




# Inflationary Gravitational Waves as a probe of the unknown post-inflationary primordial Universe

Athul K. Soman ,<sup>a</sup> Swagat S. Mishra ,<sup>b</sup> Mohammed Shafi ,<sup>a</sup>  
Soumen Basak<sup>a</sup>

<sup>a</sup>School of Physics, Indian Institute of Science Education and Research, Thiruvananthapuram, 695551, India.

<sup>b</sup>School of Physics and Astronomy, University of Nottingham, Nottingham, NG7 2RD, UK.

E-mail: [athul19@iisertvm.ac.in](mailto:athul19@iisertvm.ac.in), [swagat.mishra@nottingham.ac.uk](mailto:swagat.mishra@nottingham.ac.uk),  
[mohammedshafi18@alumni.iisertvm.ac.in](mailto:mohammedshafi18@alumni.iisertvm.ac.in), [sbasak@iisertvm.ac.in](mailto:sbasak@iisertvm.ac.in)

**Abstract.** One of the key predictions of the standard inflationary paradigm is the quantum mechanical generation of the transverse and traceless tensor fluctuations due to the rapid accelerated expansion of space, which later constitute a stochastic background of primordial gravitational waves (GWs). The amplitude of the (nearly) scale-invariant inflationary tensor power spectrum at large scales provides us with crucial information about the energy scale of inflation in the case of the minimal inflaton coupling to gravity. Furthermore, the spectral energy density,  $\Omega_{\text{GW}}(f)$ , of the GWs at sufficiently small scales (or, large frequencies  $f$ ) serves as an important observational probe of post-inflationary primordial dynamics. In fact, the small-scale spectral tilt,  $n_{\text{GW}} = \frac{d \log \Omega_{\text{GW}}}{d \log f}$ , of the spectral energy density of GWs is sensitive to the (unknown) post-inflationary equation of state (EoS),  $w$ , of the universe; with a softer EoS ( $w < 1/3$ ) leading to a red tilt:  $n_{\text{GW}} < 0$ , while a stiffer EoS ( $w > 1/3$ ) resulting in a blue tilt:  $n_{\text{GW}} > 0$ . The post-inflationary dynamics, however, is generically expected to be quite complex, potentially involving a number of distinct phases. Hence, in this work, we discuss the possibility of multiple sharp transitions, namely  $w_1 \rightarrow w_2 \rightarrow w_3 \rightarrow \dots \rightarrow w_n$ , in the EoS of the post-inflationary universe and compute the corresponding spectral energy density of the inflationary GWs. We explicitly determine the region of the parameter space  $\{w_1, w_2, w_3, \dots, w_n\}$  which leads to a potentially detectable signal in the upcoming GW detectors, without violating the current constraints.

**Keywords:** Inflation, Early Universe, Gravitational Waves, String Cosmology

---

## Contents

|          |  |           |
|----------|--|-----------|
| <b>1</b> | <b>Introduction</b>  | <b>1</b>  |
| <b>2</b> | <b>Inflationary dynamics</b>   | <b>4</b>  |
| 2.1      | Quantum fluctuations during Inflation  | 5         |
| 2.1.1    | Scalar fluctuations during inflation   | 5         |
| 2.1.2    | Tensor fluctuations during inflation   | 6         |
| 2.2      | Implications of the observational constraints  | 8         |
| <b>3</b> | <b>Primordial gravitational waves in the post-inflationary universe</b>                | <b>9</b>  |
| 3.1      | Evolution of gravitational waves   | 10        |
| 3.1.1    | Universe with a single equation of state during reheating                              | 11        |
| 3.1.2    | Universe with multiple equations of state during reheating                             | 13        |
| 3.2      | Spectral energy density of gravitational waves   | 14        |
| <b>4</b> | <b>Inflationary gravitational waves as a probe of the primordial equation of state</b> | <b>20</b> |
| <b>5</b> | <b>Post-inflationary evolution in a scenario inspired from String Theory</b>           | <b>27</b> |
| <b>6</b> | <b>Discussion and conclusions</b>  | <b>30</b> |
| <b>7</b> | <b>Acknowledgements</b>  | <b>32</b> |
| <b>A</b> | <b>Analytical solution to the Mukhanov-Sasaki equation</b>                             | <b>33</b> |
| <b>B</b> | <b>Expression for the conformal Hubble parameter</b>                                   | <b>34</b> |
| <b>C</b> | <b>Energy-momentum tensor of gravitational waves</b>                                   | <b>34</b> |
| <b>D</b> | <b>Derivation of the present-day GW spectral energy density</b>                        | <b>35</b> |
| <b>E</b> | <b>Energy density of photons and neutrinos</b>   | <b>36</b> |
| <b>F</b> | <b>Effect of varying reheating temperature on GW spectral energy density</b>           | <b>37</b> |
| F.1      | Effect of varying tensor-to-scalar ratio on GW signal                                  | 37        |
| F.2      | Two-epoch reheating with different reheating temperature                               | 38        |

---

## 1 Introduction

Cosmic inflation [1–14] is currently the leading paradigm in providing natural initial conditions for the hot Big Bang phase [6, 15–17]. In the simplest scenario, inflation is assumed to be sourced by a single (real) scalar field  $\phi$ , called the *inflaton field*, which rolls slowly down its potential  $V(\phi)$ , and couples minimally to the Ricci scalar [6, 8, 9, 14]. Of particular importance is the spectrum of (nearly) scale-invariant scalar perturbations on super-Hubble scales, generated *via* quantum fluctuations due to the rapid accelerated expansion of space during inflation [6, 18–21]. Upon their Hubble-entry, the scalar curvature fluctuations induce the temperature and density inhomogeneities in the primordial plasma, which later grow *via* gravitational instability, leading to the formation of the *large-scale structure* (LSS) in the universe [6, 16, 22–24]. The latest *Cosmic Microwave Background* (CMB) observations [25–28] provide strong support for the single field slow-roll inflationary paradigm.

Another important aspect of the inflationary dynamics is the quantum mechanical generation of a nearly scale-invariant spectrum of transverse and traceless tensor fluctuations [29] on super-Hubble scales. The inflationary tensor fluctuations, upon their Hubble-entry in the post-inflationary epochs, constitute a stochastic background of primordial gravitational waves (GWs) [30–32]. Both scalar and tensor primordial fluctuations leave distinct imprints on the CMB, which can be parameterised in terms of two sets of inflationary observables, namely, the amplitudes and the spectral indices of the primordial power spectra. In particular, the parameter space comprising of the scalar spectral index  $n_s - 1$  and the tensor-to-scalar ratio  $r$  is quite illustrative in ruling out a large class of inflationary models [8, 26, 27, 33–35]. The latest CMB observations [26, 28] impose constraints on the amplitude of primordial GWs, expressed as an upper bound on the tensor-to-scalar ratio, namely,  $r < 0.036$  at 95% confidence, which already disfavors a large class of single field inflationary models, see Ref. [35]. Moreover, the inflationary tensor fluctuations may potentially be important in distinguishing between different competing frameworks of the pre-hot Big Bang universe [36–57] observationally.

Since these GWs originate during the pre-hot Big Bang universe and propagate towards the present epoch, they encode important information about the physical processes during inflation as well as the post-inflationary dynamics of the universe. In particular, given that they are generated due to the exponential expansion during inflation, the amplitude of the spectral energy density  $\Omega_{\text{GW}}(f)$  of the primordial GWs at large length scales (or small frequencies  $f$ ) is related to the energy scale (Hubble scale  $H$ ) of inflation [30, 31, 34, 58, 59]. Additionally, the spectral index of  $\Omega_{\text{GW}}(f)$ , defined by  $n_{\text{GW}} = \frac{d \log \Omega_{\text{GW}}}{d \log f}$ , is sensitive to the equation of state (EoS) of the post-inflationary evolution [31]. In particular, the spectral tilt  $n_{\text{GW}}$  at small scales (or high frequencies  $f$ ) is determined by the (unknown) post-inflationary EoS  $w$  of the primordial universe prior to the commencement of the Big Bang Nucleosynthesis (BBN) [31, 34]. A softer EoS ( $w < 1/3$ ) leads to a red tilt:  $n_{\text{GW}} < 0$ , while a stiffer EoS ( $w > 1/3$ ) results in a blue tilt:  $n_{\text{GW}} > 0$ . A combination of the amplitude and tilt of  $\Omega_{\text{GW}}(f)$  across a broad range of frequency bands would then enable us to probe the dynamics of the early universe at energy scales far beyond the reach of the most powerful terrestrial particle accelerators [31, 34, 58–63]. Hence the search for the primordial GWs is often regarded as one of the key future targets in Cosmology.

A number of GW detectors are already operational at present, while more sensitive and advanced future detectors, both ground-based and space-based, at different frequency ranges are under construction. The existing (and upcoming) GW detectors can be primarily classified into three categories, namely, (i) CMB B-mode polarisation probes operating in the ultra-low frequency range ( $10^{-18} \text{ Hz} \lesssim f \lesssim 10^{-16} \text{ Hz}$ ), (ii) pulsar timing arrays (PTAs) sensitive to GWs in the low frequency range ( $10^{-9} \text{ Hz} \lesssim f \lesssim 10^{-7} \text{ Hz}$ ), and (iii) atomic and laser interferometers operating in the relatively high frequency range ( $10^{-5} \text{ Hz} \lesssim f \lesssim 10^3 \text{ Hz}$ ) [64]. Amongst the ultra-low frequency GW detectors, there are CMB probes such as the BICEP/Keck Array [65], LiteBIRD [66], and POLARBEAR/Simons Array [67], which are designed to measure the B-mode polarisation of the CMB photons, induced by the quadrupolar primordial GWs [68, 69]. The recent data release by the PTA observations, such as the NANOGrav collaboration [70–72], the EPTA/InPTA [73–75] and IPTA [76] provide tentative evidence for the detection of a background of stochastic GWs at low frequencies ( $\sim \mathcal{O}(10^1)$  nHz range), whose primary origin, whether astrophysical or primordial, is yet to be established [77, 78]. The currently operational interferometers such as the advanced Laser Interferometer Gravitational-wave Observatory (aLIGO) [79, 80], Virgo [81], KAGRA [82] and the upcoming/proposed interferometers, such as the Laser Interferometer Space Antenna (LISA) [83–85], Cosmic Explorer (CE) [86], Einstein Telescope (ET) [87], Big Bang Observer (BBO) [88], and the DECi-hertz Interferometer Gravitational wave Observatory (DECIGO) [89, 90], will be able to probe the (relatively) large frequency GWs from the early universe associated with the small-scale inflationary dynamics, as well as the post-inflationary expansion history of the universe, prior to the epoch of Quantum Chromodynamics (QCD) phase transition.

During the period of single field slow-roll inflation, the energy density of the universe is primarily

comprised of the homogeneous inflaton condensate  $\phi$ , which rolls down its potential  $V(\phi)$  in a slow terminal speed, thereby driving the near-exponential expansion of space. If the inflaton couplings to other external fields are low enough, then particle production during inflation can be neglected, since the rapid accelerated expansion of space quickly dilutes away the decay products. After the end of inflation, however, the inflaton field begins to oscillate around the minimum of its potential [91] and begins to transfer its energy to the particles of external offspring fields that it is coupled to via parametric resonance [92–96], and/or to the inflaton inhomogeneities  $\delta\phi$  *via* self-resonance (when attractive self-interactions are present in  $V(\phi)$ ) [96–100]. In certain classes of inflation, where the inflaton potential does not feature a stable minimum, rather it decays to zero at large field values, particle production *via* resonance is absent. However, the inflaton can still decay either perturbatively [101] or *via* the process of *instant preheating* [102]. Nevertheless, the offspring fields (and other decay products) undergo further interaction, scattering and thermalization; as a result, the universe eventually transitions to the radiation-dominated thermal plasma phase (or, the hot Big bang phase) before the commencement of BBN. This transient phase between the end of inflation and the beginning of the thermal radiation domination is referred to as the epoch of *reheating*, which is supposed to be the origin of all primordial matter and energy in the universe [14, 94, 96].

A number of comprehensive studies conducted in the past three decades [92–96, 103–109] demonstrate that the physical processes taking place during reheating is highly complex, and potentially non-linear. However, in most cases, the reheating dynamics can be broadly divided into three stages: (i) preheating, (ii) backreaction, and (iii) thermalization [14, 92, 94, 110]. The initial stage of preheating usually exhibits rapid and efficient particle production *via* broad parametric resonance [92, 94, 109]. Eventually, the backreaction of the produced particles leads to the complete/partial fragmentation of the coherent inflaton condensate. Additionally, cosmological redshifting drives the momenta of produced particles away from the broad resonance band, thereby shutting the resonance down and quenching the resonant particle production. This phase is succeeded by a long and gradual perturbative decay of the inflaton, as well as the re-scattering of decay products. Hence, the final stage of thermalization is usually the longest of the three stages, which eventually leads to the hot Big Bang phase, as discussed before. If strong attractive self-interaction of the inflaton field is present, then it can lead to the formation of quasi-solitonic structures like oscillons, resulting in the production of GWs [96–100, 111–113]. Depending upon the type of inflaton potential and the inflaton couplings to external fields, the duration and EoS of each of these phases can be different.

Despite the profusion of theoretical and numerical work in the field, the epoch of reheating remains observationally inaccessible at present. In general, there exist two distinct types of observational probes of the early universe physics, namely (1) primordial relics such as ultra long-lived solitons (*e.g.* strings, domain walls, oscillons), and (2) propagating primordial messengers (signals) such as primordial GWs. Furthermore, these primordial GWs may either originate from the physical processes during reheating or from an earlier epoch, such as inflation. In this work, we focus on the GW signal which gets generated during inflation and propagates towards us, encoding the unknown primordial dynamics of reheating after inflation. In particular, the duration of and the equation of state (EoS) during reheating can be inferred from the spectral energy density of primordial GWs at higher frequencies [34, 59, 110]. Furthermore, the GW spectrum is also influenced by a number of other factors, such as the anisotropic stress from the free-streaming relativistic neutrinos [114] and the variation in the effective number of relativistic degrees of freedom throughout the history of the universe [115–117]. Since our interest lies with in the gross features of the GW spectrum, we will not consider these factors in our computation.

There has been a number of interesting papers in the recent literature [34, 59, 118–129] investigating the possibility of probing the epoch of reheating *via* inflationary GWs, where the kinematics during reheating is parameterised by the expansion rate during ( $\sim$  at the end of) inflation  $H_{\text{inf}}$ , the temperature achieved at the end of reheating  $T_{\text{re}}$ , the duration and the EoS  $w_{\text{re}}$  during reheating. However, a majority of the papers has primarily assumed a single (average) EoS,  $w_{\text{re}}$ , throughout the

reheating history<sup>1</sup>. As mentioned earlier, the dynamics of reheating features a number of complex non-linear phases, and hence, the universe is likely to have undergone multiple transitions through different equations of state during reheating [104, 130]. Additionally, the universe might have undergone multiple phase-transitions [131–134] after the completion of reheating in the radiation dominated epoch, leading to a significant deviation of the EoS from  $w = 1/3$ .

Consequently, in this paper, we carry out a thorough investigation of the spectrum of primordial stochastic GWs by considering the unknown post-inflationary history of the universe to have undergone multiple phases of piece-wise (nearly) constant EoS, namely,  $w_1 \rightarrow w_2 \rightarrow w_3 \rightarrow \dots \rightarrow w_n$ . For the sake of simplicity in calculation, we further assume that the transition between any two successive epochs is sharp enough to be modelled as an *instantaneous transition*. Under the aforementioned assumptions, we first solve the evolution equation for the Fourier mode functions of the tensor fluctuations in different epochs of constant  $w_i$ , and then use the Israel junction matching conditions [31, 135, 136] to determine the full tensor mode functions. Using the thus obtained analytical expression for the mode functions, we finally compute the present-day spectral energy density of the (first-order) inflationary GWs. We highlight the subspace of the parameter space of EoS  $\{w_1, w_2, \dots, w_n\}$ , and the corresponding duration of each epoch of constant  $w_i$ , satisfying two conditions: (i) yielding a potentially detectable background of stochastic GWs in the upcoming detectors, such as LISA, BBO, DECIGO, CE, and ET; while at the same time, (ii) satisfying the constraints imposed by the already existing GW, CMB, and BBN observations. To be specific, we provide forecasts for GWs corresponding to the unknown primordial history of the universe comprising of (up to) three different piece-wise constant EoS phases  $\{w_1, w_2, w_3\}$ . As a concrete example, we apply our method to determine the parameter space of the duration of different piece-wise constant  $w_i$  epochs before the commencement of BBN in the framework of the recently proposed String Theory inspired model of the post-inflationary universe in Ref. [137], which leads to a detectable GW background in the aforementioned detectors.

Our paper is organised as follows: we begin with a brief review of the single field slow-roll inflationary dynamics in Sec. 2, including the spectra of scalar and tensor quantum fluctuations generated during inflation. We also provide a succinct discussion about the latest CMB constraints on the inflationary observables, which serve as the initial conditions for the post-inflationary evolution. In Sec. 3, we first derive analytical expressions for the tensor mode functions in the post-inflationary epochs using junction matching conditions, and then move on to compute the corresponding spectral energy density of GWs. Sec. 4 is dedicated to determining the parameter space of the multiple equations of states (and their corresponding duration) which leads to a potentially detectable signal in the upcoming GW detectors. In Sec. 5, we focus on the post-inflationary evolution of the universe in a specific (String-inspired) model of the primordial universe, as proposed in Ref. [137]. Finally, we spell out the primary conclusions from our results, and provide further discussions on our work in Sec. 6. Various appendices provide supplementary material to the analysis carried out in the main sections.

We work with natural units  $\hbar = c = 1$  throughout this paper, and define the reduced Planck mass to be  $m_p = 1/\sqrt{8\pi G} = 2.44 \times 10^{18}$  GeV. The background universe is considered to be described by the flat Friedmann-Lemaitre-Robertson-Walker (FLRW) line element, with metric signature  $(-, +, +, +)$ . Derivative with respect to cosmic time ‘ $t$ ’ is denoted with an overdot ( $\dot{\phantom{x}}$ ), while derivative with respect to conformal time ‘ $\tau$ ’ is denoted with an overprime ( $\phantom{x}'$ ).

## 2 Inflationary dynamics

We work in the simplest scenario where inflation is sourced by a single canonical scalar field (inflaton)  $\varphi(t, \vec{x})$ , whose homogeneous part is denoted as  $\phi(t)$ , *i.e.*,  $\varphi(t, \vec{x}) = \phi(t) + \delta\varphi(t, \vec{x})$ . The action

<sup>1</sup>However, see refs. [59, 121] for earlier work involving multiple primordial equation of states.

governing the dynamics of the scalar field  $\varphi$  is given by [6, 9, 14]

$$S[g_{\mu\nu}, \varphi] = \int d^4x \sqrt{-g} \left( \frac{1}{2} m_p^2 R - \frac{1}{2} g^{\mu\nu} \partial_\mu \varphi \partial_\nu \varphi - V(\varphi) \right), \quad (2.1)$$

where  $g_{\mu\nu}$  is the metric tensor,  $R$  is the Ricci scalar curvature and  $V(\varphi)$  is the inflaton potential. The background spacetime is described by the flat FLRW line element

$$ds^2 = -dt^2 + a^2(t) [dx^2 + dy^2 + dz^2], \quad (2.2)$$

where  $a(t)$  is the scale factor whose time evolution is governed by the Friedmann equation

$$H^2 = \frac{1}{3 m_p^2} \rho_\phi \equiv \frac{1}{3 m_p^2} \left[ \frac{1}{2} \dot{\phi}^2 + V(\phi) \right], \quad (2.3)$$

where  $H = \dot{a}/a$  is the Hubble parameter. The homogeneous inflaton condensate satisfies

$$\ddot{\phi} + 3H \dot{\phi} + \frac{dV}{d\phi} = 0. \quad (2.4)$$

Departure from a pure de Sitter (exponential) expansion during inflation is characterised by the first slow-roll parameter

$$\epsilon_H = -\frac{d \ln H}{dN} = -\frac{\dot{H}}{H^2} = \frac{1}{2 m_p^2} \frac{\dot{\phi}^2}{H^2}, \quad (2.5)$$

while a small enough value of the second slow-roll parameter, defined by

$$\eta_H = -\frac{\ddot{\phi}}{H \dot{\phi}} = \epsilon_H - \frac{1}{2} \frac{d \ln \epsilon_H}{dN}, \quad (2.6)$$

ensures that inflation lasts for long enough. Note that  $N(a) = \ln(a/a_i)$  marks the number of  $e$ -folds of expansion during inflation, with  $a_i$  being the scale factor at an arbitrary initial time during inflation [9]. Slow-roll inflation is defined by

$$\epsilon_H \ll 1, \quad \text{and} \quad |\eta_H| \ll 1. \quad (2.7)$$

## 2.1 Quantum fluctuations during Inflation

The rapid accelerated expansion during inflation stretches the small-scale (sub-Hubble) vacuum fluctuations to large super-Hubble scales, which then remain frozen until their subsequent Hubble entry in the post-inflationary epochs, as illustrated in Fig. 1. In fact, the simplest scenario of single field slow-roll inflation generates both scalar- and tensor-type fluctuations, see Refs. [9, 14]; the former induce temperature and density fluctuations in the primordial plasma, while the latter lead to a stochastic GW background, as discussed in Sec. 3. Since CMB observations suggest that the primordial fluctuations are small, their dynamics is well described by the framework of linear (cosmological) perturbation theory, where the scalar and the tensor perturbations are decoupled (SVT decomposition theorem). Thus, they can be treated independently of each other [9].

### 2.1.1 Scalar fluctuations during inflation

Scalar fluctuations during inflation are described by the gauge-invariant comoving curvature perturbation  $\zeta(\tau, \vec{x})$ , whose action, in the comoving gauge ( $\delta\varphi = 0$ ), takes the form [9, 138]

$$S[\zeta(\tau, \vec{x})] = \frac{1}{2} \int d\tau d^3\vec{x} \left( \frac{a \phi'}{\mathcal{H}} \right)^2 \left[ (\zeta')^2 - (\vec{\nabla} \zeta)^2 \right], \quad (2.8)$$

where  $\mathcal{H} = a'/a$ , is the conformal Hubble rate. To transform the action into its Minkowski equivalent, we define the Mukhanov-Sasaki (MS) variable  $v = (a \phi'/\mathcal{H}) \zeta$ . For simplification, we denote  $z = a \phi'/\mathcal{H} = \sqrt{2\epsilon_H} a m_p$ , where Eq. (2.5) has been used to get the second equality. The equation of motion in terms of the MS variable in Fourier space is given by

$$v_k'' + \left( k^2 - \frac{z''}{z} \right) v_k = 0, \quad (2.9)$$

where

$$\frac{z''}{z} = \mathcal{H}^2 \left[ 2 + 2\epsilon_H - 3\eta_H + 2\epsilon_H^2 + \eta_H^2 - 3\epsilon_H \eta_H - \frac{\eta_H'}{\mathcal{H}} \right]. \quad (2.10)$$

To solve the MS equation analytically, we define a new parameter  $\nu$  such that  $z''/z = \mathcal{H}^2(\nu^2 - 1/4)$ . For slow-roll inflation ( $\epsilon_H, |\eta_H|, |\eta_H'| \ll 1$ ), we can treat  $\nu$  to be (approximately) a constant. The MS Eq. (2.9) can be written in terms of  $\nu$  as

$$v_k'' + \left( k^2 - \frac{\nu^2 - 1/4}{\tau^2} \right) v_k = 0, \quad (2.11)$$

where we have substituted  $\mathcal{H} = -\tau^{-1}$  due to the quasi-de Sitter expansion during inflation. Eq. (2.11) is similar to the dynamic equation of a simple harmonic oscillator with a time-dependent frequency. Imposing the Bunch-Davies initial condition [139, 140],  $v_k \xrightarrow{-k\tau \gg 1} e^{-ik\tau}/\sqrt{2k}$ , results in a unique solution [136]

$$v_k(\tau) = \frac{1}{\sqrt{2k}} \sqrt{\frac{\pi}{2}} e^{i(\nu + \frac{1}{2})\frac{\pi}{2}} \sqrt{-k\tau} H_\nu^{(1)}(-k\tau), \quad (2.12)$$

where  $H_\nu^{(1)}$  is the Hankel function of first kind [141]. The derivation of Eq. (2.12) is given in App. A. For slow-roll inflation,  $\nu$  can be approximated as  $\nu \approx 3/2$ . Substituting this into Eq. (2.12) leads to the following expression for the mode function

$$v_k(\tau) = \frac{1}{\sqrt{2k}} \left( 1 - \frac{i}{k\tau} \right) e^{-ik\tau}. \quad (2.13)$$

The power spectrum for scalar fluctuations is defined as

$$\mathcal{P}_\zeta(k) = \frac{k^3}{2\pi^2} |\zeta_k|^2 = \frac{k^3}{2\pi^2} \left| \frac{v_k}{z} \right|^2. \quad (2.14)$$

Substituting  $z = am_p \sqrt{2\epsilon_H}$ ,  $a = -1/(H\tau)$  and taking the super-Hubble limit  $-k\tau \rightarrow 0$ , we obtain the scalar power spectrum during inflation to be

$$\mathcal{P}_\zeta(k) = \frac{1}{8\pi^2 \epsilon_H} \left( \frac{H}{m_p} \right)^2. \quad (2.15)$$

### 2.1.2 Tensor fluctuations during inflation

The action for the gauge-invariant, transverse and traceless tensor fluctuations  $h_{ij}$  is given by [10, 138]

$$S[h_{ij}] = \frac{m_p^2}{8} \int d\tau d^3\vec{x} a^2 \left[ (h'_{ij})^2 - (\vec{\nabla} h_{ij})^2 \right]. \quad (2.16)$$

Using the rotational symmetry of the background metric, we align the z-axis along the direction of the momentum of the tensor mode, *i.e.*,  $\vec{k} = (0, 0, k)$ , and upon decomposing the tensor perturbation into its two polarization components, we obtain

$$h_{ij} = \frac{1}{\sqrt{2}} \begin{pmatrix} h^+ & h^\times & 0 \\ h^\times & -h^+ & 0 \\ 0 & 0 & 0 \end{pmatrix} = \epsilon_{ij}^+ h^+ + \epsilon_{ij}^\times h^\times, \quad (2.17)$$

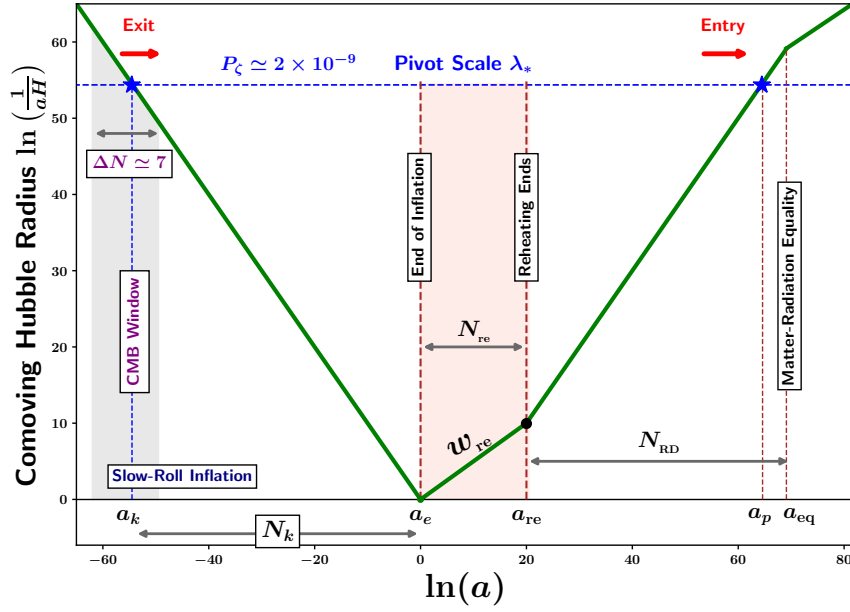


**Figure 1:** The figure illustrates the variation of the comoving Hubble radius  $(aH)^{-1}$  with the scale factor  $a(t)$  (both in the logarithmic scale). During inflation, the comoving Hubble radius decreases, causing the fluctuations to exit the comoving Hubble radius. On super-Hubble scales, the amplitude of the fluctuations remains frozen. After the end of inflation, these fluctuations enter the comoving Hubble radius, which begins to increase due to the decelerating expansion of space. Modes with larger wavelengths exit the comoving Hubble radius earlier during inflation, as compared to the ones with smaller wavelengths. The CMB pivot scale (corresponding to a wavenumber  $k_* = 0.05 \text{ Mpc}^{-1}$ ), shown in blue dashed line, makes its Hubble-exit about  $N_k$   $e$ -folds before the end of inflation, while it enters the comoving Hubble radius prior to the matter-radiation equality. The black dot represents the end of reheating. The figure has been plotted assuming a matter-like reheating equation of state, *i.e.*  $w_{\text{re}} = 0$ , for the purpose of illustration.

where  $+$ ,  $\times$  stands for the two polarisation states of GWs and

$$\epsilon_{ij}^+ = \frac{1}{\sqrt{2}} \begin{pmatrix} 1 & 0 & 0 \\ 0 & -1 & 0 \\ 0 & 0 & 0 \end{pmatrix}; \quad \epsilon_{ij}^\times = \frac{1}{\sqrt{2}} \begin{pmatrix} 0 & 1 & 0 \\ 1 & 0 & 0 \\ 0 & 0 & 0 \end{pmatrix}. \quad (2.18)$$

Hence, the action can be rewritten as [14]

$$S[h^+, h^\times] = \frac{1}{2} \int d\tau d^3\vec{x} \left( \frac{a m_p}{2} \right)^2 \sum_{\lambda=+,\times} \left[ (h'^\lambda)^2 - (\vec{\nabla} h^\lambda)^2 \right], \quad (2.19)$$

which is analogous to the action of two massless scalar fields [14] as given in Eq. (2.8). For each polarisation mode of the tensor fluctuations, we define a corresponding Mukhanov-Sasaki variable  $v^\lambda = (a m_p/2) h^\lambda$ . The full tensor power spectrum, consisting of both the aforementioned polarisation modes, is given by

$$\mathcal{P}_T(k) = \frac{k^3}{2\pi^2} \left( |h_k^+|^2 + |h_k^\times|^2 \right) = \frac{k^3}{2\pi^2} \left( \frac{2}{a m_p} \right)^2 \left( |v_k^+|^2 + |v_k^\times|^2 \right). \quad (2.20)$$



Substituting the solution for each of the polarisation mode in Eq. (2.20), as given in Eq. (2.13), the inflationary tensor power spectrum in the super-Hubble limit  $k \ll aH$  becomes

$$\mathcal{P}_T(k) = \frac{2}{\pi^2} \left( \frac{H}{m_p} \right)^2. \quad (2.21)$$

To facilitate the comparison between the inflationary predictions and the observational data, it is instructive to express the scalar and tensor power spectra as power laws around a pivot scale  $k_*$ , such as

$$\mathcal{P}_T(k) = A_T \left( \frac{k}{k_*} \right)^{n_T}; \quad \mathcal{P}_\zeta(k) = A_S \left( \frac{k}{k_*} \right)^{n_S-1}, \quad (2.22)$$

where  $A_S$  and  $A_T$  are the amplitudes of the scalar and tensor power spectra, respectively, at the CMB pivot scale  $k_* = 0.05 \text{ Mpc}^{-1}$ ; while  $n_S - 1$  and  $n_T$  are the scalar and tensor spectral indices, given by

$$n_S - 1 = 2\eta_H - 4\epsilon_H; \quad n_T = -2\epsilon_H. \quad (2.23)$$

The tensor-to-scalar ratio is defined as,

$$r = \frac{A_T}{A_S}. \quad (2.24)$$

From Eqs. (2.15) and (2.21), the tensor-to-scalar ratio can be related to the Hubble slow-roll parameter as

$$r = 16\epsilon_H, \quad (2.25)$$

which, using Eq. (2.23), leads to the *single field consistency relation*

$$r = -8n_T. \quad (2.26)$$

## 2.2 Implications of the observational constraints

Latest observations of the anisotropies of CMB temperature and polarisation fluctuations, combined with an absence of detection of the primordial tensor fluctuations on large cosmological scales, allow us to put stringent constraints on the inflationary power spectra in the single field slow-roll paradigm. In particular, the primordial scalar fluctuations are observed to be predominantly adiabatic, highly Gaussian, and nearly scale-invariant on CMB scales, which is in accordance with the predictions of the standard single field slow-roll models [142]. The amplitude of the scalar power spectrum at CMB scales is obtained from the Planck mission to be  $A_S \simeq 2.1 \times 10^{-9}$  [25, 35]. The scalar spectral index is constrained to be  $n_S = 0.9649 \pm 0.0012$  at 68% confidence [27]. The improved constraints from the BICEP/Keck Array [28], combined with the Planck 2018 observations, lead to an upper bound on the tensor-to-scalar ratio  $r < 0.036$  at the CMB pivot scale  $k_* = 0.05 \text{ Mpc}^{-1}$ . This further constrains the amplitude of the tensor fluctuations to be  $A_T < 7.56 \times 10^{-11}$  on CMB scales.

The corresponding upper bounds on the expansion rate and energy scale during inflation can be found using Eq. (2.21). The Hubble expansion rate during (slow-roll) inflation is bounded by  $H_{\text{inf}} < 4.64 \times 10^{13} \text{ GeV}$ . Using the Friedmann equation  $H_{\text{inf}}^2 \simeq \rho_{\text{inf}}/3m_p^2$ , the bound on  $E_{\text{inf}}$  is given by

$$E_{\text{inf}} = (\rho_{\text{inf}})^{1/4} \implies E_{\text{inf}} < 1.39 \times 10^{16} \text{ GeV}, \quad (2.27)$$

which is orders of magnitude below the Planck scale ( $\sim 10^{18} \text{ GeV}$ ). For slow-roll inflation, the constraint on the tensor-to-scalar ratio, along with Eq. (2.25) and Eq. (2.26) leads to  $\epsilon_H < 2.25 \times 10^{-3}$ ,  $|\eta_H| \simeq 0.02$  and  $|n_T| < 4.5 \times 10^{-3}$ . These constraints further reinforce the near-scale invariance of the inflationary power spectra; in particular, the tensor power spectrum has a negligible scale dependence [35].

### 3 Primordial gravitational waves in the post-inflationary universe

The rapid accelerated expansion during inflation leads to the generation of almost scale-invariant primordial tensor fluctuations on super-Hubble scales, as discussed in Sec. 2.1.2. These tensor fluctuations, upon making their Hubble-entry in the post-inflationary (decelerating) epochs, then propagate as waves and thus, they constitute a stochastic gravitational wave (GW) background. In this section, we carry out a detailed study of the evolution of these primordial tensor fluctuations in the post-inflationary universe. There has been a number of important papers in the literature in this direction, *e.g.* Refs. [34, 59, 119–121, 131], to quote a few. In particular, we would like to emphasize the work carried out in Refs. [119] where the authors determined the parameter space of the post-inflationary epoch which leads to a detectable signal in the aLIGO and LISA GW observatories. To be specific, their analysis primarily focused on the estimation of the post-inflationary parameter space, such as the expansion rate during (at the end of) inflation ( $H_{\text{inf}}$ ), the duration of reheating (characterised by the temperature achieved at the end of reheating,  $T_{\text{r}*}$ ), and the EoS during reheating ( $w_{\text{re}}$ ).

It is important to note that the authors of Ref. [119] modelled the post-inflationary reheating epoch by assuming a single EoS. However, as mentioned earlier, since the dynamics of reheating is quite complex, the universe is likely to have undergone multiple transitions through different equations of state during reheating [104, 130]. Furthermore, the early universe might have undergone a number of phase-transitions after the completion of reheating in the radiation dominated epoch, resulting in a significant deviation of the EoS from  $w = 1/3$ . Therefore, it is important to extend the analysis of Ref. [119] by allowing for the possibility of multiple phases of piece-wise constant EoS.

Before proceeding to determine the post-inflationary evolution of the tensor fluctuations, let us lay out the primary assumptions under which we base our analysis of multiple primordial EoS. Our technique is similar to the one carried out in Ref. [136] for multiple transitions during inflation in the context of primordial black hole formation.

1. We assume the universe to have undergone multiple sharp (instantaneous) transitions in the EoS,  $w_{\text{re}}$ , *i.e.*  $w_1 \rightarrow w_2$  at  $\tau = \tau_1$ ;  $w_2 \rightarrow w_3$  at  $\tau = \tau_2$ ;  $w_3 \rightarrow w_4$  at  $\tau = \tau_3$ ; and so on, in the post-inflationary epoch before the commencement of BBN. Hence, the EoS can be written as

$$w_{\text{re}}(\tau) = w_1 + (w_2 - w_1) \Theta(\tau - \tau_1) + (w_3 - w_2) \Theta(\tau - \tau_2) + (w_4 - w_3) \Theta(\tau - \tau_3) + \dots, \quad (3.1)$$

where  $\Theta(\tau - \tau_n)$  is the Heaviside step function.

2. The inflationary tensor modes are frozen on the super-Hubble scales, with amplitude  $h_{k,\text{inf}}^\lambda$ , before their Hubble-entry. Hence they serve as the initial conditions for the post-inflationary evolution as,

$$h_k^\lambda(\tau_k) = h_{k,\text{inf}}^\lambda \quad ; \quad h_k^{\prime\lambda}(\tau_k) = 0, \quad (3.2)$$

where  $\tau_k$  is the conformal time when the tensor mode of interest with the (comoving) wavenumber  $k$  enters the comoving Hubble radius.

3. We match the solutions of the equation of motion of tensor fluctuations across two adjacent epochs with different (constant) EoS at the time of the instantaneous transition,  $\tau = \tau_n$ , by using the Israel Junction conditions [135], *i.e.*

$$h_{k,b}^\lambda(\tau_n) = h_{k,a}^\lambda(\tau_n), \quad (\text{Continuity}), \quad (3.3)$$

$$h_{k,b}^{\prime\lambda}(\tau) \Big|_{\tau=\tau_n} = h_{k,a}^{\prime\lambda}(\tau) \Big|_{\tau=\tau_n}, \quad (\text{Differentiability}), \quad (3.4)$$

where  $h_{k,b}^\lambda$  and  $h_{k,a}^\lambda$  correspond to the tensor amplitude before and after the transition respectively.

### 3.1 Evolution of gravitational waves

First, we solve the equation of motion for the tensor mode functions in the post-inflationary epoch. The action in Eq. (2.19) leads to the field equation

$$h_{ij}''^{\lambda} + 2 \frac{a'}{a} h_{ij}'^{\lambda} - \bar{\nabla}^2 h_{ij}^{\lambda} = 0, \quad (3.5)$$

and the corresponding equation for the evolution of Fourier mode functions (for each polarisation) becomes

$$h_k''^{\lambda} + 2 \frac{a'}{a} h_k'^{\lambda} + k^2 h_k^{\lambda} = 0. \quad (3.6)$$

For an epoch with a constant EoS, say  $w$ , the conformal Hubble parameter can be written as (see App. B)

$$\mathcal{H} = \frac{a'}{a} = aH = a_i H_i \left[ 1 + \frac{a_i H_i (\tau - \tau_i)}{\alpha} \right]^{-1}, \quad (3.7)$$

where ‘ $i$ ’ denotes the beginning of the epoch and the parameter  $\alpha = 2/(1 + 3w)$ . We introduce the variable  $y(\tau) = k/[a(\tau)H(\tau)]$  as the new independent variable in order to rewrite Eq. (3.6) in the desired form

$$\frac{d^2 h_k^{\lambda}}{dy^2} + 2 \frac{\alpha}{y} \frac{dh_k^{\lambda}}{dy} + \alpha^2 h_k^{\lambda} = 0. \quad (3.8)$$

Note that  $y < 1$  for super-Hubble modes and  $y > 1$  for sub-Hubble modes. Defining  $f_k^{\lambda}(x) = x^{(\alpha-1/2)} h_k^{\lambda}$  with  $x = \alpha y$ , we can convert Eq. (3.8) to the following expression

$$\frac{d^2 f_k^{\lambda}}{dx^2} + \frac{1}{x} \frac{df_k^{\lambda}}{dx} + \left[ 1 - \frac{(\alpha - \frac{1}{2})^2}{x^2} \right] f_k^{\lambda} = 0, \quad (3.9)$$

which is of the form of a Bessel equation. Hence, the general solution of this equation can be written in terms of a linear combination of two independent Bessel functions of the first-kind,  $J_{(\alpha-\frac{1}{2})}(x)$  and  $J_{-(\alpha-\frac{1}{2})}(x)$  [141],

$$h_k^{\lambda}(y) = \frac{1}{(\alpha y)^{\alpha-\frac{1}{2}}} \left[ A_k J_{(\alpha-\frac{1}{2})}(\alpha y) + B_k J_{-(\alpha-\frac{1}{2})}(\alpha y) \right], \quad (3.10)$$

$$h_k'^{\lambda}(y) = \frac{-k}{(\alpha y)^{\alpha-\frac{1}{2}}} \left[ A_k J_{(\alpha+\frac{1}{2})}(\alpha y) - B_k J_{-(\alpha+\frac{1}{2})}(\alpha y) \right]. \quad (3.11)$$

The coefficients  $A_k$  and  $B_k$  in the solution are obtained by junction matching conditions at the transitions of two adjacent epochs as specified in Eqs. (3.3) and (3.4). Specifically, consider a sharp transition from the  $(n-1)^{\text{th}}$  epoch to the  $n^{\text{th}}$  epoch with the equations of state  $w_{(n-1)}$  and  $w_n$  respectively, at time  $\tau = \tau_{(n-1)}$ . The expression for the corresponding tensor amplitude can be written as

$$h_k^{\lambda}(y) = \begin{cases} \frac{\left[ A_{k,m} J_{(\alpha_m-\frac{1}{2})}(\alpha_m y) + B_{k,m} J_{-(\alpha_m-\frac{1}{2})}(\alpha_m y) \right]}{(\alpha_m y)^{\alpha_m-\frac{1}{2}}}, & y_{(m-1)} \leq y \leq y_m, \\ \frac{\left[ A_{k,n} J_{(\alpha_n-\frac{1}{2})}(\alpha_n y) + B_{k,n} J_{-(\alpha_n-\frac{1}{2})}(\alpha_n y) \right]}{(\alpha_n y)^{\alpha_n-\frac{1}{2}}}, & y_m \leq y \leq y_n, \end{cases} \quad (3.12)$$

where  $m = n - 1$  and  $y_n = k/[a(\tau_n)H(\tau_n)]$ . Similarly the derivatives of the tensor amplitude is given by

$$h_k^{\prime\lambda}(y) = \begin{cases} -k \frac{[A_{k,m} J_{(\alpha_m + \frac{1}{2})}(\alpha_m y) - B_{k,m} J_{-(\alpha_m + \frac{1}{2})}(\alpha_m y)]}{(\alpha_m y)^{\alpha_m - \frac{1}{2}}}, & y_{(m-1)} \leq y \leq y_m, \\ -k \frac{[A_{k,n} J_{(\alpha_n + \frac{1}{2})}(\alpha_n y) - B_{k,n} J_{-(\alpha_n + \frac{1}{2})}(\alpha_n y)]}{(\alpha_n y)^{\alpha_n - \frac{1}{2}}}, & y_m \leq y \leq y_n. \end{cases} \quad (3.13)$$

Imposing junction matching conditions (3.3) and (3.4) on Eqs. (3.12) and (3.13), we obtain

$$\frac{A_{k,n} g_1 + B_{k,n} f_1}{(\alpha_n y_m)^{(\alpha_n - \frac{1}{2})}} = \frac{A_{k,m} g_2 + B_{k,m} f_2}{(\alpha_m y_m)^{(\alpha_m - \frac{1}{2})}}, \quad (3.14)$$

$$\frac{A_{k,n} g_3 - B_{k,n} f_3}{(\alpha_n y_m)^{(\alpha_n - \frac{1}{2})}} = \frac{A_{k,m} g_4 - B_{k,m} f_4}{(\alpha_m y_m)^{(\alpha_m - \frac{1}{2})}}, \quad (3.15)$$

where

$$g_1 = J_{(\alpha_n - \frac{1}{2})}(\alpha_n y_m), \quad f_1 = J_{-(\alpha_n - \frac{1}{2})}(\alpha_n y_m), \quad (3.16)$$

$$g_2 = J_{(\alpha_m - \frac{1}{2})}(\alpha_m y_m), \quad f_2 = J_{-(\alpha_m - \frac{1}{2})}(\alpha_m y_m), \quad (3.17)$$

$$g_3 = J_{(\alpha_n + \frac{1}{2})}(\alpha_n y_m), \quad f_3 = J_{-(\alpha_n + \frac{1}{2})}(\alpha_n y_m), \quad (3.18)$$

$$g_4 = J_{(\alpha_m + \frac{1}{2})}(\alpha_m y_m), \quad f_4 = J_{-(\alpha_m + \frac{1}{2})}(\alpha_m y_m). \quad (3.19)$$

A slight rearrangement of the terms yields the following relations between the coefficients before and after transition

$$A_{k,n} = \frac{(\alpha_n y_m)^{(\alpha_n - \frac{1}{2})}}{(\alpha_m y_m)^{(\alpha_m - \frac{1}{2})}} \frac{[A_{k,m} (g_2 f_3 + g_4 f_1) + B_{k,m} (f_2 f_3 - f_4 f_1)]}{f_1 g_3 + g_1 f_3}, \quad (3.20)$$

$$B_{k,n} = \frac{(\alpha_n y_m)^{(\alpha_n - \frac{1}{2})}}{(\alpha_m y_m)^{(\alpha_m - \frac{1}{2})}} \frac{[A_{k,m} (g_2 g_3 - g_4 g_1) + B_{k,m} (f_2 g_3 + f_4 g_1)]}{f_1 g_3 + g_1 f_3}. \quad (3.21)$$

Utilizing Eqs. (3.20) and (3.21), we can find the coefficients  $A_k$  and  $B_k$  for any epoch in the post-inflationary universe, except for the first epoch right after the end of inflation as they have to be calculated using Eq. (3.2). We stress that the expression for mode functions given in Eq. (3.10) is applicable at all scales in the post-inflationary universe, irrespective of whether the mode functions are sub-Hubble<sup>2</sup> or super-Hubble, with the junction matching conditions having been imposed at the time of sharp transition.

### 3.1.1 Universe with a single equation of state during reheating

We begin by providing expressions for the coefficients of the tensor mode functions in Eq. (3.10) for the simplest case, where the post-inflationary reheating epoch is characterized by a single constant EoS.

---

<sup>2</sup>Note that we do not consider the deep-UV modes that never exited the Hubble-radius during inflation. In this sense, we have a UV cutoff around  $k_{UV} = k_{end}$ . For a thorough discussion on regularization and renormalization of tensor modes, see Refs. [143, 144].

- **Reheating epoch**

Assume that the reheating epoch is characterised by a single effective EoS,  $w_{\text{re}}$ . Then, the resultant tensor amplitude Eq. (3.10) for reheating epoch can be written as

$$h_{k,\text{re}}^\lambda(y) = \frac{1}{(\alpha_{\text{re}} y)^{\alpha_{\text{re}} - \frac{1}{2}}} \left[ A_{k,\text{re}} J_{(\alpha_{\text{re}} - \frac{1}{2})}(\alpha_{\text{re}} y) + B_{k,\text{re}} J_{-(\alpha_{\text{re}} - \frac{1}{2})}(\alpha_{\text{re}} y) \right], \quad (3.22)$$

where  $\alpha_{\text{re}} = 2/(1 + 3w_{\text{re}})$ . In order to use the initial conditions, we need the super-Hubble limits of the tensor mode and its derivative, for which we make use of the small argument limit of the Bessel function,  $J_\nu(y \ll 1) \approx (y/2)^\nu / \Gamma(\nu + 1)$ , in the super-Hubble regime. The tensor mode function and its derivative on super-Hubble scales take the form

$$\lim_{y \rightarrow 0} h_{k,\text{re}}^\lambda(y) = A_{k,\text{re}} \frac{1}{2^{(\alpha_{\text{re}} - \frac{1}{2})}} \frac{1}{\Gamma(\alpha_{\text{re}} + \frac{1}{2})} + B_{k,\text{re}} \frac{2^{(\alpha_{\text{re}} - \frac{1}{2})}}{(\alpha_{\text{re}} y)^{2(\alpha_{\text{re}} - \frac{1}{2})}} \frac{1}{\Gamma(-\alpha_{\text{re}} + \frac{3}{2})}, \quad (3.23)$$

$$\lim_{y \rightarrow 0} h_{k,\text{re}}^{\lambda'}(y) = -k \left[ A_{k,\text{re}} \frac{\alpha_{\text{re}} y}{2^{(\alpha_{\text{re}} + \frac{1}{2})}} \frac{1}{\Gamma(\alpha_{\text{re}} + \frac{3}{2})} - B_{k,\text{re}} \frac{2^{(\alpha_{\text{re}} + \frac{1}{2})}}{(\alpha_{\text{re}} y)^{2\alpha_{\text{re}}}} \frac{1}{\Gamma(-\alpha_{\text{re}} + \frac{1}{2})} \right]. \quad (3.24)$$

Incorporating this into Eq. (3.2), we obtain

$$A_{k,\text{re}} = 2^{(\alpha_{\text{re}} - \frac{1}{2})} \Gamma(\alpha_{\text{re}} + 1/2) h_{k,\text{inf}}^\lambda, \quad B_{k,\text{re}} = 0. \quad (3.25)$$

- **Radiation-dominated epoch**

The tensor mode functions in the RD epoch ( $w = 1/3$ ,  $\alpha = 1$ ) take the form

$$h_{k,\text{RD}}^\lambda(y) = \frac{1}{y^{\frac{1}{2}}} \left[ A_{k,\text{RD}} J_{\frac{1}{2}}(y) + B_{k,\text{RD}} J_{-\frac{1}{2}}(y) \right]. \quad (3.26)$$

The coefficients for this epoch are determined using Eqs. (3.20) and (3.21) at the end of reheating (denoted by ‘r\*’)

$$A_{k,\text{RD}} = \frac{y_{\text{r}^*}^{(1-\alpha_{\text{re}})}}{\alpha_{\text{re}}^{(\alpha_{\text{re}} - \frac{1}{2})}} \times A_{k,\text{re}} \left[ \frac{J_{(\alpha_{\text{re}} - \frac{1}{2})}(\alpha_{\text{re}} y_{\text{r}^*}) J_{-\frac{3}{2}}(y_{\text{r}^*}) + J_{(\alpha_{\text{re}} + \frac{1}{2})}(\alpha_{\text{re}} y_{\text{r}^*}) J_{-\frac{1}{2}}(y_{\text{r}^*})}{J_{-\frac{1}{2}}(y_{\text{r}^*}) J_{\frac{3}{2}}(y_{\text{r}^*}) + J_{\frac{1}{2}}(y_{\text{r}^*}) J_{-\frac{3}{2}}(y_{\text{r}^*})} \right], \quad (3.27)$$

$$B_{k,\text{RD}} = \frac{y_{\text{r}^*}^{(1-\alpha_{\text{re}})}}{\alpha_{\text{re}}^{(\alpha_{\text{re}} - \frac{1}{2})}} \times A_{k,\text{re}} \left[ \frac{J_{(\alpha_{\text{re}} - \frac{1}{2})}(\alpha_{\text{re}} y_{\text{r}^*}) J_{\frac{3}{2}}(y_{\text{r}^*}) - J_{(\alpha_{\text{re}} + \frac{1}{2})}(\alpha_{\text{re}} y_{\text{r}^*}) J_{\frac{1}{2}}(y_{\text{r}^*})}{J_{-\frac{1}{2}}(y_{\text{r}^*}) J_{\frac{3}{2}}(y_{\text{r}^*}) + J_{\frac{1}{2}}(y_{\text{r}^*}) J_{-\frac{3}{2}}(y_{\text{r}^*})} \right], \quad (3.28)$$

where  $y_{\text{r}^*} = k/k_{\text{r}^*}$  with  $k_{\text{r}^*}$  being the comoving wavenumber that made its Hubble-entry at the end of reheating (beginning of radiation domination).

- **Matter-dominated epoch**

The tensor mode functions in the MD epoch ( $w = 0$ ,  $\alpha = 2$ ) take the form

$$h_{k,\text{MD}}^\lambda(y) = \frac{1}{(2y)^{\frac{3}{2}}} \left[ A_{k,\text{MD}} J_{\frac{3}{2}}(2y) + B_{k,\text{MD}} J_{-\frac{3}{2}}(2y) \right]. \quad (3.29)$$

Again, Eqs. (3.20) and (3.21) at matter-radiation equality (denoted by ‘eq’) lead to

$$A_{k,\text{MD}} = 2^{\frac{3}{2}} y_{\text{eq}} \times \left\{ A_{k,\text{RD}} \left[ \frac{J_{\frac{1}{2}}(y_{\text{eq}}) J_{-\frac{5}{2}}(2y_{\text{eq}}) + J_{\frac{3}{2}}(y_{\text{eq}}) J_{-\frac{3}{2}}(2y_{\text{eq}})}{J_{-\frac{3}{2}}(2y_{\text{eq}}) J_{\frac{5}{2}}(2y_{\text{eq}}) + J_{\frac{3}{2}}(2y_{\text{eq}}) J_{-\frac{5}{2}}(2y_{\text{eq}})} \right] \right. \\ \left. + B_{k,\text{RD}} \left[ \frac{J_{-\frac{1}{2}}(y_{\text{eq}}) J_{-\frac{5}{2}}(2y_{\text{eq}}) - J_{-\frac{3}{2}}(y_{\text{eq}}) J_{-\frac{3}{2}}(2y_{\text{eq}})}{J_{-\frac{3}{2}}(2y_{\text{eq}}) J_{\frac{5}{2}}(2y_{\text{eq}}) + J_{\frac{3}{2}}(2y_{\text{eq}}) J_{-\frac{5}{2}}(2y_{\text{eq}})} \right] \right\}, \quad (3.30)$$

$$B_{k,\text{MD}} = 2^{\frac{3}{2}} y_{\text{eq}} \times \left\{ A_{k,\text{RD}} \left[ \frac{J_{\frac{1}{2}}(y_{\text{eq}}) J_{\frac{5}{2}}(2 y_{\text{eq}}) - J_{\frac{3}{2}}(y_{\text{eq}}) J_{\frac{3}{2}}(2 y_{\text{eq}})}{J_{-\frac{3}{2}}(2 y_{\text{eq}}) J_{\frac{5}{2}}(2 y_{\text{eq}}) + J_{\frac{3}{2}}(2 y_{\text{eq}}) J_{-\frac{5}{2}}(2 y_{\text{eq}})} \right] \right. \\ \left. + B_{k,\text{RD}} \left[ \frac{J_{-\frac{1}{2}}(y_{\text{eq}}) J_{\frac{5}{2}}(2 y_{\text{eq}}) + J_{-\frac{3}{2}}(y_{\text{eq}}) J_{\frac{3}{2}}(2 y_{\text{eq}})}{J_{-\frac{3}{2}}(2 y_{\text{eq}}) J_{\frac{5}{2}}(2 y_{\text{eq}}) + J_{\frac{3}{2}}(2 y_{\text{eq}}) J_{-\frac{5}{2}}(2 y_{\text{eq}})} \right] \right\}, \quad (3.31)$$

where  $y_{\text{eq}} = k/k_{\text{eq}}$  with  $k_{\text{eq}}$  being the comoving wavenumber that made its Hubble-entry at the time of matter-radiation equality.

### 3.1.2 Universe with multiple equations of state during reheating

As stressed before, since reheating is a complex phase involving non-linear processes, it is natural to represent it by multiple equation of state parameters, as illustrated in Fig. 2. We model reheating by multiple epochs of piece-wise constant EoS parameters with sharp (instantaneous) transitions in between. The procedure to obtain the coefficients appearing in the solution for the tensor mode functions is therefore the same as that given in Sec. 3.1.1, with some additional (minor) changes that one need to take into account when considering multiple equations of state parameters, as detailed below.

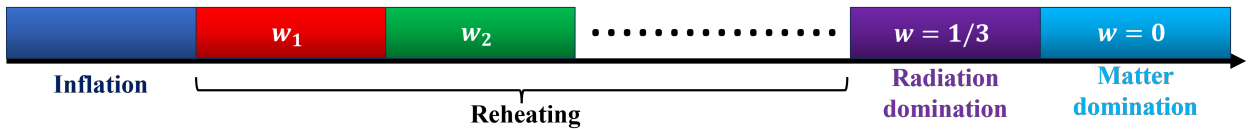


**Figure 2:** A schematic depiction of the timeline of the universe with a post-inflationary reheating phase consisting of multiple equations of state. Note, the horizontal length is not a representation of the actual duration.

The coefficients for the first epoch following the end of inflation are the same as that given in Eq. (3.25), for reheating with single EoS. The main difference comes while labelling them. For example, if the equation of state of the first epoch is  $w_1$ , then the coefficients of the mode functions are

$$A_{k,1} = 2^{(\alpha_1 - \frac{1}{2})} \Gamma(\alpha_1 + 1/2) h_{k,\text{inf}}^\lambda, \quad B_{k,1} = 0, \quad (3.32)$$

where  $\alpha_1 = 2/(1 + 3w_1)$ . Suppose, there are  $n$  epochs during reheating, each with a constant EoS ( $w_i$  being the EoS of the  $i^{\text{th}}$  epoch, with  $i \in \mathbb{Z}^+$ ). Then, the coefficients  $A_{k,i}$  and  $B_{k,i}$  corresponding to all subsequent epochs ( $i > 1$ ) during reheating need to be computed using Eqs. (3.20) and (3.21). For the sake of completeness, we provide closed-form expressions for the coefficients at the onset of radiation domination following the final transition ( $i = n$ ), which are different from the ones corresponding to a single transition as given in Eqs. (3.27) and (3.28), to be

$$A_{k,\text{RD}} = \frac{y_{\text{r}*}^{(1-\alpha_n)}}{\alpha_n^{(\alpha_n - \frac{1}{2})}} \left\{ A_{k,i} \left[ \frac{J_{(\alpha_n - \frac{1}{2})}(\alpha_n y_{\text{r}*}) J_{-\frac{3}{2}}(y_{\text{r}*}) + J_{(\alpha_n + \frac{1}{2})}(\alpha_n y_{\text{r}*}) J_{-\frac{1}{2}}(y_{\text{r}*})}{J_{-\frac{1}{2}}(y_{\text{r}*}) J_{\frac{3}{2}}(y_{\text{r}*}) + J_{\frac{1}{2}}(y_{\text{r}*}) J_{-\frac{3}{2}}(y_{\text{r}*})} \right] \right. \\ \left. + B_{k,i} \left[ \frac{J_{-(\alpha_n - \frac{1}{2})}(\alpha_n y_{\text{r}*}) J_{-\frac{3}{2}}(y_{\text{r}*}) - J_{-(\alpha_n + \frac{1}{2})}(\alpha_n y_{\text{r}*}) J_{-\frac{1}{2}}(y_{\text{r}*})}{J_{-\frac{1}{2}}(y_{\text{r}*}) J_{\frac{3}{2}}(y_{\text{r}*}) + J_{\frac{1}{2}}(y_{\text{r}*}) J_{-\frac{3}{2}}(y_{\text{r}*})} \right] \right\}, \quad (3.33)$$

$$B_{k, \text{RD}} = \frac{y_{\text{r}*}^{(1-\alpha_n)}}{\alpha_n^{(\alpha_n-\frac{1}{2})}} \left\{ A_{k,n} \left[ \frac{J_{(\alpha_n-\frac{1}{2})}(\alpha_n y_{\text{r}*}) J_{\frac{3}{2}}(y_{\text{r}*}) - J_{(\alpha_n+\frac{1}{2})}(\alpha_n y_{\text{r}*}) J_{\frac{1}{2}}(y_{\text{r}*})}{J_{-\frac{1}{2}}(y_{\text{r}*}) J_{\frac{3}{2}}(y_{\text{r}*}) + J_{\frac{1}{2}}(y_{\text{r}*}) J_{-\frac{3}{2}}(y_{\text{r}*})} \right] \right. \\ \left. + B_{k,n} \left[ \frac{J_{-(\alpha_n-\frac{1}{2})}(\alpha_n y_{\text{r}*}) J_{\frac{3}{2}}(y_{\text{r}*}) + J_{-(\alpha_n+\frac{1}{2})}(\alpha_n y_{\text{r}*}) J_{\frac{1}{2}}(y_{\text{r}*})}{J_{-\frac{1}{2}}(y_{\text{r}*}) J_{\frac{3}{2}}(y_{\text{r}*}) + J_{\frac{1}{2}}(y_{\text{r}*}) J_{-\frac{3}{2}}(y_{\text{r}*})} \right] \right\}, \quad (3.34)$$

where  $\alpha_n = 2/(1 + 3w_n)$ . While, the analytical expression for  $A_{k, \text{MD}}$  and  $B_{k, \text{MD}}$  remains the same as in Eqs. (3.30) and (3.31).

### 3.2 Spectral energy density of gravitational waves

A cosmological background of stochastic gravitational waves at a given time is characterized in terms of the spectral energy density of GWs, defined as the energy density of GWs per unit logarithmic wavenumber interval relative to the critical energy density of the universe,  $\rho_c(\tau) = 3m_p^2 H^2(\tau)$  at that epoch [145, 146], *i.e.*,

$$\Omega_{\text{GW}}(\tau, k) = \frac{1}{\rho_c} \frac{d\rho_{\text{GW}}}{d \ln k}. \quad (3.35)$$

The energy density of GWs obtained from the time-time component of the energy-momentum tensor  $T^\mu_\nu$  of tensor fluctuations in the FLRW background (see App. C) is

$$\hat{\rho}_{\text{GW}}(\tau, \vec{x}) = -\hat{T}^0_0(\tau, \vec{x}) = \frac{m_p^2}{8a^2(\tau)} \left[ (\hat{h}'_{ij}(\tau, \vec{x}))^2 + (\vec{\nabla} \hat{h}_{ij}(\tau, \vec{x}))^2 \right]. \quad (3.36)$$

The vacuum expectation value of  $\rho_{\text{GW}}$  (with summation over the two polarisation states) is given by

$$\rho_{\text{GW}}(\tau) = \langle 0 | \hat{\rho}_{\text{GW}}(\tau, \vec{x}) | 0 \rangle = \frac{m_p^2}{8a^2(\tau)} \int d \ln k \frac{k^3}{\pi^2} \left[ |h'_k{}^\lambda(\tau)|^2 + k^2 |h_k{}^\lambda(\tau)|^2 \right], \quad (3.37)$$

where we used the following Fourier representation of the tensor operator  $\hat{h}_{ij}$

$$\hat{h}_{ij}(\tau, \vec{x}) = \sum_{\lambda=+, \times} \int \frac{d^3 \vec{k}}{(2\pi)^3} \epsilon_{ij}^\lambda \left[ h_k{}^\lambda(\tau) \hat{a}_{\vec{k}} e^{i\vec{k}\cdot\vec{x}} + \left( h_k{}^\lambda(\tau) \right)^* \hat{a}_{\vec{k}}^\dagger e^{-i\vec{k}\cdot\vec{x}} \right], \quad (3.38)$$

and the vacuum state is defined by  $\hat{a}_{\vec{k}} |0\rangle = 0$ . Using Eq. (3.37), expression for the GW spectral energy density becomes

$$\Omega_{\text{GW}}(\tau, k) = \frac{k^2}{24 a^2(\tau) H^2(\tau)} \mathcal{P}_T(\tau, k) \left[ 1 + \frac{1}{k^2} \frac{|h'_k{}^\lambda(\tau)|^2}{|h_k{}^\lambda(\tau)|^2} \right]. \quad (3.39)$$

Considering modes that are deep in the Hubble radius so that the frequency of GWs is substantially larger than the expansion rate of the universe, *i.e.*,  $k \gg aH$ , the second term inside the square bracket becomes [147, 148]

$$\frac{1}{k^2} \frac{|h'_k{}^\lambda(\tau)|^2}{|h_k{}^\lambda(\tau)|^2} = 1 + \mathcal{O}\left(\frac{a^2 H^2}{k^2}\right) \simeq 1. \quad (3.40)$$

Therefore, in the sub-Hubble regime, expression for the GW spectral energy density becomes

$$\Omega_{\text{GW}}(\tau, k) = \frac{k^2}{12 a^2(\tau) H^2(\tau)} \mathcal{P}_T(\tau, k), \quad (3.41)$$

which coincides with the standard Isaacson approximation [149, 150]. We again emphasize that this approximation is valid as long as the wavelength of GWs are much shorter than the Hubble radius of the universe<sup>3</sup>.

In order to calculate the spectral energy density at the present epoch, we compute tensor mode functions deep inside the Hubble radius, in the limit  $y \gg 1$ , during the MD epoch by making use of the large argument expansion of Bessel function, namely,  $J_\nu(y) \approx \sqrt{2/(\pi y)} \cos(y - \nu\frac{\pi}{2} - \frac{\pi}{4})$ . Accordingly, Eq. (3.29) reduces to

$$h_{k,\text{MD}}^\lambda(y \gg 1) = -\frac{1}{(2y)^{\frac{3}{2}}} \frac{1}{\sqrt{\pi y}} [A_{k,\text{MD}} \cos(2y) + B_{k,\text{MD}} \sin(2y)] . \quad (3.42)$$

Consequently, the average of the modulus squared value of tensor amplitude becomes

$$\overline{|h_{k,\text{MD}}^\lambda(y \gg 1)|^2} = \frac{1}{(2y)^4} \frac{1}{\pi} [|A_{k,\text{MD}}|^2 + |B_{k,\text{MD}}|^2] . \quad (3.43)$$

Upon substituting  $y(\tau) = y_{\text{eq}} \frac{a_{\text{eq}} H_{\text{eq}}}{a(\tau) H(\tau)} = y_{\text{eq}} \left( \frac{a(\tau)}{a_{\text{eq}}} \right)^{1/2}$ , for  $\tau > \tau_{\text{eq}}$ , into the above expression, we can observe that the term  $\overline{|h_{k,\text{MD}}^\lambda(y \gg 1)|^2} \propto a^{-2}$ . In fact, this is true in general for any epoch, *i.e.*,  $\overline{|h_k^\lambda(y \gg 1)|^2} \propto a^{-2}$ . This implies that the tensor amplitude dampens as  $h_k^\lambda \propto a^{-1}$  due to the expansion of the universe, irrespective of the EoS [119]. At late times, as the universe begins to accelerate again, no new additional tensor modes become sub-Hubble in this epoch. Instead, a narrow range of long-wavelength tensor modes, that had freshly become sub-Hubble, begin to exit the Hubble radius during this accelerated epoch. We therefore consider these tensor modes inaccessible, and only focus on sub-Hubble modes deep inside the Hubble radius at the onset of the MD epoch. Substituting Eq. (3.43) and  $k = y_{\text{eq}} a_{\text{eq}} H_{\text{eq}}$  in Eq. (3.41) we obtain

$$\overline{\Omega_{\text{GW}}(\tau_0, k)} = \frac{1}{96\pi^3} \frac{g_{*,\text{r}*}}{g_{*,0}} \left( \frac{g_{s,0}}{g_{s,\text{r}*}} \right)^{4/3} \Omega_{\text{rad},0} \frac{1}{y_{\text{eq}}^2} [\tilde{A}_{k,\text{MD}}^2 + \tilde{B}_{k,\text{MD}}^2] \frac{H_{\text{inf}}^2}{m_{\text{p}}^2} \left( \frac{k}{k_*} \right)^{n_T} , \quad (3.44)$$

where  $g_*$ ,  $g_s$  are the effective number of relativistic degrees of freedom of the universe in energy density, entropy density respectively, with the second subscript in  $g_*$  and  $g_s$  denoting the time of estimation of its value (with ‘0’ denoting the present epoch).  $H_{\text{inf}}$  corresponds to the Hubble parameter at the Hubble-exit of the CMB pivot scale during inflation, *i.e.*,  $H_{\text{inf}} = H_*$ . Note that in Eq. (3.44), the coefficients  $\tilde{A}_{k,\text{MD}}$  and  $\tilde{B}_{k,\text{MD}}$  differ from  $A_{k,\text{MD}}$  and  $B_{k,\text{MD}}$  in Eq. (3.29) by the factor  $h_{k,\text{inf}}^\lambda$  as discussed in App. D.

From detection perspective, it is important to characterize the GW spectral energy density in terms of the present-day (physical, as opposed to comoving) frequency of GWs [64, 77, 117, 119, 147]. The present-day frequency  $f_k$  of a mode of comoving wavenumber  $k$  is given by

$$f_k = \frac{k}{2\pi a_0} = \frac{1}{2\pi} \frac{a_k}{a_0} H_k , \quad (3.45)$$

where  $a_k$  and  $H_k$  are the scale factor and Hubble parameter at the time when the mode with comoving wavenumber  $k$  made its Hubble-entry.

In order for us to mark the beginning and the end of each post-inflationary epoch in our computation, we relate the present-day frequency of a mode to the temperature at the time of its

<sup>3</sup>In the cosmological context, there are long wavelength tensor modes comparable to the Hubble scale that might be of observational relevance. Hence, in general, one needs to derive the energy-momentum tensor without invoking the frequently used approximation of high frequency GWs propagating in flat background [143, 146]. Nevertheless, in this work we will continue using Eq. (3.41) since we are primarily interested in high frequency GWs that are deep inside the comoving Hubble radius in the MD epoch.



Hubble-entry. In a radiation-dominated universe, the Hubble parameter can be expressed in terms of its temperature as

$$H^2(T) = \frac{\rho_{\text{rad}}(T)}{3 m_p^2} = \frac{1}{3 m_p^2} \frac{\pi^2}{30} g_{*,T} T^4. \quad (3.46)$$

From the conservation of entropy, we have

$$\left( \frac{g_{s,0}}{g_{s,T}} \right)^{1/3} \frac{T_0}{T} = \frac{a(T)}{a_0}. \quad (3.47)$$

By incorporating Eqs. (3.46) and (3.47) to Eq. (3.45), one can relate the temperature  $T_k$  of the universe (in GeV) at the Hubble-entry of a mode to its present-day frequency  $f_k$  (in Hz) as [34]

$$\frac{f_k}{\text{Hz}} = 7.43 \times 10^{-8} \left( \frac{g_{s,0}}{g_{s,T_k}} \right)^{1/3} \left( \frac{g_{*,T_k}}{90} \right)^{1/2} \left( \frac{T_k}{\text{GeV}} \right). \quad (3.48)$$

Note that the above expression is valid for a radiation-dominated universe in thermal equilibrium. With reheating being primarily a non-thermal process, achieving thermal equilibrium only at the end of it, Eq. (3.48) cannot be used during reheating. However, we shall be using Eq. (3.48) to relate the energy scale of the universe during reheating to the physical frequency of GWs; where  $T_k$  is treated as an *effective temperature* (related to  $f_k$  via Eq. (3.48), which serves as a proxy for the energy-scale at the Hubble-entry time of the mode. In fact, to be precise, we can define the corresponding energy scale of the universe to be

$$E_k = \rho_c^{1/4}(T_k) = \left( \frac{\pi^2}{30} g_{*,T_k} \right)^{1/4} T_k. \quad (3.49)$$

Therefore, the present-day frequency of a mode making its Hubble-entry at an energy scale  $E_k$  is given by

$$\frac{f_k}{\text{Hz}} = 1.03 \times 10^{-8} \left( \frac{g_{s,0}}{g_{s,T_k}} \right)^{1/3} g_{*,T_k}^{1/4} \left( \frac{E_k}{\text{GeV}} \right). \quad (3.50)$$

Table 1 lists the present-day frequency of GWs generated at the Hubble-entry of some of the important cosmological events (and their corresponding energy scales).

While computing the spectral energy density of GWs, in order to be concrete we have fixed the energy scale during inflation to be  $E_{\text{inf}} = 5.76 \times 10^{15}$  GeV corresponding to the tensor-to-scalar ratio  $r = 0.001$ , which is a target of next generation CMB experiments. Similarly, in order to be consistent with the BBN predictions for the abundance of light nuclei, reheating must end before the onset of BBN, *i.e.*,  $T_{r^*} \gg T_{\text{BBN}} \sim 1$  MeV. Therefore, we fix the energy scale of the universe at the end of reheating to be  $E_{r^*} = 1$  GeV ( $T_{r^*} \simeq 0.45$  GeV), which is safely above the BBN bound. Note that for a given reheating history, by decreasing the tensor-to-scalar ratio, the probability of detection of GWs will become lower. Therefore, our analysis in this work must be treated as a best case scenario for the detection. By fixing the reheating temperature, we primarily focus on illustrating how to probe the duration and EoS of successive epochs during reheating.

By replacing the comoving wavenumber  $k$  with the present-day frequency  $f_k$ , and denoting the oscillation-averaged spectral energy density as  $\Omega_{\text{GW}}^{(0)}(f)$  instead of  $\Omega_{\text{GW}}^{(0)}(k)$ , we obtain

$$h^2 \Omega_{\text{GW}}^{(0)}(f_k) = \frac{1}{96\pi^3} \frac{g_{*,r^*}}{g_{*,0}} \left( \frac{g_{s,0}}{g_{s,r^*}} \right)^{4/3} h^2 \Omega_{\text{rad},0} \left( \frac{f_{\text{eq}}}{f_k} \right)^2 \left[ \tilde{A}_{k,\text{MD}}^2 + \tilde{B}_{k,\text{MD}}^2 \right] \frac{H_{\text{inf}}^2}{m_p^2}, \quad (3.51)$$

where  $h$  is a dimensionless parameter, related to the Hubble parameter at the present epoch by  $H_0 = 100 h \text{ km s}^{-1} \text{ Mpc}^{-1}$ . Values of the relativistic degrees of freedom at our fixed reheating temperature

| Event                                | Energy scale ( $E_k$ ) | Present-day frequency $f_k$ (Hz) |
|--------------------------------------|------------------------|----------------------------------|
| Matter-radiation equality            | $\sim 1$ eV            | $1.4 \times 10^{-17}$            |
| Hubble-entry time of CMB pivot scale | $\sim 5$ eV            | $7.2 \times 10^{-17}$            |
| Onset of BBN                         | $\sim 1.4$ MeV         | $1.8 \times 10^{-11}$            |
| QCD Phase Transition                 | $\sim 320$ MeV         | $3.7 \times 10^{-9}$             |
| Electro-weak symmetry breaking       | $\sim 240$ GeV         | $2.7 \times 10^{-6}$             |

**Table 1:** Present-day frequencies of primordial GWs generated at different (Hubble-entry) energy scale corresponding to some of the important events in the thermal history of our universe.

are  $g_{*,r*} = g_{s,r*} = 73.0$ ,  $g_{s,0} = 3.94$ , and  $g_{*,0} = 3.38$ . The present-day density parameter of radiation is  $h^2\Omega_{\text{rad},0} = 4.16 \times 10^{-5}$  (see Eq. (E.7)). The spectral-tilt of relic GWs is defined as [58]

$$n_{\text{GW}} = \frac{d \ln \Omega_{\text{GW}}^{(0)}(f_k)}{d \ln f_k}, \quad (3.52)$$

which, for a range of frequencies corresponding to modes making their Hubble-entry at the beginning and end of a post-inflationary cosmic epoch with constant EoS  $w$ , reduces to<sup>4</sup> [34]

$$n_{\text{GW}} = 2 \left( \frac{w - 1/3}{w + 1/3} \right). \quad (3.53)$$

Fig. 3 shows the GW spectral energy density as a function of the present-day frequency of GWs for the case of a single constant EoS during reheating. During the MD epoch, the energy density of relic GWs redshifts faster than the background density, implying that  $\Omega_{\text{GW}}(f)$  exhibits a red-tilt, with slope  $n_{\text{GW}} \simeq -2$  as determined from Eq. (3.53). Similarly,  $\Omega_{\text{GW}}$  is (nearly) flat for the range of frequencies corresponding to modes that made their Hubble-entry in the RD epoch, since the GWs redshift at an equal rate in comparison to the background radiation. Finally, the spectrum of those modes that made their Hubble-entry during reheating can be either blue-tilted, or flat or red-tilted depending upon the EoS during reheating. For example, we see a red-tilt for a softer EoS  $w_{\text{re}} < 1/3$  (black dashed curve), and a blue-tilt for a stiff-matter phase  $w_{\text{re}} > 1/3$  (solid black curve); while for radiation like EoS  $w_{\text{re}} = 1/3$  (black dotted curve), the spectrum is flat, as expected. Therefore, we observe that if the post-inflationary reheating EoS is stiff-matter like, then the relic GWs have a greater likelihood of getting detected by the upcoming GW detectors [34, 119, 152, 153].

Keeping in mind that GW energy density contributes to the total energy density of the universe, the observations on the light nuclei abundance impose an upper bound on the GW energy density during BBN to be [61]

$$\rho_{\text{GW}}(T_{\text{BBN}}) \leq \Delta\rho_{\text{rad}}(T_{\text{BBN}}) = \frac{\pi^2}{30} \times \frac{7}{8} (2 \Delta N_\nu) T_{\text{BBN}}^4 = \frac{7}{8} \rho_\gamma(T_{\text{BBN}}) \Delta N_\nu, \quad (3.54)$$

where  $\Delta N_\nu$  is the extra neutrino (relativistic) degrees of freedom outside the Standard Model from the Standard Model value  $N_\nu = 3$ , and  $\rho_\gamma$  is the energy density of photons. Using entropy conservation from Eq. (3.47), we obtain the expression for the total energy density of primordial GWs that are sub-Hubble before the BBN to be

$$\frac{\rho_{\text{GW}}(T_{\text{BBN}})}{\rho_{\text{GW},0}} = \left( \frac{a_0}{a_{\text{BBN}}} \right)^4 = \left( \frac{g_{s,T_{\text{BBN}}}}{g_{s,0}} \right)^{4/3} \left( \frac{T_{\text{BBN}}}{T_0} \right)^4. \quad (3.55)$$

<sup>4</sup>Note that we have ignored contribution from the tiny red-tilt  $n_r \simeq -r/8$  of the inflationary tensor modes, since they are very small for  $r \leq 0.001$ , see Ref. [14].

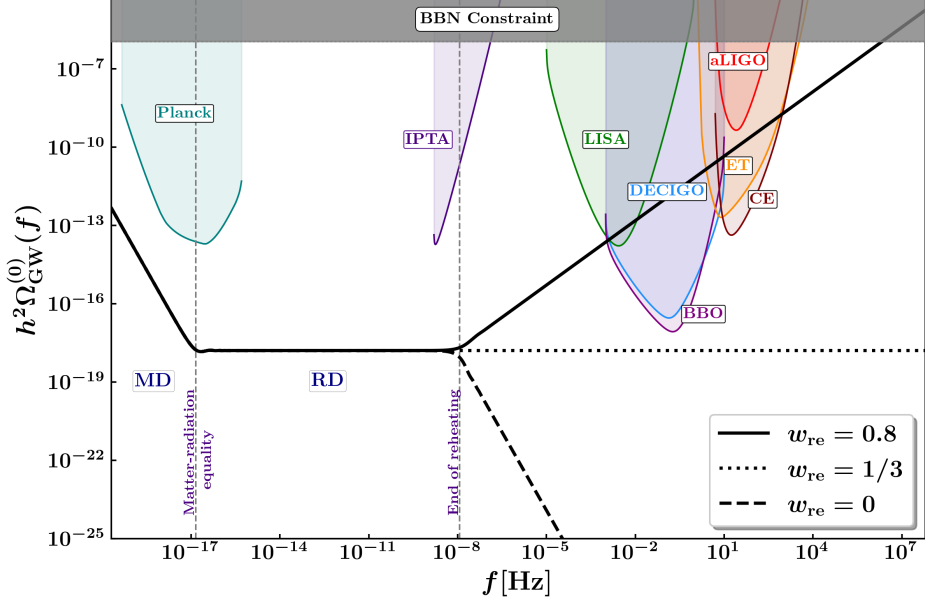


**Figure 3:** The spectral energy density of first-order inflationary GWs is shown as a function of the present-day GW frequencies for a single constant post-inflationary EoS during reheating; along with the sensitivity curves of various GW detectors [151], as well as the BBN constraint. The spectrum is shown for three different possibilities of reheating EoS above  $f \gtrsim 10^{-8}$  Hz, corresponding to a blue-tilted stiff matter phase with  $w_{\text{re}} = 0.8$  (solid black), radiative phase with  $w_{\text{re}} = 1/3$  (dotted black), and softer matter-like phase with  $w_{\text{re}} = 0$  (dashed black). The tensor-to-scalar ratio has been set to  $r = 0.001$  and the reheating energy scale is fixed at  $E_{\text{r}*} = 1$  GeV.

We can further modify Eq. (3.55) using the relation involving energy density of photons,  $\rho_\gamma(T) = (\pi^2/15)T^4$ ,

$$\frac{\rho_{\text{GW},0}}{\rho_{c,0}} = \frac{\rho_{\text{GW}}(T_{\text{BBN}})}{\rho_\gamma(T_{\text{BBN}})} \left( \frac{g_{s,0}}{g_{s,T_{\text{BBN}}}} \right)^{4/3} \Omega_{\gamma,0}. \quad (3.56)$$

Using Eqs. (3.35) and (3.54), we can rewrite Eq. (3.56) as

$$\begin{aligned} h^2 \int_{f_{\text{BBN}}}^{f_e} d \ln f \Omega_{\text{GW}}(\tau_0, f) &\leq \frac{7}{8} \Delta N_\nu \left( \frac{g_{s,0}}{g_{s,T_{\text{BBN}}}} \right)^{4/3} h^2 \Omega_{\gamma,0} \\ &= 5.64 \times 10^{-6} \Delta N_\nu < 1.13 \times 10^{-6}, \end{aligned} \quad (3.57)$$

where we have used the values  $h^2 \Omega_{\gamma,0} = 2.46 \times 10^{-5}$  (see Eq. (E.3)),  $g_{s,0} = 3.94$ ,  $g_{s,T_{\text{BBN}}} = 10.75$ . The upper bound,  $N_\nu < 3.2$ , is obtained with a 95% C.L. from combining the deuterium-to-hydrogen ratio along with CMB baryon density [154]. Eq. (3.57) is integrated from the frequencies of those modes that have entered the comoving Hubble radius at the onset of BBN ( $f_{\text{BBN}}$ ) to those at the end of inflation ( $f_e$ ). For single-epoch reheating dominated by stiff-matter, with EoS  $w_{\text{re}}$ , the aforementioned integral is dominated by the upper bound on  $\Omega_{\text{GW}}$  at  $f_e$  corresponding to the end of inflation. Hence, Ref. [119] used the following weaker constraint instead of Eq. (3.57) for numerical computation

$$h^2 \Omega_{\text{GW}}(\tau_0, f_e) < (1 - \alpha_{\text{re}}) 2.26 \times 10^{-6}, \quad (3.58)$$

where  $\alpha_{\text{re}} = 2/(1 + 3w_{\text{re}})$ . In the case of reheating with multiple epochs, we also use a similar constraint

$$h^2 \Omega_{\text{GW}}(\tau_0, f_e) < \begin{cases} (1 - \alpha_1) 2.26 \times 10^{-6}, & w_1 > \frac{1}{3}, \\ 2.24 \times 10^{-8}, & w_1 < \frac{1}{3}, \end{cases} \quad (3.59)$$

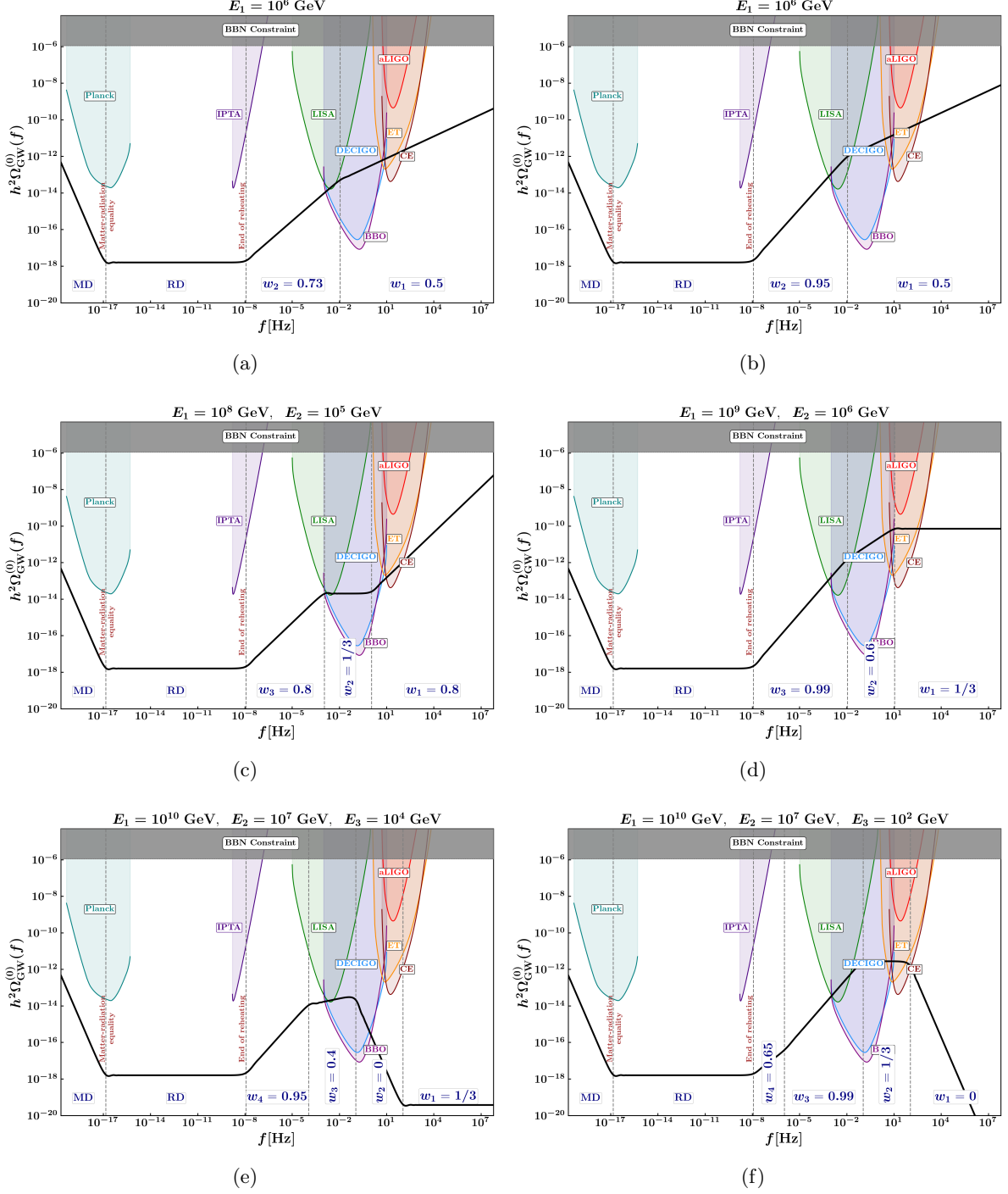


**Figure 4:** The spectral energy density ( $\Omega_{\text{GW}}$ ) of inflationary GWs associated with two (**top row**), three (**middle row**) and four (**bottom row**) epochs of piece-wise constant EoS parameters during reheating. Plots in the **left column** correspond to scenarios where  $\Omega_{\text{GW}}$  has a minimal overlap with the LISA sensitivity curve, while those in the **right column** belong to scenarios where  $\Omega_{\text{GW}}$  has a substantial overlap with LISA sensitivity region, without violating the existing BBN and aLIGO constraints. The energy scales  $E_i$  (with  $i \in \mathbb{Z}^+$ ) corresponding to the end of each epoch, are given in the top labels of each plot. The energy scales at the end of reheating and inflation are the same in all plots, namely,  $E_{\text{r}*} = 1$  GeV and  $E_{\text{inf}} = 5.76 \times 10^{15}$  GeV respectively, so as the tensor-to-scalar ratio,  $r = 0.001$ .

where  $\alpha_1 = 2/(1+3w_1)$  and  $w_1$  is the EoS parameter of the first epoch during reheating. Throughout this paper, we use Eq. (3.59) as the BBN constraint instead of Eq. (3.57) for numerical computation as the latter is computationally expensive. However, we emphasise that this particular choice leading to a weaker constraint may not be reliable for other values of  $r$  and  $E_{r*}$ , which results in an increased value of the maximum allowed area under the GW spectrum from  $f_{\text{BBN}}$  to  $f_e$ .

Fig. 4, displays the GW spectral energy density for the cases of reheating with two, three, and four epochs of piece-wise constant EoS parameters; with each epoch having a different EoS and duration. The figure helps to highlight post-inflationary scenarios where the predicted signals for the spectral energy density of GWs have, approximately, either a minimal overlap (left column) or maximal overlap (right column) with the LISA sensitivity curve, without violating the existing aLIGO and BBN constraints. Hence, it is important to analyse the possible combinations of EoS parameters and duration of these epochs resulting in signals that are detectable in the near future, not only by LISA, but also by other upcoming GW detectors.

The case of instantaneously sharp transitions, apart from being computationally simple, gives a reasonable insight into the detectable post-inflationary properties of the universe. However, we must stress that realistic sharp cosmological transitions are not expected to be instantaneous, but rather smooth [59]. Hence, our  $\Omega_{\text{GW}}$  curves are not fully accurate for frequencies right around the transitions.

#### 4 Inflationary gravitational waves as a probe of the primordial equation of state

In this section, we determine the subspace of equation of state parameters (and their corresponding duration) during reheating, comprising of two and three epochs of piece-wise constant EoS, which leads to a detectable signal for the inflationary GWs in the upcoming GW detectors<sup>5</sup> such as LISA, CE, ET, BBO, and DECIGO. As mentioned earlier, all of the following results are obtained assuming a tensor-to-scalar ratio  $r = 0.001$ , and for a fixed reheating energy scale  $E_{r*} = 1$  GeV. Note that even though the post-inflationary EoS can vary between  $-1/3 < w \leq 1$ , we restrict ourselves to  $-0.28 \leq w \leq 1$  due to computational limitations associated with the values of EoS closer to  $w = -1/3$ , which lead to divergences in our numerical computation. The aforementioned GW detectors can be classified into three groups based on their optimal frequency range of operation (see Fig. 5):  $10^{-4} - 10^{-1}$  Hz for LISA,  $10^{-3} - 10$  Hz for BBO and DECIGO, and  $1 - 10^3$  Hz for aLIGO, CE and ET [88, 157–161].

The EoS parameter space,  $\{w_1, w_2\}$ , for reheating with two epochs is shown in Fig. 6, with  $E_1$  being the energy scale of the universe at the transition between the two epochs. In order for the signal to possess a greater likelihood of detection with the upcoming GW detectors (without violating BBN and aLIGO bounds), a higher value of  $w_2$  is preferred, as evident from Fig. 6. However, having higher values of both  $w_1$  and  $w_2$  would violate the BBN constraint given in Eq. (3.59) as indicated by the grey shaded region. Similarly, the dark maroon-shaded region represents the subspace outside the BBN constraint that are ruled out by the null detection of stochastic GWs by aLIGO. From Fig. 6, we also notice that with an increase in the value of  $E_1$ , the range of values of  $w_2$  that leads to a detection in the future detectors actually decreases; while that of  $w_1$  becomes relatively unconstrained. This is because the physical frequency of GWs corresponding to the Hubble-entry at the end of the first epoch during reheating becomes higher than the frequency ranges of the aforementioned GW detectors. As a result, these GW detectors fails to put any constraint on  $w_1$ ; as evident from Figs. 6(c), 6(d) and 6(e). Similar things happen for each detector, albeit at different values of  $E_1$ . Specifically, the detectable values of  $w_2$  for LISA reaches its minimum around  $E_1 \geq 10^6$  GeV. For BBO and DECIGO, this happens around  $E_1 \geq 10^8$  GeV, while for CE and ET, operating at higher frequencies, the same takes place around  $E_1 \geq 10^{10}$  GeV.

<sup>5</sup>Important additional constraints come from the bound on CMB spectral distortions [155, 156] which are more relevant for relatively lower frequency GW signals in between the CMB and PTA sensitivity curves.

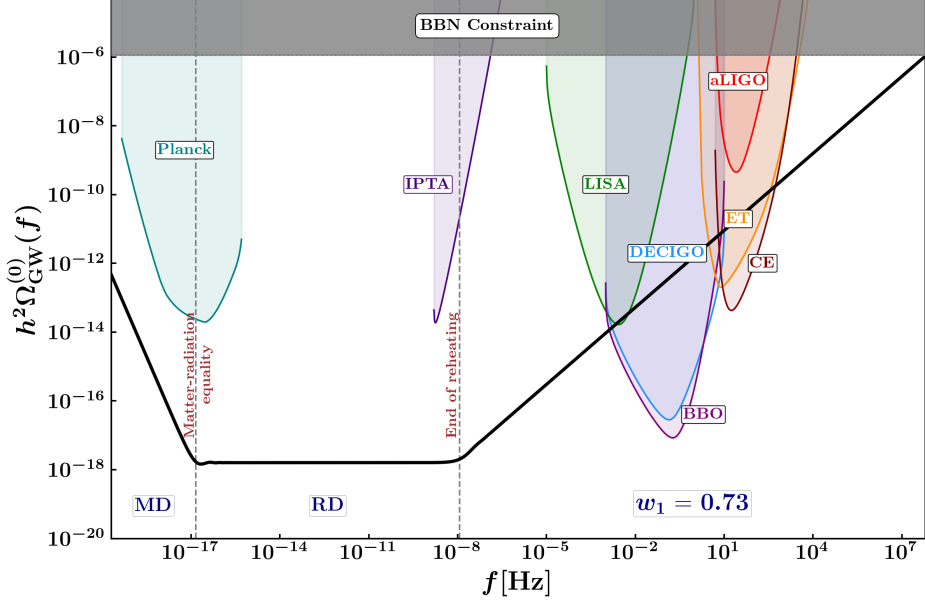


**Figure 5:** GW spectral energy density for single-epoch reheating with  $w_{re} = 0.73$ . In this scenario,  $\Omega_{\text{GW}}$  has a (near) minimal overlap with the LISA sensitivity curve. The spectrum is plotted for  $r = 0.001$  and  $E_{r^*} = 1$  GeV.

Furthermore, we can also constrain the duration of each epoch, in terms of the number of  $e$ -folds  $N$ , corresponding to an EoS ( $w$ ), given the energy scales at the beginning ( $E_i$ ) and end ( $E_f$ ) of that epoch. Since the energy density scales as  $\rho \simeq E^4 \propto a^{-3(1+w)}$ , the relation between  $N$  and  $w$  is given by

$$N = \ln\left(\frac{a_f}{a_i}\right) = \frac{4}{3(1+w)} \ln\left(\frac{E_i}{E_f}\right). \quad (4.1)$$

Accordingly, we have also provided the corresponding number of  $e$ -folds in the plots appearing in Fig. 6 for each value of  $w$ .

Following the above procedure, one can obtain the parameter space for a three-epoch reheating phase with the EoS parameters  $\{w_1, w_2, w_3\}$ . In order to clearly describe the constraints on such a 3-dimensional parameter space, we have considered illustrating the results by using the 2-dimensional projections of the full plots. The projected two-dimensional plots for different values of  $E_1$  and  $E_2$  (energy scales of the universe at the end of the first and the second epochs, respectively) are shown in Figs. 7, 8 and 9.

A careful reader must take caution in interpreting these plots since they are projections. In fact, the subspace of  $\{w_1, w_2, w_3\}$  that leads to a potentially detectable GW signal in the future detectors, is actually smaller than that shown in these projected plots. Specifically, the interpretation of whether a point in the projected space will lead to a potential detection is quite murky towards the edges of the shaded regions. Keeping this in mind, we shall briefly discuss a general prescription that the reader may follow while interpreting these plots, where we use a *tuple*  $(w_1, w_2, w_3)$  to represent a point in the EoS parameter space  $\{w_1, w_2, w_3\}$ . The prescription may seem complicated at first, but with practice, it becomes much easier to interpret the 2-dimensional plots correctly.

**Step-1:** Start by selecting a GW detector that is of interest to the reader, amongst LISA, BBO, CE, ET and DECIGO.

**Step-2:** Pick a value for  $w_1$  (denoting it as  $w_1^*$ ) within the shaded region (of interest) in the left column of Figs. 7, or 8 or 9 for that detector. For this choice ( $w_1^*$ ), find the range of  $w_2$  and  $w_3$  from the left and the middle columns, respectively, which leads to a detectable signal.

**Step-3:** Succeeding this step, choose a value for  $w_2$  (denoting it as  $w_2^*$ ) from the aforementioned range of  $w_2$ . For that particular choice ( $w_2^*$ ), determine the range of detectable values of  $w_3$  from the right columns.

**Step-4:** Next, obtain the intersection from aforementioned ranges of values of  $w_3$ , as obtained from the second and the third steps. We denote this resultant range as  $W_3$ , which may lead to a detectable GW signal. However, one has to be careful as we are dealing with projected 2-dimensional constraints of the fully three-dimensional parameter space. Thus, not all values in  $W_3$  will guarantee a detection. To confirm whether any chosen ( $w_1^*, w_2^*, w_3^*$ ), with  $w_3^* \in W_3$ , results in a detection, we have to check if  $w_3^* > w_3^{\min}$ , where  $w_3^{\min} \in W_3$  is the minimum value that leads to a detectable signal.

In general, it is difficult to find  $w_3^{\min}$  for a given  $w_1^*$  and  $w_2^*$  from the projected plots. However, if the lower boundary of the sensitivity curve of the detector near  $w_1^*$  is (nearly) flat in the left column plots, then  $w_3^{\min}$  will approximately be equal to the lower bound of  $W_3$ .

**Step-5:** If the projection of a given point ( $w_1^*, w_2^*, w_3^*$ ) is outside BBN and aLIGO constraint curves in any of the three columns, then we can conclude that the combination ( $w_1^*, w_2^*, w_3^*$ ) satisfies the BBN and aLIGO constraints. On the other hand, it is difficult, in general, to conclusively infer whether a point violates the BBN or aLIGO constraints or not.

In the following, we will demonstrate how to utilize the aforementioned prescription with a number of key examples.

**Example 1:** Consider the case with  $E_1 = 10^6$  GeV and  $E_2 = 10^3$  GeV which is shown in Fig. 7(a). Suppose we are interested in determining whether a given combination of the three EoS parameters results in a detectable signal in the LISA detector (purple-shaded region) (following *step-1*). The range of  $w_1$  that leads to a potential detection is  $[-0.28, 0.74]$ . Fixing  $w_1^* = 0.4$  in the left and middle columns, we obtain the range of  $w_2$  which likely to give detection to be  $[0.54, 1]$ , and that of  $w_3$  to be  $[0.56, 1]$  (following *step-2*). Note that this does not imply any combination ( $0.4, w_2^*, w_3^*$ ) with  $w_2^*$  and  $w_3^*$  within the aforementioned ranges will result in a potential detection, as stressed before. Choosing  $w_2^* = 0.6 \in [0.54, 1]$ , we observe that the allowed range of  $w_3$  to be  $[0.84, 1]$  from the right column in Fig. 7(a) (following *step-3*), with this range being independent of  $w_1^*$ . After taking the intersection of the two aforementioned ranges of  $w_3$ , we obtain  $W_3 = [0.84, 1]$ . In the left column, we observe that the lower boundary near  $w_1^* = 0.4$  is quite flat for LISA. Hence, the value  $w_3^{\min}$  will be approximately equal to the lower bound of  $W_3$ , *i.e.*,  $w_3^{\min} \simeq 0.84$  (following *step-4*). We can, therefore, be almost certain that the combination, ( $0.4, 0.6, w_3^*$ ) for  $w_3^* \in [0.84, 1]$  will result in a GW signal that will be detectable by LISA.

Finally, we carry out the last check regarding whether any point ( $0.4, 0.6, w_3^*$ ) for  $w_3^* \in [0.84, 1]$  violates the BBN and aLIGO constraints. From the left column, we find that  $w_1 = 0.4$  lies outside the BBN-constrained region. Therefore, for  $w_1 = 0.4$ , all values of  $w_2 \in [0.54, 1]$  and  $w_3 \in [0.56, 1]$  satisfy the BBN constraint (following *step-5*). Similarly, we find that there is no region ruled out by the aLIGO constraints in Fig. 7(a). Hence, the aforementioned collection of EoS parameters leads to a potentially detectable GW signal in the LISA detector, without violating the existing constraints.

**Example 2:** Consider the case of  $E_1 = 10^8$  GeV and  $E_2 = 10^5$  GeV shown in Fig. 8(c). This time, let us look for a detectable signal in the CE detector (red-shaded region) (following *step-1*). The detectable range for  $w_1$  from the left column is  $[-0.05, 1]$ . Fixing  $w_1^* = 0$ , we obtain  $w_2 \in [0.66, 1]$  and  $w_3 \in [0.76, 1]$  from the left and the middle columns, respectively (following *step-2*).

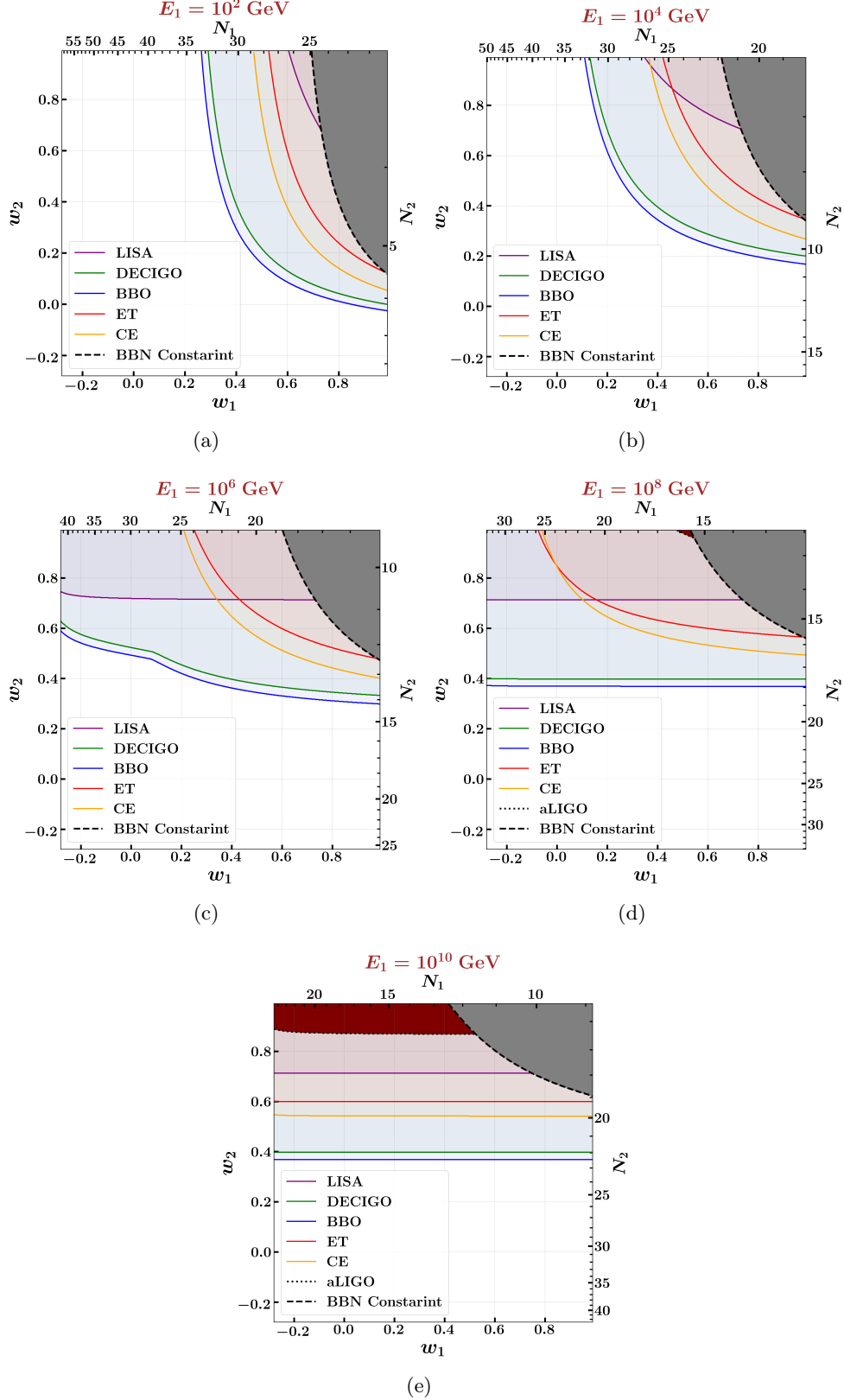


**Figure 6:** The parameter space for two-epoch reheating phase with EoS parameters  $w_1$  and  $w_2$  that leads to a potentially detectable GW signal in the LISA, BBO, DECIGO, CE, ET, and aLIGO detectors. The grey-shaded region in each plot corresponds to the combination of  $w_1$  and  $w_2$  that violate the BBN constraint (as provided in Eq. (3.59)), while the maroon-shaded region represents those that are ruled out by the aLIGO null detection. Energy scale of the universe at the end of the first post-inflationary epoch is labelled above in each plot. Note that, the duration of each epoch (number of  $e$ -folds) has been provided opposite to the corresponding EoS axis.



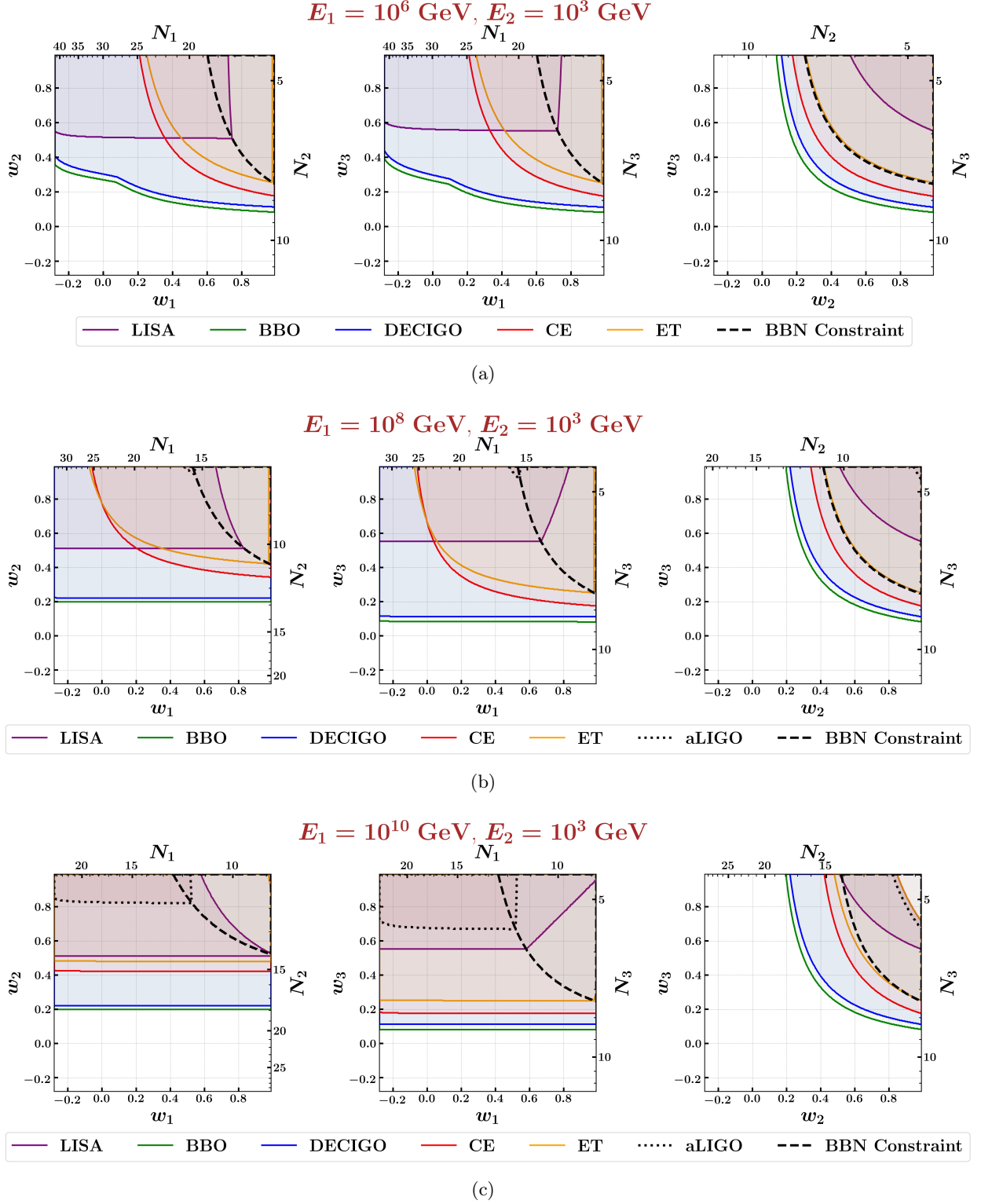


**Figure 7:** The parameter space for three-epoch reheating phase with EoS parameters  $w_1$ ,  $w_2$  and  $w_3$  that leads to a potentially detectable GW signal in the LISA, BBO, DECIGO, CE, ET, and aLIGO detectors. The plots are obtained by taking 2-dimensional projections of the full 3-dimensional subspace of EoS parameters. Energy scales at which the first and second post-inflationary epochs end are given as  $E_1$  and  $E_2$ . The duration of each epoch (number of  $e$ -folds) has been provided opposite to the corresponding EoS axis. The projections of the BBN-constrained and aLIGO-constrained regions are enclosed by the dashed and dotted black lines respectively.

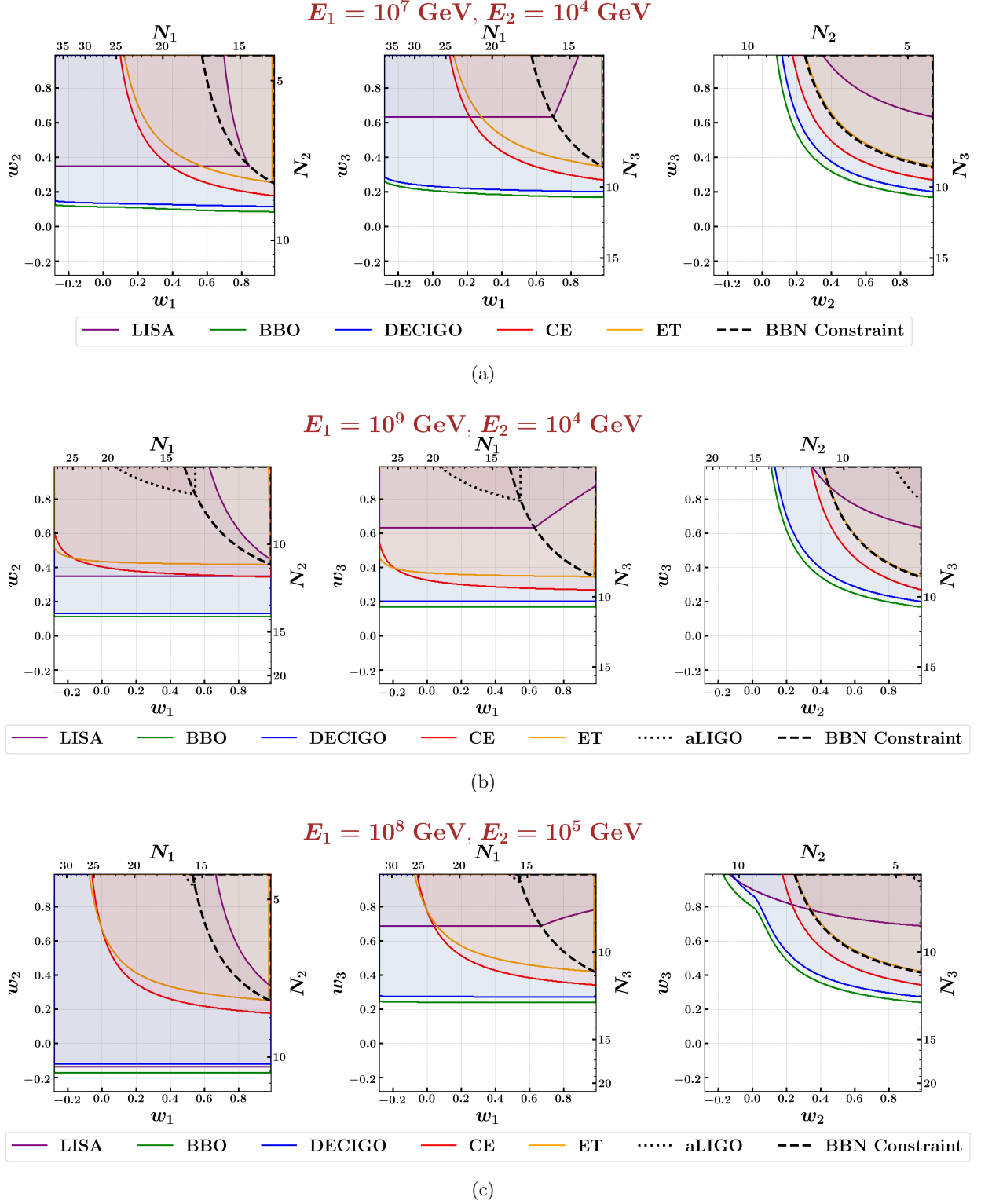


**Figure 8:** The parameter space for three-epoch reheating phase with EoS parameters  $w_1$ ,  $w_2$  and  $w_3$  that leads to a potentially detectable GW signal in the LISA, BBO, DECIGO, CE, ET, and aLIGO detectors. The plots are obtained by taking 2-dimensional projections of the full 3-dimensional subspace of EoS parameters. Energy scales at which the first and second post-inflationary epochs end are given as  $E_1$  and  $E_2$ . The duration of each epoch (number of  $e$ -folds) has been provided opposite to the corresponding EoS axis. The projections of the BBN-constrained and aLIGO-constrained regions are enclosed by the dashed and dotted black lines respectively.

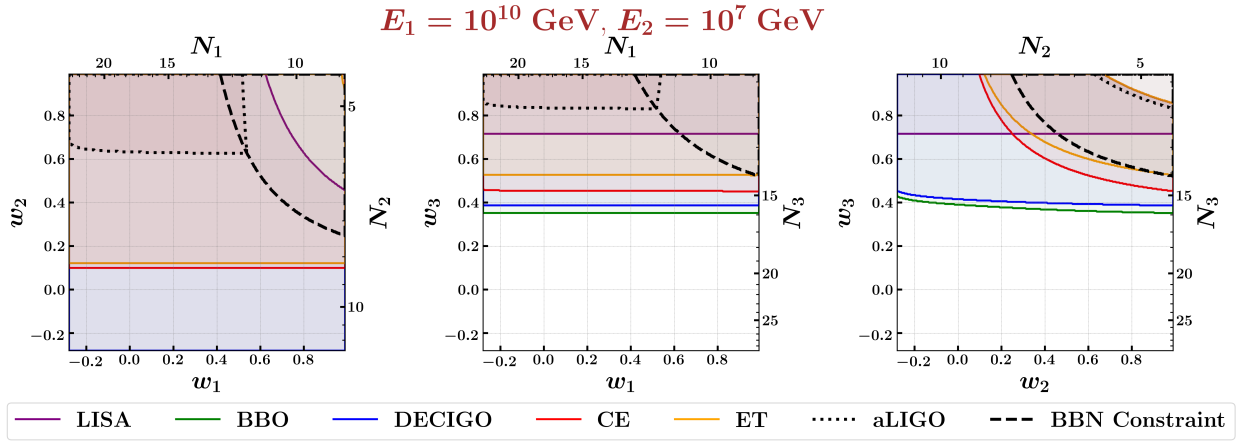
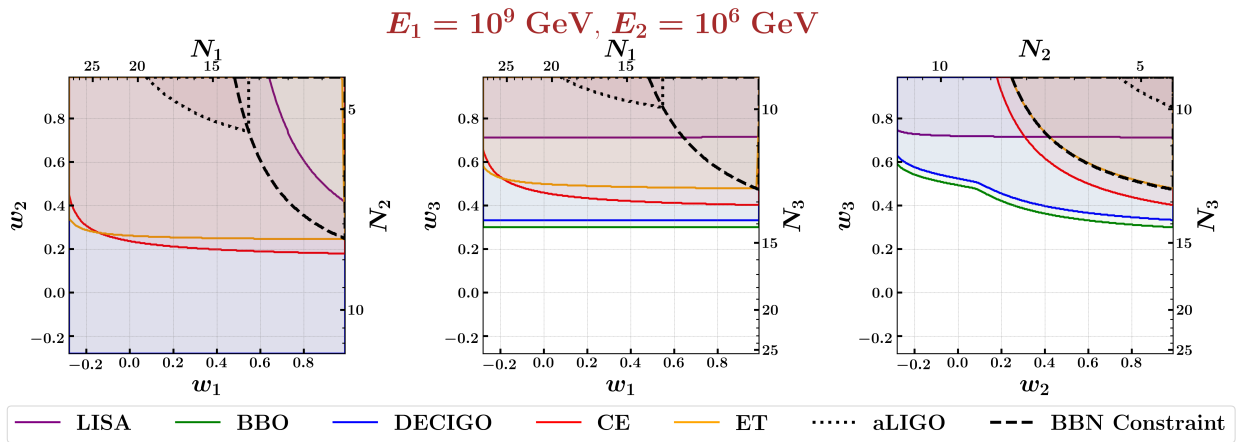
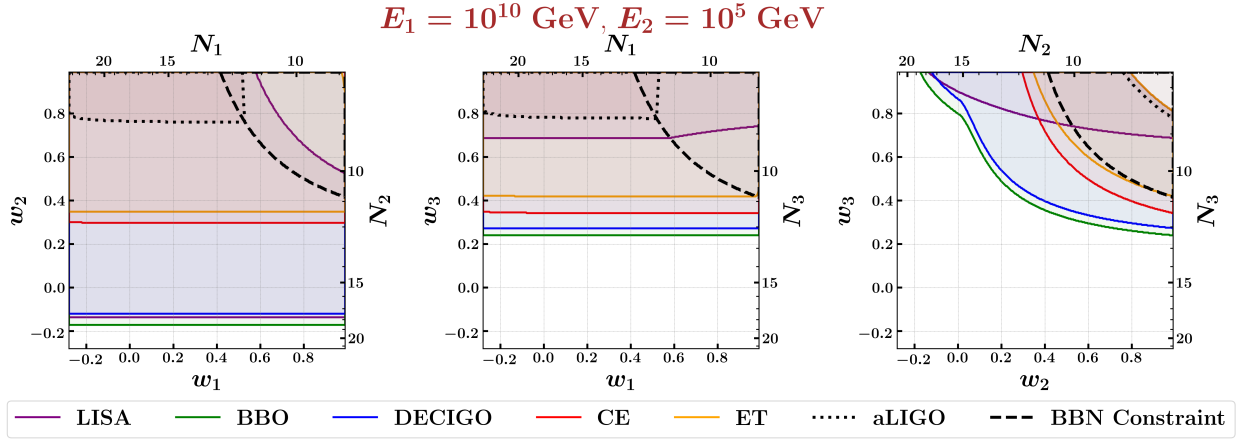


**Figure 9:** The parameter space for three-epoch reheating phase with EoS parameters  $w_1$ ,  $w_2$  and  $w_3$  that leads to a potentially detectable GW signal in the LISA, BBO, DECIGO, CE, ET, and aLIGO detectors. The plots are obtained by taking 2-dimensional projections of the full 3-dimensional subspace of EoS parameters. Energy scales at which the first and second post-inflationary epochs end are given as  $E_1$  and  $E_2$ . The duration of each epoch (number of  $e$ -folds) has been provided opposite to the corresponding EoS axis. The projections of the BBN-constrained and aLIGO-constrained regions are enclosed by the dashed and dotted black lines respectively.

Choosing  $w_2^* = 0.7 \in [0.66, 1]$  leads to  $w_3 \in [0.4, 1]$  from the right column plot (following *step-3*). Taking the intersection of the aforementioned two ranges of  $w_3$  results in  $W_3 = [0.76, 1]$ . In the left column, the lower boundary of the parameter space for CE around  $w_1^* = 0$  is curved in this case. Hence, we cannot be fully certain about  $w_3^{\min}$  (following *step-4*). For example, we find that the point  $(0, 0.7, 0.8)$  which *appears to lie inside the projected CE region* will actually not be detectable by CE.

**Example 3:** Let us now consider  $E_1 = 10^7$  GeV and  $E_2 = 10^4$  GeV, as shown in Fig. 8(a). Focusing on detection with the ET detector (orange-shaded region) (following *step-1*), the range for  $w_1$  is  $[0.12, 0.97]$ . Note that there is a short interval  $w_1 \in [0.97, 1]$ , which does not result in a detection with ET for any values of  $w_2$  and  $w_3$ . This is due to the fact that for  $w_1 \in [0.97, 1]$  (independent of the values of  $w_2$  and  $w_3$ ), either the GW signal is not large enough to be detected by ET or it violates the BBN constraint.

Let us fix  $w_1^* = 0.8 \in [0.12, 0.97]$ , leading to  $w_2 \in [0.28, 1]$  (from the left column plot) and  $w_3 \in [0.37, 1]$  (from the middle column plot) (following *step-2*). Choosing  $w_2^* = 0.6 \in [0.28, 1]$ , the range of  $w_3$  (from the right column plot) is found to be  $[0.48, 1]$  (following *step-3*). The intersection of these two ranges of  $w_3$  results in  $W_3 = [0.48, 1]$ . From the left column plot in Fig. 8(a), we observe that lower boundary of ET region near  $w_1^* = 0.8$  is again not flat. Hence, we can only conclude that for  $w_1^* = 0.8$  and  $w_2^* = 0.6$ , and not-all-values of  $w_3 \in [0.48, 1]$  will result in a detection in ET (following *step-4*).

For example, as per *step-5*, the point  $(0.8, 0.6, 0.8)$  appears to fall inside the region which is ruled out by the BBN constraint in all of three subplots shown in Fig. 8(a). But we restrict ourselves from conclusively concluding whether this combination of EoS parameters actually satisfies the BBN constraint or not, since these are just 2-dimensional projections of the full three-dimensional parameter space.

Since interpreting conclusively from the projected plots for three-epoch reheating phase is quite difficult, and at times ambiguous, we provide a link to the GitHub repository [🔗](#) which contains a Python code to directly plot the spectral energy density of first-order GWs. The reader can use this as a tool to conclusively determine whether a particular combination of EoS parameters would result in a potentially detectable GW signal (which is consistent with BBN and aLIGO constraints) for multiple transitions during reheating.

As mentioned in the case of two-epoch reheating, higher values of  $E_1$  implies a shorter duration of the first epoch during reheating following the end of inflation. As a result, the aforementioned GW detectors will be able to impose weaker constraints on  $w_1$  for large values of  $E_1$ , as evident from Fig. 9. This is because if the first post-inflationary epoch is short, then the detectability essentially relies on the subsequent epochs, specifically on the final epoch before BBN. Similarly, higher values of  $E_2$  widen the range of detectable values of  $w_2$  further, with the range of  $w_3$  being shortened (see Figs. 9(b) and 9(c)). To conclude, our results in this section indicate that higher values of  $w_2$  and  $w_3$  would result in detectable GW signal, as expected.

## 5 Post-inflationary evolution in a scenario inspired from String Theory

In our analysis of the spectral energy density of GWs in Sec. 4, we remained agnostic about the exact values of the post-inflationary EoS parameters and focused on determining the sub-space of the post-inflationary parameter space that results in a potentially detectable signal in the upcoming GW detectors, without violating the existing constraints. In this section, we focus on a particular post-inflationary scenario considered in a recent study [137], which is phenomenologically inspired from String Theory [162–166].

In type IIB String Theory within the large volume scenario (LVS) [165], a resultant *moduli field*  $\chi$  (which is an artifact of string compactification) may persist throughout the universe, potentially long enough until the onset of BBN. During inflation, the moduli field is sub-dominant and remains nearly frozen in its potential, while after the end of inflation, the volume modulus comes to dominate the universe and commences rolling swiftly down its steep exponential potential. The moduli field eventually reaches the minimum of its potential around which it oscillates and later decays, thereby reheating the universe to the hot Big Bang phase. Thus, the dynamics of the universe from the end of inflation until the onset of BBN is primarily dictated by the moduli field in this scenario [137].

The succeeding epoch after the end of inflation is therefore a *kination epoch*<sup>6</sup> during which the moduli exhibits a fast-roll phase, with  $\dot{\chi}^2 \gg V(\chi)$ , down a steep region of its potential of the form

$$V(\chi) \simeq V_0 e^{-\lambda \frac{\chi}{m_p}}, \quad (5.1)$$

where  $\lambda = \sqrt{27/2}$  and  $V_0 = m_p^4$  for LVS. The EoS during this kination epoch is  $w = \frac{\dot{\chi}^2 - 2V(\chi)}{\dot{\chi}^2 + 2V(\chi)} \simeq 1$ . While the universe, at this epoch, is also filled with a small fraction of radiative degrees of freedom that was generated from the decay of the inflaton at the end of inflation. Due to a sharp decline of the moduli energy density during kination, the universe enters into a radiation-dominated epoch, following the kination phase.

The moduli field, rolling down its steep potential in the radiation dominated epoch, then enters into a tracker regime [167–171], as illustrated in Fig. 10, where its energy density scales proportionally to the energy density of the background universe. Eventually, the field leaves the steep region of its potential and rolls down to its stable (quadratic) local minimum about which it begins to oscillate. The oscillating moduli field then dominates the energy budget of the universe again, leading to a matter-dominated universe. The oscillating field then decays, potentially non-perturbatively (hence efficiently), thereby reheating the universe to give rise to the hot Big Bang phase.

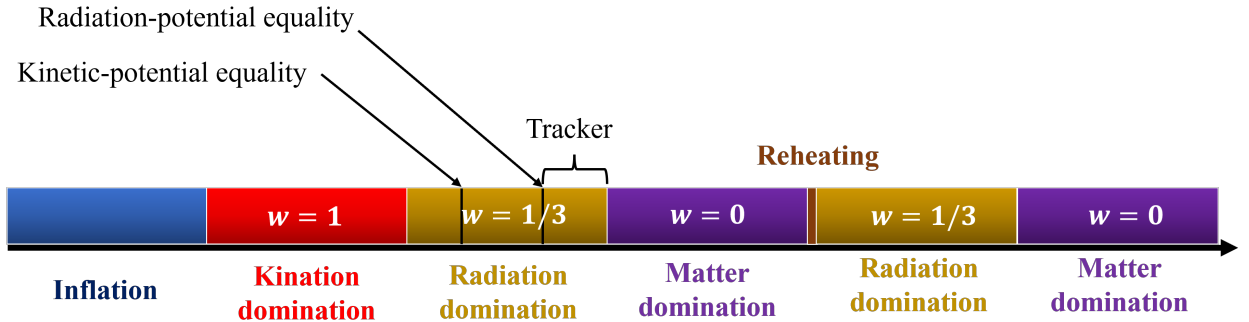


**Figure 10:** A schematic depiction of the chronology of post-inflationary epochs in the String-inspired model considered in Ref. [137], where the final epoch of reheating is assumed to be instantaneous. Note that the horizontal length is not an accurate representation of the duration of each epoch.

In short, the specific chronology of post-inflationary epochs in this scenario involves an early kination epoch ( $w \approx 1$ ) following the end of inflation, followed by a radiation-dominated epoch ( $w = 1/3$ ), and subsequently, a matter-dominated epoch ( $w = 0$ ), before reheating the universe prior to the commencement of the BBN. Note that this final epoch of reheating is assumed to be instantaneous. Fig. 11 depicts a typical plot of spectral energy density against the current frequency of GWs for this particular model.

Following the methodology as spelled out systematically in Sec. 4, we determine the parameter space of the energy scales at the end of each of the aforementioned epochs. To be consistent with our previous analyses, let us assume the energy scale at the end of inflation to be  $E_{\text{inf}} = 5.76 \times 10^{15}$  GeV,

<sup>6</sup>See Refs. [131, 132] for discussions on kination cosmology.

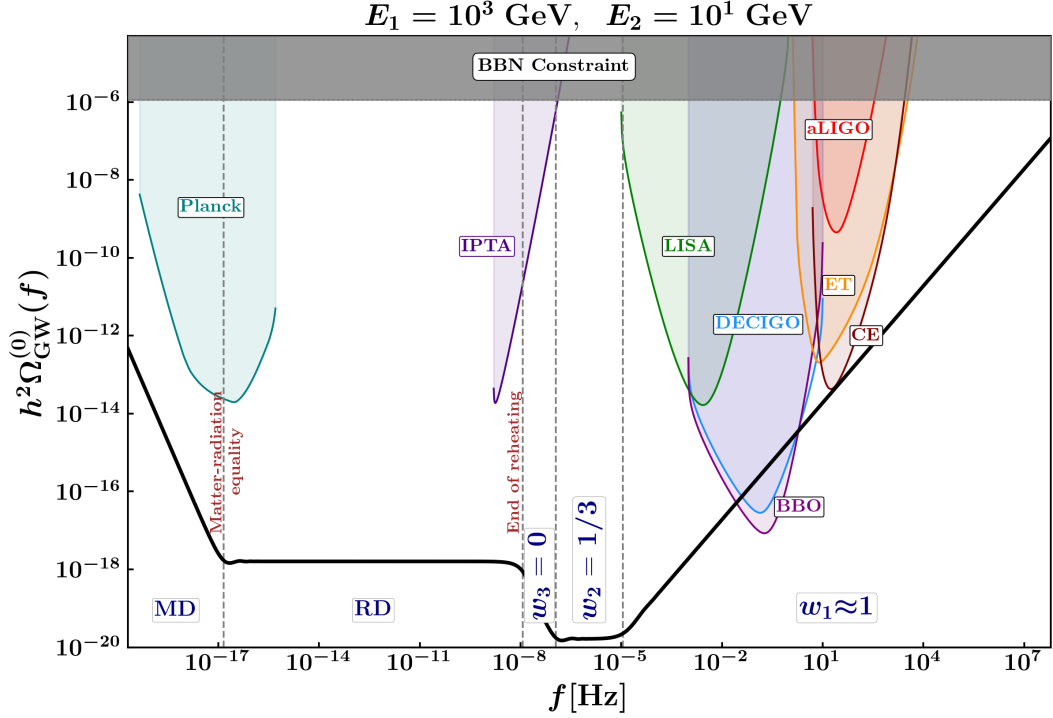


**Figure 11:** The spectral energy density ( $\Omega_{\text{GW}}$ ) of inflationary GWs for the String-inspired scenario as illustrated in Fig. 10, where we have an early kination epoch ( $w \simeq 1$ ) following the end of inflation, which was later followed by a radiation-dominated epoch ( $w = 1/3$ ) and subsequently by a matter-dominated epoch ( $w = 0$ ). The final epoch of reheating is assumed to be instantaneous at an energy scale  $E_{r^*} = 1 \text{ GeV}$ . The energy scales  $E_i$  (with  $i \in \mathbb{Z}^+$ ) corresponding to the end of each epoch, are given in the top label of the plot. The energy scale at the end of inflation is the same as in our previous plots, namely,  $E_{\text{inf}} = 5.76 \times 10^{15} \text{ GeV}$ , so as to have the tensor-to-scalar ratio  $r = 0.001$ .

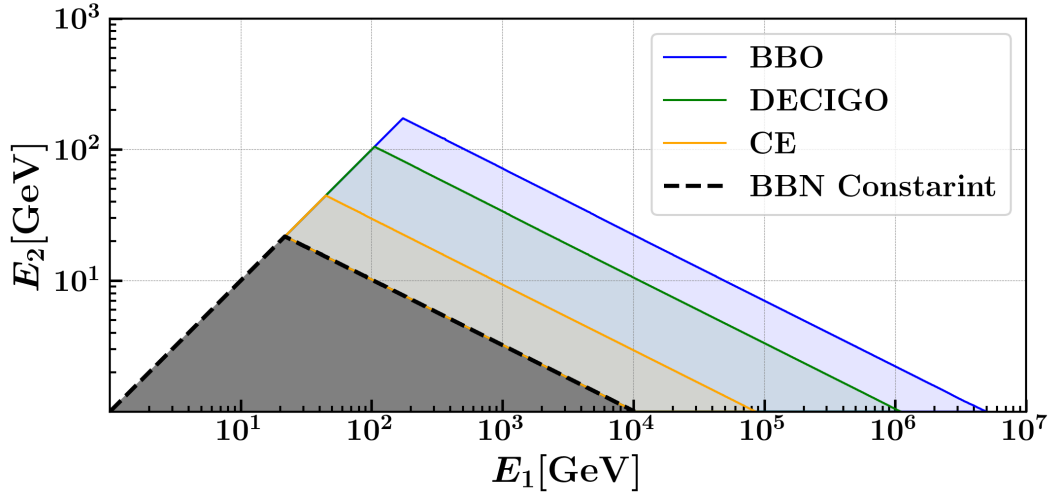


**Figure 12:** The parameter-space plot for the energy scale at the end of the kination epoch ( $E_1$ ), and that at the beginning of the early matter domination ( $E_2$ ), which leads to a detectable GW signal in the future detectors (assuming the final epoch of reheating to be instantaneous) for the case of a String-inspired scenario considered in Ref. [137] and illustrated in Fig. 10.

and that at the end of (the instantaneous period of) reheating to be  $E_{r^*} = 1$  GeV. Specifically, we determine the range of energy scale at the end of the kination epoch ( $E_1$ ) and that at the end of (the early) radiation domination epoch ( $E_2$ ), which results in detectable GW signals. The corresponding parameter-space plot is shown in Fig. 12.

From Fig. 12, we observe that this particular scenario results in a GW signal which will be detectable by BBO, DECIGO, and CE (for our choice of  $E_{\text{inf}}$  and  $E_{r^*}$ ) for a large range of  $E_1$  and  $E_2$ . However, the combination of  $E_1$  and  $E_2$ , that leads to a detectable signal in LISA and ET, actually violates the BBN constraint given in Eq. (3.59). Furthermore, the spectrum of only those tensor modes that entered the Hubble radius during the kination epoch are high enough to intersect the sensitivity curves of the detectors, since the kination epoch results in a highly blue-tilted GW spectrum. The plot also demonstrates that a detection of primordial GWs is possible in this scenario only if  $E_2 \lesssim \mathcal{O}(10^2)$  GeV, or equivalently, if the duration of the early matter-dominated epoch is roughly less than 7  $e$ -folds, *i.e.*,  $N_{\text{matter}} \lesssim 7$ .

## 6 Discussion and conclusions

One of the key predictions of the inflationary paradigm is the generation of tensor fluctuations which later constitute a stochastic background of gravitational waves (GWs) upon their Hubble-entry after the end of inflation [30]. These primordial GWs encode crucial information about the state of the universe, both at the time of their production, and the subsequent epochs through which they propagate before reaching the terrestrial and celestial detectors. Below the Planck scale, the GWs interact minimally with matter and energy, making them the most ideal candidate for probing the dynamics of the very early universe [30, 58–60, 62, 63]. Numerous studies have recently examined the feasibility of detecting these GWs using both the current and upcoming GW detectors [63, 64, 119, 147, 172–176].

In this paper, we focused on the possibility of probing the unknown post-inflationary history of the universe via primordial GWs. Since the dynamics of reheating involves a number of complex phases during which the universe transits from a highly non-thermal state at the end of inflation to the thermal hot Big Bang phase [93, 110, 177], it is important to describe reheating by a series of epochs with distinct EoS parameters [104, 130]. Hence, it is phenomenologically important to determine the possible post-inflationary scenarios that would result in a detectable stochastic GW signal in the upcoming GW detectors, without violating the existing constraints. Therefore, we have dedicated this paper in computing the spectral energy density of (first-order) inflationary GWs at the present epoch by considering the post-inflationary universe to feature multiple successive phases, each with a (nearly) constant EoS parameter. We determined the subspace of the EoS parameters of different epochs, as well as the corresponding duration of each epoch, during reheating that leads to a potentially detectable GW signal.

After a brief review of the inflationary dynamics, both at background and perturbation levels, in Sec. 2, we focused on studying the evolution of inflationary (first-order) tensor fluctuations in the post-inflationary universe in Sec. 3. We began by solving the evolution equation for the tensor mode functions, where we obtained the general solution for a given post-inflationary epoch described by a constant EoS parameter in terms of the Bessel functions. By assuming the transitions between successive epochs of constant EoS to be instantaneous, we obtained expressions for the unknown coefficients appearing in the general solutions for the tensor mode functions; be it for the epoch immediately following the end of inflation, as given by Eq. (3.32), or any other epoch succeeding that, as given by Eqs. (3.20) and (3.21). We computed the spectral energy density  $\Omega_{\text{GW}}(f)$  of GWs using Eq. (3.51), and checked whether their resulting spectrum will be detectable by the upcoming GW observatories, such as LISA, ET, CE, DECIGO and BBO; for a variety of reheating scenarios as demonstrated in Fig. 4. In the case of a reheating scenario consisting of two successive phases, the EoS parameter space which results in a detectable GW signal is plotted in Fig. 6. Similarly for

a three-epoch reheating phase, the projections of the three-dimensional EoS parameter space are shown in Figs. 7-9.

Our results primarily indicate that if inflationary GWs are detected by the aforementioned observatories in the near future, then it is highly likely that the temperature at the end of reheating was low enough, and that the universe evolved through one or more epochs of stiff-matter ( $w > 1/3$ ) dominated phase towards the end of reheating. More importantly, our analysis demonstrates that a predicted GW signal, that could have violated the BBN and/or aLIGO constraints when modelled by a single stiff EoS,  $w_{\text{stiff}} > 1/3$ , may actually be consistent with the aforementioned constraints if the post-inflationary history is comprised of additional phases with softer EoS parameters,  $w \leq 1/3$ , along with the stiff-matter phase. Therefore, our work highlights the drawback of using a single average EoS to describe the post-inflationary expansion, and opens up a broad range of parameter space which generates robust forecasts for the upcoming GW observatories.

Finally, in Sec. 5 we applied our techniques to a particular post-inflationary scenario described in Ref. [137], which is phenomenologically inspired from String Theory, in which a scalar moduli field plays a cosmologically important role, and dictates the evolution of the universe in between the end of inflation and the onset of BBN. In this scenario, the post-inflationary universe transits through a series of chronological epochs, namely, a kination-dominated epoch, an intermediate radiation-dominated epoch, and an early matter-dominated epoch (see Fig. 10), prior to the standard radiative hot Big Bang phase. We explored the possibility of observing the imprints of this scenario in the inflationary GW spectrum via upcoming GW observatories. Representing the duration of each epoch in terms of the energy scale at the end of that epoch, we obtained the corresponding parameter space that results in a detectable signal, as shown in Fig. 12; with the assumption that the final stage reheating is instantaneous. We found that GWs, corresponding to tensor modes that made their Hubble-entry during the kination phase, will be detected by BBO, DECIGO and CE, and not by LISA and ET (due to violation of BBN constraints). Furthermore, we obtain a necessary condition for this scenario to result in a detectable GW signal to be that the early matter-dominated epoch prior to the end of reheating must be shorter in duration, lasting no more than 7  $e$ -folds of expansion.

Before concluding, we emphasize that the specific analysis carried out in this work comes with a number of caveats, which we list in the following.

- Throughout this paper, we have fixed the value of the tensor-to-scalar ratio at  $r = 0.001$  which is a standard target for the upcoming CMB missions [178, 179]. In this sense, our analysis was focused on the question: ‘*if low-frequency primordial GWs get detected by their imprints on the CMB B-mode polarization in the upcoming decade, then what will the implications be for the upcoming GW observatories functioning at higher frequencies?*’. However, one can easily consider lower values of tensor-to-scalar ratio and incorporate our computational scheme to generate updated forecast for GWs. Nevertheless, we provide a detailed discussion on the effect of changing reheating temperature on the GW spectral energy density in App. F.
- Similarly, the energy scale of the universe at the end of reheating was fixed to be  $E_{\text{T*}} = 1$  GeV in this paper in order to demonstrate our approach and to focus on the EoS parameter and duration of each post-inflationary (pre-BBN) epoch. However, the hot Big bang phase might have commenced at a much lower temperature (as low as  $\mathcal{O}(1)$  MeV) or even at higher temperatures (as high as  $\mathcal{O}(10^{15})$  GeV). The lower reheating temperature is of greater phenomenological interest, and one can utilize our scheme to generate the corresponding GW forecast. However, much higher reheating temperature usually results in a low amplitude of GWs which may be of phenomenological interest for the high-frequency resonant cavity GW detectors [180–183].
- More importantly, while realistic transitions (no matter how sharp they are) in the early universe are expected to be smooth [102, 119], in this work we modelled the transitions between different post-inflationary epochs to be instantaneous, primarily for two reasons: (i) for the convenience of solving the tensor mode equations analytically in terms of Bessel functions, and (ii) to



remain agnostic about the exact functional form of the EoS  $w(\tau)$ . However, it is possible to carry out a fully numerical approach by either using a (phenomenologically) smoothed EoS parameter, or by considering a specific model where the exact evolution of  $w(\tau)$  is known. It has been shown that a smoothed reheating EoS in the perturbative regime leads to transient oscillatory features in the GW spectrum [59]. Nevertheless, since we primarily focused on determining the detectable parameter space of post-inflationary dynamics, the implementation of instantaneous transitions suffices for our purpose.

- In our analysis, we did not take into account the finer effects coming from the variation in the effective number of relativistic degrees of freedom,  $g_*(T)$ , in the early universe [116] as well as due to the anisotropic stress induced by freely streaming relativistic neutrinos [114] on the spectrum of GWs.
- We assumed a (nearly-) flat primordial tensor power spectrum (at the end of inflation) to be the initial condition for evolving the tensor modes post inflation and for computing the present-day GW spectrum. However, towards the end of inflation, the tensor power-spectrum acquires a scale dependence which affects the GW spectrum [59] closer to the highest frequency values  $f_e$ . Additionally, we did not consider the UV tail of GWs [184] corresponding to tensor modes that never became super-Hubble during inflation. However, the aforementioned effects are more relevant for detecting ultra-high frequency GWs, potentially via resonant cavity detectors, which was not the primary focus of our work.
- Our treatment of tensor modes in this paper was based on first-order inflationary GWs. However, at second-order in cosmological perturbation theory, GWs can be induced by the presence of potentially large scalar perturbations in the primordial universe [43, 145, 185, 186]. They get amplified by the enhancement of scalar curvature perturbations at small scales and/or by the presence of an early matter-dominated epoch in the post-inflationary universe [145, 187], which might lead to a larger background of second-order GWs in comparison to their first-order counterparts. The CMB observations can probe scalar fluctuations with comoving wavenumber only in the range around  $k = 0.05 \text{ Mpc}^{-1}$ , hence they are insensitive to small scale primordial fluctuations. Large enough fluctuations at smaller cosmological scales may also lead to the formation of copious amounts of primordial black holes (PBHs), a plausible candidate for dark matter. Hence, a potential detection of these induced GWs would allow us to put strong constraints on the small-scale primordial density perturbations [188] and on the abundance of PBHs [189–191]. We will revert to second-order GWs in a future project.
- Finally, it is plausible that non-linear solitonic and non-solitonic configurations can contribute considerably towards the energy budget during the early stages of the post-inflationary evolution [100, 112, 192]. They further induce second and higher-order GWs that is expected to be detected by the planned GW detectors. For example, high-frequency (GHz-scale) stochastic GWs can result from oscillon formation (and inflaton fragmentation in general) during reheating [112, 193]. However, such signals are beyond the sensitivities of the current and proposed detectors, and are relevant for the resonant cavity detectors [194]. Another example would be the stochastic GW associated with cosmic strings which can be picked up by LISA, DECIGO and BBO [133, 134, 195, 196]. Thus, it is important to classify the possible GW signal resulting from such differing scenarios, which is outside the scope of this paper.

## 7 Acknowledgements

SSM is supported by the STFC Consolidated Grant [ST/T000732/1] at the University of Nottingham. AKS was supported by the INSPIRE scholarship of the Department of Science and Technology (DST), Govt. of India, during his Master’s thesis work. SSM is grateful to IUCAA for the hospitality

during the earliest stage of this work. SSM thanks Varun Sahni for insightful discussions over the years which led to the inception of this project. SSM is also thankful to Ed Copeland, Oliver Gould, Sanjit Mitra, Ranjeev Misra and P. P. Divakaran for helpful discussions at various stages of this project. Numerical computations were performed on the Padmanabha HPC cluster at IISER TVM. For the purpose of open access, the authors have applied a CC BY public copyright license to any Author Accepted Manuscript version arising.

**Data Availability Statement:** This work is entirely theoretical and has no associated data. A Python code to generate the plots of spectral energy density of first-order inflationary GWs can be found at the GitHub repository [🔗](#).

## Appendices

### A Analytical solution to the Mukhanov-Sasaki equation

The Mukhanov-Sasaki (MS) Eq. (2.9) can be written as

$$v_k + \left( k^2 - \frac{\nu^2 - \frac{1}{4}}{\tau^2} \right) v_k = 0, \quad (\text{A.1})$$

where  $\frac{z''}{z} = (aH)^2(\nu^2 - 1/4)$  with  $z = am_p \sqrt{2\epsilon_H}$ . For slow-roll inflation, at early times all relevant scales were sub-Hubble, ( $\tau \rightarrow -\infty$  or  $|k\tau| \gg 1$ ). In this limit, Eq. (A.1) reduces to the form

$$v_k + k^2 v_k = 0, \quad (\text{A.2})$$

which is similar to the equation for a simple harmonic oscillator with a time-independent frequency. A unique solution to Eq. (A.2) is obtained by fixing the vacuum in the sub-Hubble regime to be the Bunch-Davies vacuum [139, 140], namely,

$$\lim_{k\tau \rightarrow -\infty} v_k \simeq \frac{1}{\sqrt{2k}} e^{-ik\tau}. \quad (\text{A.3})$$

In terms of the variable to be  $T = -k\tau$ , the MS equation becomes

$$\frac{d^2 v_k}{dT^2} + \left( 1 - \frac{\nu^2 - \frac{1}{4}}{T^2} \right) v_k = 0. \quad (\text{A.4})$$

Furthermore, we also introduce the variable  $v_k = F\sqrt{T}$ , in order to transform Eq. (A.4) to the Bessel equation

$$\frac{d^2 F}{dT^2} + \frac{1}{T} \frac{dF}{dT} + \left( 1 - \frac{\nu^2}{T^2} \right) F = 0, \quad (\text{A.5})$$

whose general solution can be written in terms of Hankel functions as

$$F(T) = C_1 H_\nu^{(1)}(T) + C_2 H_\nu^{(2)}(T). \quad (\text{A.6})$$

Hence, the general solution of the MS equation can be written as

$$v_k(T) = \sqrt{T} \left[ C_1 H_\nu^{(1)}(T) + C_2 H_\nu^{(2)}(T) \right]. \quad (\text{A.7})$$

In the sub-Hubble limit,  $T \gg 1$ , the Hankel functions become

$$H_\nu^{(1)}(T) \Big|_{T \rightarrow \infty} \simeq \sqrt{\frac{2}{\pi T}} e^{iT} e^{-i(\nu + \frac{1}{2})\frac{\pi}{2}}, \quad (\text{A.8})$$

$$H_\nu^{(2)}(T) \Big|_{T \rightarrow \infty} \simeq \sqrt{\frac{2}{\pi T}} e^{-iT} e^{i(\nu + \frac{1}{2})\frac{\pi}{2}}. \quad (\text{A.9})$$

From the Bunch-Davies initial condition in Eq. (A.3), we have

$$v_k(T) \Big|_{T \rightarrow \infty} = \frac{1}{\sqrt{2k}} e^{iT} = \sqrt{T} C_1 H_\nu^{(1)}(T) \Big|_{T \rightarrow \infty}, \quad (\text{A.10})$$

which implies that the coefficients in Eq. (A.7) are

$$C_1 = \frac{1}{\sqrt{2k}} \sqrt{\frac{\pi}{2}} e^{i(\nu+\frac{1}{2})\frac{\pi}{2}}, \quad C_2 = 0. \quad (\text{A.11})$$

Ultimately, the expression for the mode function becomes

$$v_k(T) = \frac{1}{\sqrt{2k}} \sqrt{\frac{\pi}{2}} e^{i(\nu+\frac{1}{2})\frac{\pi}{2}} \sqrt{T} H_\nu^{(1)}(T). \quad (\text{A.12})$$

## B Expression for the conformal Hubble parameter

Consider an epoch with EoS,  $w$ . Let ‘ $i$ ’ denote the beginning of that epoch, then the energy density evolves as

$$\rho(\tau) = \rho_i \left( \frac{a(\tau)}{a_i} \right)^{-3(1+w)}. \quad (\text{B.1})$$

Hence, we can write the Hubble rate during the epoch to be,  $H^2 = H_i^2 (a/a_i)^{-3(1+w)}$ . Integrating the above expression from  $a_i$  to an arbitrary  $a$  during this epoch, we obtain

$$\int_{a_i}^a da \left( \frac{a^{3(1+w)/2-1}}{a_i^{3(1+w)/2}} \right) = \int_{\tau_i}^{\tau} a_i H_i d\tau, \quad (\text{B.2})$$

which leads to the expression for the scale factor  $a(\tau)$  during that epoch as

$$a(\tau) = a_i \left[ 1 + \frac{a_i H_i (\tau - \tau_i)}{\alpha} \right]^\alpha, \quad (\text{B.3})$$

where  $\alpha = 2/(1 + 3w)$ . Hence, the conformal Hubble parameter  $\mathcal{H}$  becomes

$$\begin{aligned} \mathcal{H} &= aH = \frac{d \ln a}{d\tau}, \\ \ln a &= \ln a_i + \alpha \ln \left[ 1 + \frac{a_i H_i (\tau - \tau_i)}{\alpha} \right], \\ \Rightarrow aH &= \frac{a_i H_i}{\left[ 1 + \frac{a_i H_i (\tau - \tau_i)}{\alpha} \right]}. \end{aligned} \quad (\text{B.4})$$

## C Energy-momentum tensor of gravitational waves

The quadratic action for the tensor fluctuations  $h_{ij}$  is given by

$$S_2[h_{ij}] = \frac{m_p^2}{8} \int d^4x \sqrt{-\bar{g}} \left[ -\bar{g}^{\mu\nu} (\partial_\mu h_{ij}) (\partial_\nu h^{ij}) \right], \quad (\text{C.1})$$

where  $\bar{g}_{\mu\nu}$  is the background metric and  $\bar{g} \equiv \det \bar{g}_{\mu\nu}$ . The energy-momentum tensor is obtained from the variation of this action with respect to the background (inverse) metric [148]

$$\delta S = -\frac{1}{2} \int d^4x \sqrt{-\bar{g}} T_{\mu\nu} \delta \bar{g}^{\mu\nu}, \quad (\text{C.2})$$

leading to

$$\begin{aligned} T_{\alpha\beta} &= \frac{m_p^2}{4} \left[ -\frac{1}{2} \bar{g}_{\alpha\beta} \bar{g}^{\mu\nu} (\partial_\mu h_{ij}) (\partial_\nu h^{ij}) + (\partial_\alpha h_{ij}) (\partial_\beta h^{ij}) \right], \\ T^\mu{}_\nu &= \frac{m_p^2}{4} \left[ -\frac{1}{2} \delta^\mu{}_\nu \bar{g}^{\alpha\beta} (\partial_\alpha h_{ij}) (\partial_\beta h^{ij}) + (\partial^\mu h_{ij}) (\partial_\nu h^{ij}) \right]. \end{aligned} \quad (\text{C.3})$$

The time-time component of the energy-momentum tensor is the energy density of GWs, given by

$$\rho_{\text{GW}}(\tau, \vec{x}) = -T^0{}_0 = \frac{m_p^2}{8a^2(\tau)} \left[ (h'_{ij}(\tau, \vec{x}))^2 + (\vec{\nabla} h_{ij}(\tau, \vec{x}))^2 \right]. \quad (\text{C.4})$$

## D Derivation of the present-day GW spectral energy density

The derivation is done for the general case of reheating consisting of multiple equation of state parameters. For  $\tau = \tau_0$  in Eq. (3.41)

$$\Omega_{\text{GW}}(\tau_0, k) = \frac{k^2}{12 a^2(\tau_0) H^2(\tau_0)} \mathcal{P}_T(\tau_0, k). \quad (\text{D.1})$$

Substituting  $k = y_{\text{eq}} a_{\text{eq}} H_{\text{eq}}$  and  $\mathcal{P}_T(\tau_0, k) = (k^3/\pi^2) \overline{|h_{k,\text{MD}}^\lambda(y \gg 1)|^2}$  in Eq. (D.1), we obtain

$$\Omega_{\text{GW}}(\tau_0, k) = \frac{1}{12 a_0^2 H_0^2} (y_{\text{eq}} a_{\text{eq}} H_{\text{eq}})^2 \frac{k^3}{\pi^2} \frac{1}{(2y_0)^4} \frac{1}{\pi} [|A_{k,\text{MD}}|^2 + |B_{k,\text{MD}}|^2], \quad (\text{D.2})$$

where  $\overline{|h_{k,\text{MD}}^\lambda(y \gg 1)|^2}$  was substituted from Eq. (3.43). We can rewrite  $y_0$  as

$$\begin{aligned} y_0 &= \frac{k}{a_0 H_0} = y_{\text{eq}} \frac{a_{\text{eq}} H_{\text{eq}}}{a(\tau_0) H(\tau_0)} = y_{\text{eq}} \left[ 1 + \frac{a_{\text{eq}} H_{\text{eq}} (\tau_0 - \tau_{\text{eq}})}{2} \right], \\ &\Rightarrow y_0 = y_{\text{eq}} \left( \frac{a(\tau_0)}{a_{\text{eq}}} \right)^{1/2}. \end{aligned} \quad (\text{D.3})$$

Incorporating Eq. (D.3) into Eq. (D.2), we obtain

$$\begin{aligned} \Omega_{\text{GW}}(\tau_0, k) &= \frac{1}{192} \frac{a_{\text{eq}}^4 H_{\text{eq}}^2}{a_0^4 H_0^2} \frac{k^3}{\pi^3} \frac{1}{y_{\text{eq}}^2} \left[ \tilde{A}_{k,\text{MD}}^2 + \tilde{B}_{k,\text{MD}}^2 \right] \left| h_{k,\text{inf}}^\lambda \right|^2, \\ &= \frac{1}{96\pi^3} \frac{a_{\text{r}*}^4 H_{\text{r}*}^2}{a_0^4 H_0^2} \frac{1}{y_{\text{eq}}^2} \left[ \tilde{A}_{k,\text{MD}}^2 + \tilde{B}_{k,\text{MD}}^2 \right] \frac{H_{\text{inf}}^2}{m_p^2} \left( \frac{k}{k_*} \right)^{n_T}, \end{aligned} \quad (\text{D.4})$$

where  $\tilde{A}_{k,\text{MD}} = \frac{A_{k,\text{MD}}}{h_{k,\text{inf}}^\lambda}$  and similarly,  $\tilde{B}_{k,\text{MD}} = \frac{B_{k,\text{MD}}}{h_{k,\text{inf}}^\lambda}$ . Furthermore, we have made use of the following relations:

$$\mathcal{P}_{T,\text{inf}}(\tau_0, k) = \frac{k^3}{\pi^2} \left| h_{k,\text{inf}}^\lambda \right|^2 = \frac{2}{\pi^2} \left( \frac{H_{\text{inf}}}{m_p} \right)^2 \left( \frac{k}{k_*} \right)^{n_T}, \quad (\text{D.5})$$

$$a_{\text{eq}}^4 H_{\text{eq}}^2 = (a_{\text{eq}} H_{\text{eq}})^2 a_{\text{eq}}^2 = \left[ \frac{a_{\text{r}*} H_{\text{r}*}}{1 + a_{\text{r}*} H_{\text{r}*} (\tau_{\text{eq}} - \tau_{\text{r}*})} \right]^2 a_{\text{r}*}^2 [1 + a_{\text{r}*} H_{\text{r}*} (\tau_{\text{eq}} - \tau_{\text{r}*})]^2 = a_{\text{r}*}^4 H_{\text{r}*}^2. \quad (\text{D.6})$$

where  $H_{\text{inf}}$  corresponds to the Hubble scale during inflation at the Hubble-exit time of the CMB pivot scale, *i.e.*,  $H_{\text{inf}} = H_*$ . The Hubble parameter can be written as

$$H^2(\tau) = \frac{\rho_{\text{rad}}}{3 m_p^2 \Omega_{\text{rad}}} = \frac{\rho_{\text{rad}} \Omega_{\text{rad},0} H_0^2}{\rho_{\text{rad},0} \Omega_{\text{rad}}}. \quad (\text{D.7})$$

Radiation energy density is given by

$$\rho_{\text{rad}}(T) = \frac{\pi^2}{30} g_*(T) T^4, \quad (\text{D.8})$$

while the conservation of entropy implies

$$T \propto g_s^{-1/3} a^{-1}. \quad (\text{D.9})$$

Substituting Eq. (D.8) and Eq. (D.9) in Eq. (D.7), we obtain

$$H^2(T) = \frac{g_*(T) g_s^{-4/3}(T) a^{-4}(T) \Omega_{\text{rad},0} H_0^2}{g_{*,0} g_{s,0}^{-4/3} a_0^{-4} \Omega_{\text{rad}}(T)}, \quad (\text{D.10})$$

which can be rewritten as

$$\frac{a_k^4 H_k^2}{a_0^4 H_0^2} = \frac{g_{*,k}}{g_{*,0}} \left( \frac{g_{s,0}}{g_{s,k}} \right)^{4/3} \frac{\Omega_{\text{rad},0}}{\Omega_{\text{rad}}(\tau_k)}, \quad (\text{D.11})$$

where  $g_{*,k}$ ,  $g_{s,k}$  are the number of relativistic degrees of freedom in energy density and entropy density, respectively, at the time when the tensor mode with comoving wavenumber  $k$  makes its Hubble-entry, while  $g_{*,0}$ ,  $g_{s,0}$  correspond to the same at the present epoch. When the tensor mode of interest enters during the RD epoch,  $\Omega_{\text{rad}} \approx 1$ . So, (D.11) becomes

$$\frac{a_k^4 H_k^2}{a_0^4 H_0^2} \approx \frac{g_{*,k}}{g_{*,0}} \left( \frac{g_{s,0}}{g_{s,k}} \right)^{4/3} \Omega_{\text{rad},0}, \quad (\text{D.12})$$

where the label ‘ $k$ ’ refers to any mode that entered the Hubble radius during the RD epoch. Using Eq. (D.12) in Eq. (D.4) at  $\tau = \tau_{r^*}$  (beginning of RD epoch), we arrive at the final expression for the spectral energy density of GWs

$$\Omega_{\text{GW}}(\tau_0, k) = \frac{1}{96\pi^3} \frac{g_{*,r^*}}{g_{*,0}} \left( \frac{g_{s,0}}{g_{s,r^*}} \right)^{4/3} \Omega_{\text{rad},0} \frac{1}{y_{\text{eq}}^2} \left[ \tilde{A}_{k,\text{MD}}^2 + \tilde{B}_{k,\text{MD}}^2 \right] \frac{H_{\text{inf}}^2}{m_p^2} \left( \frac{k}{k_*} \right)^{n_T}. \quad (\text{D.13})$$

## E Energy density of photons and neutrinos

From the present-day CMB temperature,  $T_0 = 2.73 \text{ K}$  [197], we obtain the energy density of CMB photons

$$\rho_{\gamma,0} = \frac{\pi^2}{30} \times 2 \times T_0^4 = 2.00 \times 10^{-51} \text{ GeV}^4, \quad (\text{E.1})$$

where the factor ‘2’ accounts for the internal degrees of freedom of photons. The present-day critical density of the universe is

$$\rho_{c,0} = 3 H_0^2 m_p^2 = 8.12 \times 10^{-47} h^2 \text{ GeV}^4, \quad (\text{E.2})$$

where  $H_0 = 100 h \text{ km s}^{-1} \text{ Mpc}^{-1} = 2.132 \times 10^{-42} h \text{ GeV}$  [25]. Hence, the density parameter of CMB photons is given by

$$h^2 \Omega_{\gamma,0} = h^2 \frac{\rho_{\gamma,0}}{\rho_{c,0}} = 2.46 \times 10^{-5}. \quad (\text{E.3})$$

Post electron-positron annihilation, the neutrino temperature is given by [23]

$$T_\nu = \left( \frac{4}{11} \right)^{1/3} T_\gamma, \quad (\text{E.4})$$

from which, we can derive a relation between the energy density of SM neutrinos and CMB photons to be

$$\rho_\nu = \frac{7}{8} N_{\text{eff}} \left( \frac{4}{11} \right)^{4/3} \rho_\gamma, \quad (\text{E.5})$$

where  $N_{\text{eff}} = 3.046$  [198] is the effective number of neutrino species in the SM. Using Eq. (E.5), the present-day density parameter for neutrinos becomes

$$h^2 \Omega_{\nu,0} = \frac{7}{8} N_{\text{eff}} \left( \frac{4}{11} \right)^{4/3} h^2 \Omega_{\gamma,0} = 1.70 \times 10^{-5}. \quad (\text{E.6})$$

Hence, the present-day density parameter of radiation becomes

$$h^2 \Omega_{\text{rad},0} = h^2 (\Omega_{\gamma,0} + \Omega_{\nu,0}) = 4.16 \times 10^{-5}. \quad (\text{E.7})$$

## F Effect of varying reheating temperature on GW spectral energy density

In the main text of this paper, we had fixed the reheating temperature to be  $T_{r^*} = 0.45 \text{ GeV}$ , or equivalently, the energy scale at the end of reheating to be  $E_{r^*} = 1 \text{ GeV}$ , for the purpose of illustration. However, in general, the reheating energy scale can range from the end of inflation all the way down to the onset of BBN. Hence, in this appendix, we discuss the impact of varying the reheating temperature on the spectral energy density of inflationary GWs.

Additionally, in the main text of the paper, we had fixed the tensor-to-scalar ratio during inflation to be  $r = 0.001$ , or equivalently, the energy scale at the end of inflation to be  $E_{\text{inf}} = 5.76 \times 10^{15} \text{ GeV}$ , keeping in mind that the upcoming CMB detectors will be able to probe  $r$  up to  $\mathcal{O}(10^{-3})$ . Since inflation does not make a prediction for  $r$ , it is possible that  $r \ll 10^{-3}$ . Therefore, we proceed to first discuss the impact of small  $r$  on the detectability of inflationary GWs *via* the upcoming GW observatories, before moving on to determine the detectable parameter space of equation of states for fixed  $r = 0.001$ , but different values of the reheating energy scales  $E_{r^*}$ .

### F.1 Effect of varying tensor-to-scalar ratio on GW signal

A quantity of central importance is the minimum value of reheating temperature corresponding to a given value of tensor-to-scalar ratio which leads to a detectable GW signal in various GW detectors. In fact, for a given GW detector, and for a fixed value of  $r$ , we find that upon increasing the reheating temperature, there is a critical value of  $T_{r^*}$  (or  $E_{r^*}$ ) above which the inflationary GW signal will lie outside the sensitivity region of that detector, even if the EoS during reheating is that of a stiff-matter, *i.e.*  $w \simeq 1$ .

In Fig. 13, we show the (shaded) region in the parameter space of  $r$  and  $T_{r^*}$  (or  $E_{r^*}$ ) for different GW detectors that will never lead to a detectable inflationary GW signal. This does not necessarily mean that the unshaded region corresponding to each detector will guarantee a detection in that detector, which of course depends upon the EoS and duration of reheating, as well as on whether the GW spectrum satisfies the current observational constraints.

For large enough values of  $r \gtrsim \mathcal{O}(10^{-2})$ , height of flat (nearly scale-invariant) region of  $\Omega_{\text{GW}}(f)$ , corresponding to modes making their Hubble-entry during the thermal RD epoch, increases enough to reach the sensitivity curves of BBO and DECIGO, as long as the reheating temperature is also large enough. In such cases, at large reheating temperatures, these detectors will detect a GW signal with certainty. That is why we see nearly vertical curves for BBO and DECIGO at high values of  $r$  in Fig. 13 (blue and green curves).

However, the same is not true for other GW detectors, because their sensitivity curves are above the highest allowed height of  $\Omega_{\text{GW}}$ , corresponding to  $r = 0.036$ , for modes that entered in the RD epoch. Therefore, if  $T_{r^*}$  is high enough, then the GW signal will be absent in these detectors, independent of the EoS during reheating.

Note that the small kinks seen in the solid curves are due to the sudden drop in the relativistic degrees of freedom in the early Universe, within the Standard Model of particle physics. In particular, the prominent horizontal shift in all curves around  $T_{r^*} \simeq 150 \text{ MeV}$  is due to a large drop in relativistic degrees of freedom closer to QCD phase transition.

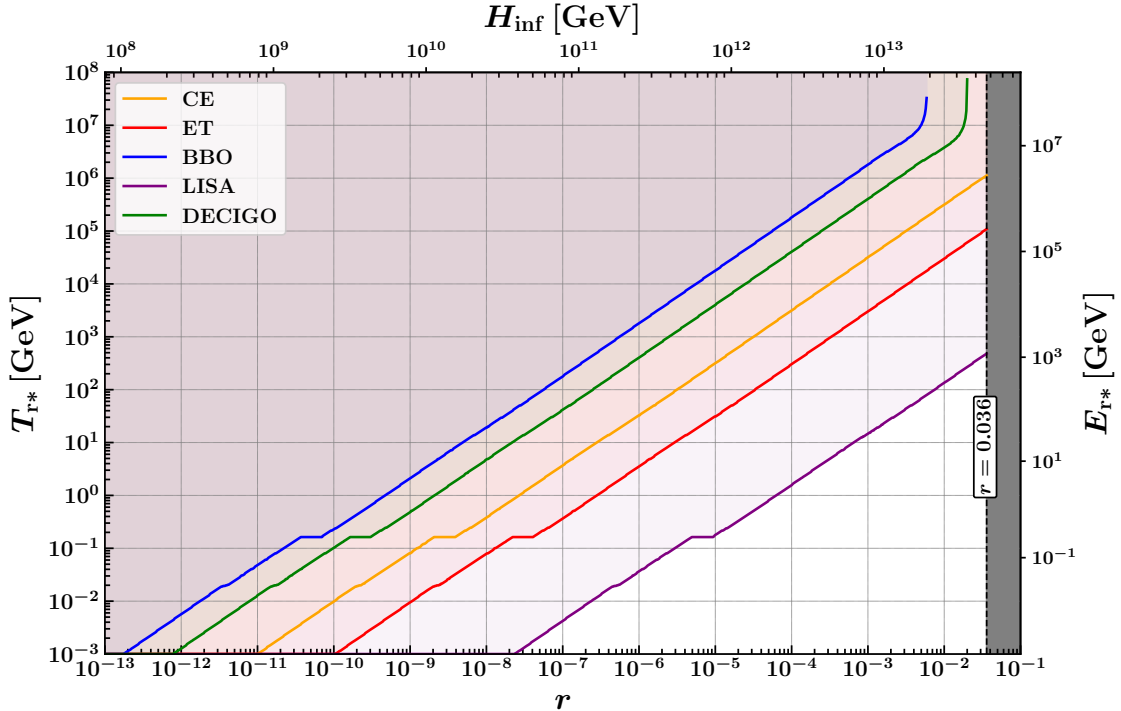


**Figure 13:** The figure illustrates the effect of varying tensor-to-scalar ratio ( $r$ ), and reheating temperature ( $T_{r*}$ ) on the detectability of inflationary GWs in various GW detectors. The coloured shaded regions indicate the parameter space of the  $r$ , and  $T_{r*}$ , that can never yield a potential detection of inflationary GW signal in CE, ET, BBO, LISA and DECIGO detectors. The grey-shaded region is ruled out by the CMB observations, namely,  $r \leq 0.036$ . The Hubble parameter during (at the end of) inflation ( $H_{\text{inf}}$ ) corresponding to each value of  $r$  and the energy scale corresponding to each value of  $T_{r*}$  are provided in the respective opposite axes.

## F.2 Two-epoch reheating with different reheating temperature

In Sec. 4, we determined the parameter space of EoS  $w_1$  and  $w_2$ , that results in a potentially detectable inflationary GW signal in future GW detectors, for fixed values  $E_{r*} = 1 \text{ GeV}$  and  $r = 0.001$  ( $E_{\text{inf}} = 5.76 \times 10^{15} \text{ GeV}$ ). As stressed before, the aforementioned values of  $r$  and reheating temperature were used purely for the purpose of illustrating how to use our calculations of  $\Omega_{\text{GW}}$  to check whether a particular set of parameters leads to a detectable signal.

However, for a given value of  $r$ , reheating temperature can be very different, ranging in between  $1 \text{ MeV} \leq T_{r*} \lesssim E_{\text{inf}}$ . Therefore, in this appendix, we include the parameter space plots of  $w_1$  and  $w_2$  corresponding to a two-epoch reheating scenario (similar to Fig. 6), specifically for  $E_{r*} = 100 \text{ GeV}$  and  $10 \text{ MeV}$  in Figs. 14 and 15, respectively. We fix the value of  $E_{\text{inf}}$  to be the same as before. Note that the BBN constraint that we have imposed in this appendix is slightly weaker than the one quoted in Eq. (3.59). Here, we only make sure whether the GW spectrum intersects the BBN constraint curve at  $h^2 \Omega_{\text{GW}}(\tau_0) = 1.13 \times 10^{-6}$ .

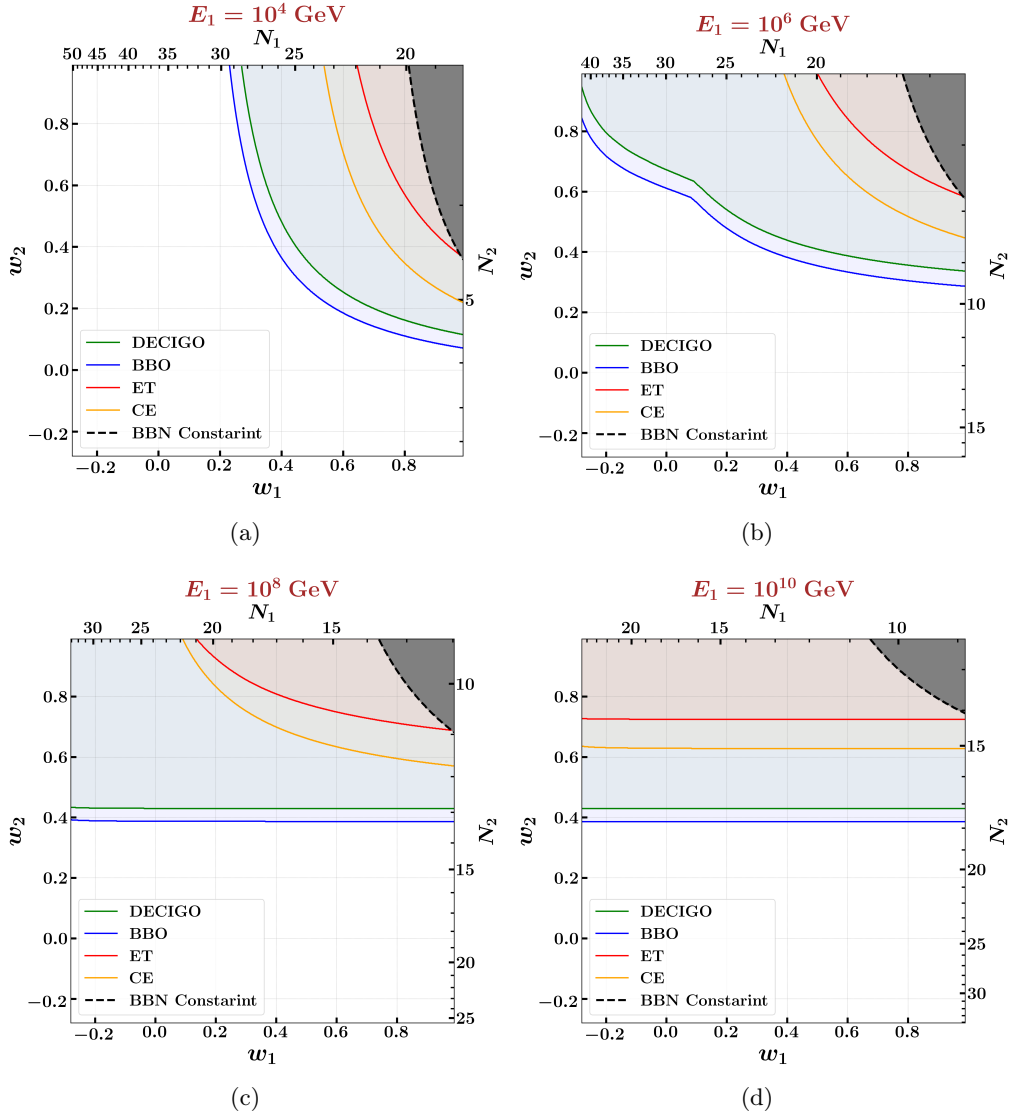


**Figure 14:** The parameter space for two-epoch reheating phase with EoS parameters  $w_1$  and  $w_2$  that leads to a potentially detectable GW signal in the LISA, BBO, DECIGO, CE, and ET detectors for  $E_{\text{r}*} = 100$  GeV and  $r = 0.001$ . The grey-shaded region in each plot corresponds to the combination of  $w_1$  and  $w_2$  that crosses the BBN constraint curve at  $h^2 \Omega_{\text{GW}}(\tau_0) = 1.13 \times 10^{-6}$ , while the maroon-shaded region represents those that are ruled out by the aLIGO null detection. Energy scale of the universe at the end of the first post-inflationary epoch is labelled above in each plot. The duration of each epoch (number of  $e$ -folds) has been provided opposite to the corresponding EoS axis.



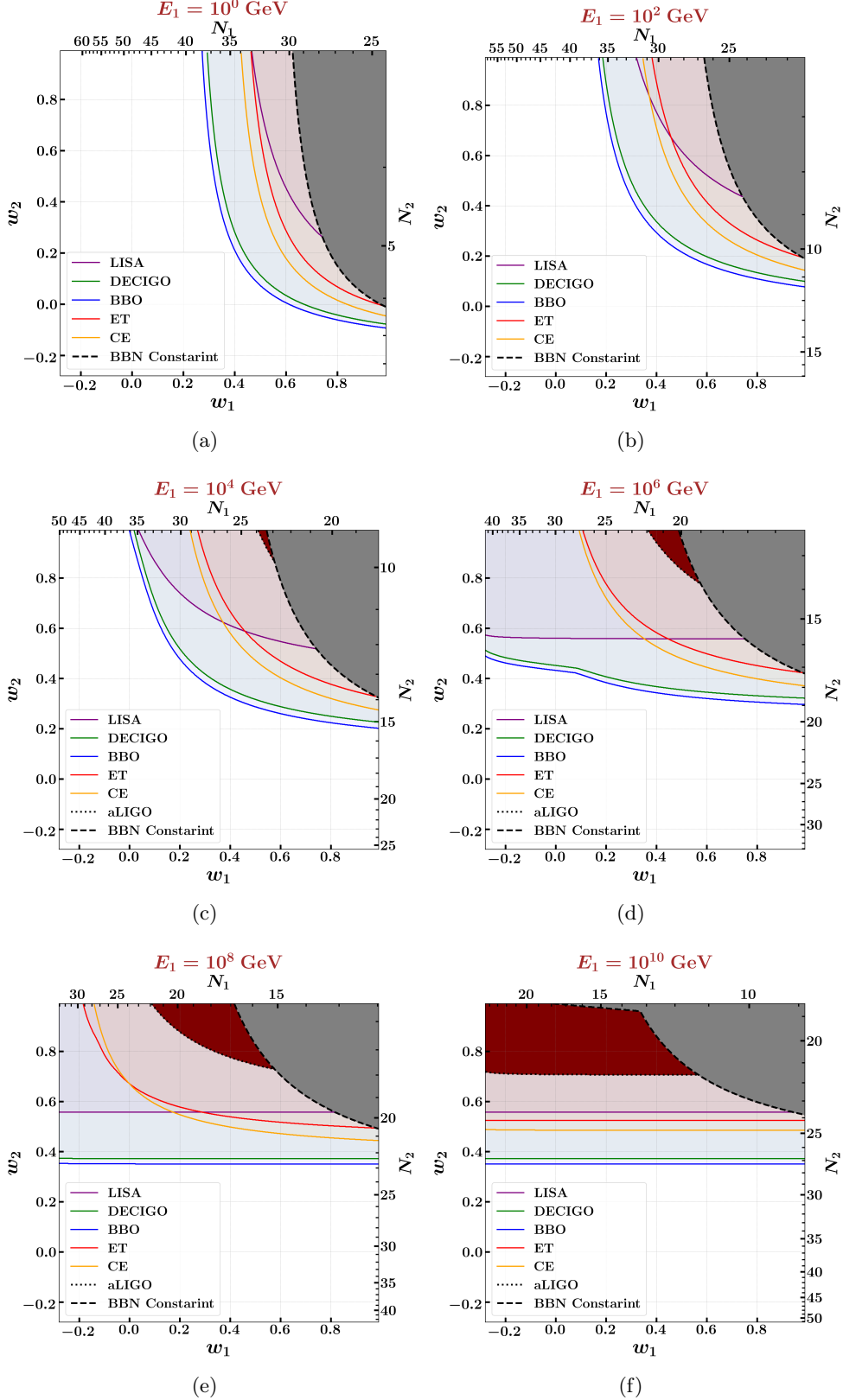


**Figure 15:** The parameter space for two-epoch reheating phase with EoS parameters  $w_1$  and  $w_2$  that leads to a potentially detectable GW signal in the LISA, BBO, DECIGO, CE, and ET detectors for  $E_{T*} = 10$  MeV and  $r = 0.001$ . The grey-shaded region in each plot corresponds to the combination of  $w_1$  and  $w_2$  that crosses the BBN constraint curve at  $h^2 \Omega_{\text{GW}}(\tau_0) = 1.13 \times 10^{-6}$ , while the maroon-shaded region represents those that are ruled out by the aLIGO null detection. Energy scale of the universe at the end of the first post-inflationary epoch is labelled above in each plot. The duration of each epoch (number of  $e$ -folds) has been provided opposite to the corresponding EoS axis.

## References

- [1] Alexei A. Starobinsky. “A New Type of Isotropic Cosmological Models Without Singularity”. In: *Phys. Lett. B* 91 (1980). Ed. by I. M. Khalatnikov and V. P. Mineev, pp. 99–102. DOI: [10.1016/0370-2693\(80\)90670-X](https://doi.org/10.1016/0370-2693(80)90670-X).
- [2] Alan H. Guth. “The Inflationary Universe: A Possible Solution to the Horizon and Flatness Problems”. In: *Phys. Rev. D* 23 (1981). Ed. by Li-Zhi Fang and R. Ruffini, pp. 347–356. DOI: [10.1103/PhysRevD.23.347](https://doi.org/10.1103/PhysRevD.23.347).
- [3] Andrei D. Linde. “A New Inflationary Universe Scenario: A Possible Solution of the Horizon, Flatness, Homogeneity, Isotropy and Primordial Monopole Problems”. In: *Phys. Lett. B* 108 (1982). Ed. by Li-Zhi Fang and R. Ruffini, pp. 389–393. DOI: [10.1016/0370-2693\(82\)91219-9](https://doi.org/10.1016/0370-2693(82)91219-9).
- [4] Andreas Albrecht and Paul J. Steinhardt. “Cosmology for Grand Unified Theories with Radiatively Induced Symmetry Breaking”. In: *Phys. Rev. Lett.* 48 (1982). Ed. by Li-Zhi Fang and R. Ruffini, pp. 1220–1223. DOI: [10.1103/PhysRevLett.48.1220](https://doi.org/10.1103/PhysRevLett.48.1220).
- [5] Andrei D. Linde. “Chaotic Inflation”. In: *Phys. Lett. B* 129 (1983), pp. 177–181. DOI: [10.1016/0370-2693\(83\)90837-7](https://doi.org/10.1016/0370-2693(83)90837-7).
- [6] Andrei D. Linde. *Particle physics and inflationary cosmology*. Vol. 5. 1990. arXiv: [hep-th/0503203](https://arxiv.org/abs/hep-th/0503203).
- [7] William H. Kinney. *TASI Lectures on Inflation*. 2009. arXiv: [0902.1529](https://arxiv.org/abs/0902.1529) [[astro-ph.CO](https://arxiv.org/abs/0902.1529)].
- [8] Jerome Martin, Christophe Ringeval, and Vincent Vennin. “Encyclopædia Inflationaris”. In: *Phys. Dark Univ.* 5-6 (2014), pp. 75–235. DOI: [10.1016/j.dark.2014.01.003](https://doi.org/10.1016/j.dark.2014.01.003). arXiv: [1303.3787](https://arxiv.org/abs/1303.3787) [[astro-ph.CO](https://arxiv.org/abs/1303.3787)].
- [9] Daniel Baumann. “Inflation”. In: *Theoretical Advanced Study Institute in Elementary Particle Physics: Physics of the Large and the Small*. 2011, pp. 523–686. DOI: [10.1142/9789814327183\\_0010](https://doi.org/10.1142/9789814327183_0010). arXiv: [0907.5424](https://arxiv.org/abs/0907.5424) [[hep-th](https://arxiv.org/abs/0907.5424)].
- [10] Daniel Baumann. “Primordial Cosmology”. In: *PoS TASI2017* (2018), p. 009. DOI: [10.22323/1.305.0009](https://doi.org/10.22323/1.305.0009). arXiv: [1807.03098](https://arxiv.org/abs/1807.03098) [[hep-th](https://arxiv.org/abs/1807.03098)].
- [11] Hideo Kodama and Misao Sasaki. “Cosmological Perturbation Theory”. In: *Progress of Theoretical Physics Supplement* 78 (Jan. 1984), pp. 1–166. ISSN: 0375-9687. DOI: [10.1143/PTPS.78.1](https://doi.org/10.1143/PTPS.78.1). eprint: <https://academic.oup.com/ptps/article-pdf/doi/10.1143/PTPS.78.1/5321391/78-1.pdf>. URL: <https://doi.org/10.1143/PTPS.78.1>.
- [12] Antonio Riotto. “Inflation and the theory of cosmological perturbations”. In: *ICTP Lect. Notes Ser.* 14 (2003). Ed. by G. Dvali et al., pp. 317–413. arXiv: [hep-ph/0210162](https://arxiv.org/abs/hep-ph/0210162).
- [13] John Ellis and David Wands. “Inflation (2023)”. In: (Dec. 2023). arXiv: [2312.13238](https://arxiv.org/abs/2312.13238) [[astro-ph.CO](https://arxiv.org/abs/2312.13238)].
- [14] Swagat S. Mishra. “Cosmic Inflation: Background dynamics, Quantum fluctuations and Reheating”. Other thesis. Mar. 2024. arXiv: [2403.10606](https://arxiv.org/abs/2403.10606) [[gr-qc](https://arxiv.org/abs/2403.10606)].
- [15] Edward W. Kolb and Michael S. Turner. *The Early Universe*. Vol. 69. 1990. ISBN: 978-0-201-62674-2. DOI: [10.1201/9780429492860](https://doi.org/10.1201/9780429492860).
- [16] Scott Dodelson. *Modern Cosmology*. Amsterdam: Academic Press, 2003. ISBN: 978-0-12-219141-1.
- [17] Valery A. Rubakov and Dmitry S. Gorbunov. *Introduction to the Theory of the Early Universe: Hot big bang theory*. Singapore: World Scientific, 2017. ISBN: 978-981-320-987-9. DOI: [10.1142/10447](https://doi.org/10.1142/10447).
- [18] Viatcheslav F. Mukhanov and G. V. Chibisov. “Quantum Fluctuations and a Nonsingular Universe”. In: *JETP Lett.* 33 (1981), pp. 532–535.

- [19] S. W. Hawking. “The Development of Irregularities in a Single Bubble Inflationary Universe”. In: *Phys. Lett. B* 115 (1982), p. 295. DOI: [10.1016/0370-2693\(82\)90373-2](https://doi.org/10.1016/0370-2693(82)90373-2).
- [20] Alexei A. Starobinsky. “Dynamics of Phase Transition in the New Inflationary Universe Scenario and Generation of Perturbations”. In: *Phys. Lett. B* 117 (1982), pp. 175–178. DOI: [10.1016/0370-2693\(82\)90541-X](https://doi.org/10.1016/0370-2693(82)90541-X).
- [21] Alan H. Guth and S. Y. Pi. “Fluctuations in the New Inflationary Universe”. In: *Phys. Rev. Lett.* 49 (1982), pp. 1110–1113. DOI: [10.1103/PhysRevLett.49.1110](https://doi.org/10.1103/PhysRevLett.49.1110).
- [22] V. Mukhanov. *Physical Foundations of Cosmology*. Oxford: Cambridge University Press, 2005. ISBN: 978-0-521-56398-7. DOI: [10.1017/CB09780511790553](https://doi.org/10.1017/CB09780511790553).
- [23] Daniel Baumann. *Cosmology*. Cambridge University Press, July 2022. ISBN: 978-1-108-93709-2. DOI: [10.1017/9781108937092](https://doi.org/10.1017/9781108937092).
- [24] Dmitry S. Gorbunov and Valery A. Rubakov. *Introduction to the theory of the early universe: Cosmological perturbations and inflationary theory*. 2011. DOI: [10.1142/7873](https://doi.org/10.1142/7873).
- [25] N. Aghanim et al. “Planck 2018 results. VI. Cosmological parameters”. In: *Astron. Astrophys.* 641 (2020). [Erratum: *Astron. Astrophys.* 652, C4 (2021)], A6. DOI: [10.1051/0004-6361/201833910](https://doi.org/10.1051/0004-6361/201833910). arXiv: [1807.06209](https://arxiv.org/abs/1807.06209) [[astro-ph.CO](https://arxiv.org/archive/ph)].
- [26] N. Aghanim et al. “Planck 2018 results. I. Overview and the cosmological legacy of Planck”. In: *Astron. Astrophys.* 641 (2020), A1. DOI: [10.1051/0004-6361/201833880](https://doi.org/10.1051/0004-6361/201833880). arXiv: [1807.06205](https://arxiv.org/abs/1807.06205) [[astro-ph.CO](https://arxiv.org/archive/ph)].
- [27] Y. Akrami et al. “Planck 2018 results. X. Constraints on inflation”. In: *Astron. Astrophys.* 641 (2020), A10. DOI: [10.1051/0004-6361/201833887](https://doi.org/10.1051/0004-6361/201833887). arXiv: [1807.06211](https://arxiv.org/abs/1807.06211) [[astro-ph.CO](https://arxiv.org/archive/ph)].
- [28] P. A. R. Ade et al. “Improved Constraints on Primordial Gravitational Waves using Planck, WMAP, and BICEP/Keck Observations through the 2018 Observing Season”. In: *Phys. Rev. Lett.* 127.15, 151301 (Oct. 2021), p. 151301. DOI: [10.1103/PhysRevLett.127.151301](https://doi.org/10.1103/PhysRevLett.127.151301). arXiv: [2110.00483](https://arxiv.org/abs/2110.00483) [[astro-ph.CO](https://arxiv.org/archive/ph)].
- [29] L. P. Grishchuk. “Amplification of gravitational waves in an isotropic universe”. In: *Zh. Eksp. Teor. Fiz.* 67 (1974), pp. 825–838.
- [30] Alexei A. Starobinsky. “Spectrum of relict gravitational radiation and the early state of the universe”. In: *JETP Lett.* 30 (1979). Ed. by I. M. Khalatnikov and V. P. Mineev, pp. 682–685.
- [31] Varun Sahni. “The Energy Density of Relic Gravity Waves From Inflation”. In: *Phys. Rev. D* 42 (1990), pp. 453–463. DOI: [10.1103/PhysRevD.42.453](https://doi.org/10.1103/PhysRevD.42.453).
- [32] Bruce Allen. “The Stochastic Gravity Wave Background in Inflationary Universe Models”. In: *Phys. Rev. D* 37 (1988), p. 2078. DOI: [10.1103/PhysRevD.37.2078](https://doi.org/10.1103/PhysRevD.37.2078).
- [33] Scott Dodelson, William H. Kinney, and Edward W. Kolb. “Cosmic microwave background measurements can discriminate among inflation models”. In: *Phys. Rev. D* 56 (1997), pp. 3207–3215. DOI: [10.1103/PhysRevD.56.3207](https://doi.org/10.1103/PhysRevD.56.3207). arXiv: [astro-ph/9702166](https://arxiv.org/abs/astro-ph/9702166).
- [34] Swagat S. Mishra, Varun Sahni, and Alexei A. Starobinsky. “Curing inflationary degeneracies using reheating predictions and relic gravitational waves”. In: *JCAP* 05 (2021), p. 075. DOI: [10.1088/1475-7516/2021/05/075](https://doi.org/10.1088/1475-7516/2021/05/075). arXiv: [2101.00271](https://arxiv.org/abs/2101.00271) [[gr-qc](https://arxiv.org/archive/gr)].
- [35] Swagat S. Mishra and Varun Sahni. “Canonical and Non-canonical Inflation in the light of the recent BICEP/Keck results”. In: (Feb. 2022). arXiv: [2202.03467](https://arxiv.org/abs/2202.03467) [[astro-ph.CO](https://arxiv.org/archive/ph)].
- [36] Robert H. Brandenberger. “Alternatives to the inflationary paradigm of structure formation”. In: *Int. J. Mod. Phys. Conf. Ser.* 01 (2011). Ed. by Sang Pyo Kim, pp. 67–79. DOI: [10.1142/S2010194511000109](https://doi.org/10.1142/S2010194511000109). arXiv: [0902.4731](https://arxiv.org/abs/0902.4731) [[hep-th](https://arxiv.org/archive/hep)].

- [37] Robert H. Brandenberger. “Beyond Standard Inflationary Cosmology”. In: *Beyond Spacetime*. Ed. by Nick Huggett, Keizo Matsubara, and Christian Wüthrich. Apr. 2020, pp. 79–104. DOI: [10.1017/9781108655705.005](https://doi.org/10.1017/9781108655705.005). arXiv: [1809.04926](https://arxiv.org/abs/1809.04926) [hep-th].
- [38] Paolo Creminelli and Leonardo Senatore. “A Smooth bouncing cosmology with scale invariant spectrum”. In: *JCAP* 11 (2007), p. 010. DOI: [10.1088/1475-7516/2007/11/010](https://doi.org/10.1088/1475-7516/2007/11/010). arXiv: [hep-th/0702165](https://arxiv.org/abs/hep-th/0702165).
- [39] Anna Ijjas and Paul J. Steinhardt. “A new kind of cyclic universe”. In: *Phys. Lett. B* 795 (2019), pp. 666–672. DOI: [10.1016/j.physletb.2019.06.056](https://doi.org/10.1016/j.physletb.2019.06.056). arXiv: [1904.08022](https://arxiv.org/abs/1904.08022) [gr-qc].
- [40] Anna Ijjas and Paul J. Steinhardt. “Bouncing Cosmology made simple”. In: *Class. Quant. Grav.* 35.13 (2018), p. 135004. DOI: [10.1088/1361-6382/aac482](https://doi.org/10.1088/1361-6382/aac482). arXiv: [1803.01961](https://arxiv.org/abs/1803.01961) [astro-ph.CO].
- [41] Peter W. Graham, David E. Kaplan, and Surjeet Rajendran. “Born again universe”. In: *Phys. Rev. D* 97.4 (2018), p. 044003. DOI: [10.1103/PhysRevD.97.044003](https://doi.org/10.1103/PhysRevD.97.044003). arXiv: [1709.01999](https://arxiv.org/abs/1709.01999) [hep-th].
- [42] Latham A. Boyle, Paul J. Steinhardt, and Neil Turok. “The Cosmic gravitational wave background in a cyclic universe”. In: *Phys. Rev. D* 69 (2004), p. 127302. DOI: [10.1103/PhysRevD.69.127302](https://doi.org/10.1103/PhysRevD.69.127302). arXiv: [hep-th/0307170](https://arxiv.org/abs/hep-th/0307170).
- [43] Daniel Baumann et al. “Gravitational Wave Spectrum Induced by Primordial Scalar Perturbations”. In: *Phys. Rev. D* 76 (2007), p. 084019. DOI: [10.1103/PhysRevD.76.084019](https://doi.org/10.1103/PhysRevD.76.084019). arXiv: [hep-th/0703290](https://arxiv.org/abs/hep-th/0703290).
- [44] Fabio Finelli and Robert Brandenberger. “On the generation of a scale invariant spectrum of adiabatic fluctuations in cosmological models with a contracting phase”. In: *Phys. Rev. D* 65 (2002), p. 103522. DOI: [10.1103/PhysRevD.65.103522](https://doi.org/10.1103/PhysRevD.65.103522). arXiv: [hep-th/0112249](https://arxiv.org/abs/hep-th/0112249).
- [45] Robert Brandenberger and Patrick Peter. “Bouncing Cosmologies: Progress and Problems”. In: *Found. Phys.* 47.6 (2017), pp. 797–850. DOI: [10.1007/s10701-016-0057-0](https://doi.org/10.1007/s10701-016-0057-0). arXiv: [1603.05834](https://arxiv.org/abs/1603.05834) [hep-th].
- [46] David Wands. “Duality invariance of cosmological perturbation spectra”. In: *Phys. Rev. D* 60 (1999), p. 023507. DOI: [10.1103/PhysRevD.60.023507](https://doi.org/10.1103/PhysRevD.60.023507). arXiv: [gr-qc/9809062](https://arxiv.org/abs/gr-qc/9809062).
- [47] M. Gasperini and G. Veneziano. “Pre - big bang in string cosmology”. In: *Astropart. Phys.* 1 (1993), pp. 317–339. DOI: [10.1016/0927-6505\(93\)90017-8](https://doi.org/10.1016/0927-6505(93)90017-8). arXiv: [hep-th/9211021](https://arxiv.org/abs/hep-th/9211021).
- [48] James E. Lidsey, David Wands, and Edmund J. Copeland. “Superstring cosmology”. In: *Phys. Rept.* 337 (2000), pp. 343–492. DOI: [10.1016/S0370-1573\(00\)00064-8](https://doi.org/10.1016/S0370-1573(00)00064-8). arXiv: [hep-th/9909061](https://arxiv.org/abs/hep-th/9909061).
- [49] M. Gasperini and G. Veneziano. “The Pre - big bang scenario in string cosmology”. In: *Phys. Rept.* 373 (2003), pp. 1–212. DOI: [10.1016/S0370-1573\(02\)00389-7](https://doi.org/10.1016/S0370-1573(02)00389-7). arXiv: [hep-th/0207130](https://arxiv.org/abs/hep-th/0207130).
- [50] Justin Khoury et al. “The Ekpyrotic universe: Colliding branes and the origin of the hot big bang”. In: *Phys. Rev. D* 64 (2001), p. 123522. DOI: [10.1103/PhysRevD.64.123522](https://doi.org/10.1103/PhysRevD.64.123522). arXiv: [hep-th/0103239](https://arxiv.org/abs/hep-th/0103239).
- [51] Rathul Nath Raveendran and L. Sriramkumar. “Primordial features from ekpyrotic bounces”. In: *Phys. Rev. D* 99.4 (2019), p. 043527. DOI: [10.1103/PhysRevD.99.043527](https://doi.org/10.1103/PhysRevD.99.043527). arXiv: [1809.03229](https://arxiv.org/abs/1809.03229) [astro-ph.CO].
- [52] Rathul Nath Raveendran, Debika Chowdhury, and L. Sriramkumar. “Viable tensor-to-scalar ratio in a symmetric matter bounce”. In: *JCAP* 01 (2018), p. 030. DOI: [10.1088/1475-7516/2018/01/030](https://doi.org/10.1088/1475-7516/2018/01/030). arXiv: [1703.10061](https://arxiv.org/abs/1703.10061) [gr-qc].

- [53] Aaron M. Levy, Anna Ijjas, and Paul J. Steinhardt. “Scale-invariant perturbations in ekpyrotic cosmologies without fine-tuning of initial conditions”. In: *Phys. Rev. D* 92.6 (2015), p. 063524. DOI: [10.1103/PhysRevD.92.063524](https://doi.org/10.1103/PhysRevD.92.063524). arXiv: [1506.01011](https://arxiv.org/abs/1506.01011) [[astro-ph.CO](#)].
- [54] Anna Ijjas, Jean-Luc Lehners, and Paul J. Steinhardt. “General mechanism for producing scale-invariant perturbations and small non-Gaussianity in ekpyrotic models”. In: *Phys. Rev. D* 89.12 (2014), p. 123520. DOI: [10.1103/PhysRevD.89.123520](https://doi.org/10.1103/PhysRevD.89.123520). arXiv: [1404.1265](https://arxiv.org/abs/1404.1265) [[astro-ph.CO](#)].
- [55] Robert H. Brandenberger and C. Vafa. “Superstrings in the Early Universe”. In: *Nucl. Phys. B* 316 (1989), pp. 391–410. DOI: [10.1016/0550-3213\(89\)90037-0](https://doi.org/10.1016/0550-3213(89)90037-0).
- [56] Robert H. Brandenberger. “String Gas Cosmology: Progress and Problems”. In: *Class. Quant. Grav.* 28 (2011), p. 204005. DOI: [10.1088/0264-9381/28/20/204005](https://doi.org/10.1088/0264-9381/28/20/204005). arXiv: [1105.3247](https://arxiv.org/abs/1105.3247) [[hep-th](#)].
- [57] Robert H. Brandenberger. “String Gas Cosmology”. In: Aug. 2008. arXiv: [0808.0746](https://arxiv.org/abs/0808.0746) [[hep-th](#)].
- [58] Massimo Giovannini. “Stochastic gravitational waves backgrounds: a probe for inflationary and non-inflationary cosmology”. In: *3rd International Conference on Particle Physics and the Early Universe*. 2000, pp. 167–173. DOI: [10.1142/9789812792129\\_0024](https://doi.org/10.1142/9789812792129_0024). arXiv: [hep-ph/9912480](https://arxiv.org/abs/hep-ph/9912480).
- [59] Md Riajul Haque et al. “Decoding the phases of early and late time reheating through imprints on primordial gravitational waves”. In: *Phys. Rev. D* 104.6 (2021), p. 063513. DOI: [10.1103/PhysRevD.104.063513](https://doi.org/10.1103/PhysRevD.104.063513). arXiv: [2105.09242](https://arxiv.org/abs/2105.09242) [[astro-ph.CO](#)].
- [60] Massimo Giovannini. “Primordial backgrounds of relic gravitons”. In: *Prog. Part. Nucl. Phys.* 112 (2020), p. 103774. DOI: [10.1016/j.pnpnp.2020.103774](https://doi.org/10.1016/j.pnpnp.2020.103774). arXiv: [1912.07065](https://arxiv.org/abs/1912.07065) [[astro-ph.CO](#)].
- [61] Chiara Caprini and Daniel G. Figueroa. “Cosmological Backgrounds of Gravitational Waves”. In: *Class. Quant. Grav.* 35.16 (2018), p. 163001. DOI: [10.1088/1361-6382/aac608](https://doi.org/10.1088/1361-6382/aac608). arXiv: [1801.04268](https://arxiv.org/abs/1801.04268) [[astro-ph.CO](#)].
- [62] M. C. Guzzetti et al. “Gravitational waves from inflation”. In: *Riv. Nuovo Cim.* 39.9 (2016), pp. 399–495. DOI: [10.1393/ncr/i2016-10127-1](https://doi.org/10.1393/ncr/i2016-10127-1). arXiv: [1605.01615](https://arxiv.org/abs/1605.01615) [[astro-ph.CO](#)].
- [63] Yu-Tong Wang et al. “Probing the primordial universe with gravitational waves detectors”. In: *JCAP* 01 (2017), p. 010. DOI: [10.1088/1475-7516/2017/01/010](https://doi.org/10.1088/1475-7516/2017/01/010). arXiv: [1612.05088](https://arxiv.org/abs/1612.05088) [[astro-ph.CO](#)].
- [64] Paolo Campeti et al. “Measuring the spectrum of primordial gravitational waves with CMB, PTA and Laser Interferometers”. In: *JCAP* 01 (2021), p. 012. DOI: [10.1088/1475-7516/2021/01/012](https://doi.org/10.1088/1475-7516/2021/01/012). arXiv: [2007.04241](https://arxiv.org/abs/2007.04241) [[astro-ph.CO](#)].
- [65] Benjamin Racine et al. “Measurements of Degree-Scale B-mode Polarization with the BICEP/Keck Experiments at South Pole”. In: *53rd Rencontres de Moriond on Cosmology*. 2018, pp. 113–120. arXiv: [1807.02199](https://arxiv.org/abs/1807.02199) [[astro-ph.CO](#)].
- [66] M. Hazumi et al. “LiteBIRD: A Satellite for the Studies of B-Mode Polarization and Inflation from Cosmic Background Radiation Detection”. In: *J. Low Temp. Phys.* 194.5-6 (2019), pp. 443–452. DOI: [10.1007/s10909-019-02150-5](https://doi.org/10.1007/s10909-019-02150-5).
- [67] A. Suzuki et al. “The POLARBEAR-2 and the Simons Array Experiment”. In: *J. Low Temp. Phys.* 184.3-4 (2016). Ed. by Philippe Camus, Alexandre Juillard, and Alessandro Monfardini, pp. 805–810. DOI: [10.1007/s10909-015-1425-4](https://doi.org/10.1007/s10909-015-1425-4). arXiv: [1512.07299](https://arxiv.org/abs/1512.07299) [[astro-ph.IM](#)].
- [68] Uros Seljak and Matias Zaldarriaga. “Signature of gravity waves in polarization of the microwave background”. In: *Phys. Rev. Lett.* 78 (1997), pp. 2054–2057. DOI: [10.1103/PhysRevLett.78.2054](https://doi.org/10.1103/PhysRevLett.78.2054). arXiv: [astro-ph/9609169](https://arxiv.org/abs/astro-ph/9609169).

- [69] Sachiko Kuroyanagi et al. “Implications of the B-mode Polarization Measurement for Direct Detection of Inflationary Gravitational Waves”. In: *Phys. Rev. D* 90.6 (2014), p. 063513. DOI: [10.1103/PhysRevD.90.063513](https://doi.org/10.1103/PhysRevD.90.063513). arXiv: [1406.1369](https://arxiv.org/abs/1406.1369) [astro-ph.CO].
- [70] Gabriella Agazie et al. “The NANOGrav 15 yr Data Set: Evidence for a Gravitational-wave Background”. In: *Astrophys. J. Lett.* 951.1 (2023), p. L8. DOI: [10.3847/2041-8213/acdac6](https://doi.org/10.3847/2041-8213/acdac6). arXiv: [2306.16213](https://arxiv.org/abs/2306.16213) [astro-ph.HE].
- [71] Gabriella Agazie et al. “The NANOGrav 15 yr Data Set: Search for Anisotropy in the Gravitational-wave Background”. In: *Astrophys. J. Lett.* 956.1 (2023), p. L3. DOI: [10.3847/2041-8213/acf4fd](https://doi.org/10.3847/2041-8213/acf4fd). arXiv: [2306.16221](https://arxiv.org/abs/2306.16221) [astro-ph.HE].
- [72] Gabriella Agazie et al. “The NANOGrav 15 yr Data Set: Observations and Timing of 68 Millisecond Pulsars”. In: *Astrophys. J. Lett.* 951.1 (2023), p. L9. DOI: [10.3847/2041-8213/acda9a](https://doi.org/10.3847/2041-8213/acda9a). arXiv: [2306.16217](https://arxiv.org/abs/2306.16217) [astro-ph.HE].
- [73] J. Antoniadis et al. “The second data release from the European Pulsar Timing Array - III. Search for gravitational wave signals”. In: *Astron. Astrophys.* 678 (2023), A50. DOI: [10.1051/0004-6361/202346844](https://doi.org/10.1051/0004-6361/202346844). arXiv: [2306.16214](https://arxiv.org/abs/2306.16214) [astro-ph.HE].
- [74] J. Antoniadis et al. “The second data release from the European Pulsar Timing Array - I. The dataset and timing analysis”. In: *Astron. Astrophys.* 678 (2023), A48. DOI: [10.1051/0004-6361/202346841](https://doi.org/10.1051/0004-6361/202346841). arXiv: [2306.16224](https://arxiv.org/abs/2306.16224) [astro-ph.HE].
- [75] J. Antoniadis et al. “The second data release from the European Pulsar Timing Array V. Search for continuous gravitational wave signals”. In: (June 2023). arXiv: [2306.16226](https://arxiv.org/abs/2306.16226) [astro-ph.HE].
- [76] G. Agazie et al. “Comparing Recent Pulsar Timing Array Results on the Nanohertz Stochastic Gravitational-wave Background”. In: *Astrophys. J.* 966.1 (2024), p. 105. DOI: [10.3847/1538-4357/ad36be](https://doi.org/10.3847/1538-4357/ad36be). arXiv: [2309.00693](https://arxiv.org/abs/2309.00693) [astro-ph.HE].
- [77] Adeela Afzal et al. “The NANOGrav 15 yr Data Set: Search for Signals from New Physics”. In: *Astrophys. J. Lett.* 951.1 (2023), p. L11. DOI: [10.3847/2041-8213/acdc91](https://doi.org/10.3847/2041-8213/acdc91). arXiv: [2306.16219](https://arxiv.org/abs/2306.16219) [astro-ph.HE].
- [78] J. Antoniadis et al. “The second data release from the European Pulsar Timing Array: V. Implications for massive black holes, dark matter and the early Universe”. In: (June 2023). arXiv: [2306.16227](https://arxiv.org/abs/2306.16227) [astro-ph.CO].
- [79] J. Aasi et al. “Advanced LIGO”. In: *Class. Quant. Grav.* 32 (2015), p. 074001. DOI: [10.1088/0264-9381/32/7/074001](https://doi.org/10.1088/0264-9381/32/7/074001). arXiv: [1411.4547](https://arxiv.org/abs/1411.4547) [gr-qc].
- [80] Nina Bode et al. “Advanced LIGO Laser Systems for O3 and Future Observation Runs”. In: *Galaxies* 8.4 (2020), p. 84. DOI: [10.3390/galaxies8040084](https://doi.org/10.3390/galaxies8040084).
- [81] F. Acernese et al. “Advanced Virgo: a second-generation interferometric gravitational wave detector”. In: *Class. Quant. Grav.* 32.2 (2015), p. 024001. DOI: [10.1088/0264-9381/32/2/024001](https://doi.org/10.1088/0264-9381/32/2/024001). arXiv: [1408.3978](https://arxiv.org/abs/1408.3978) [gr-qc].
- [82] T. Akutsu et al. “KAGRA: 2.5 Generation Interferometric Gravitational Wave Detector”. In: *Nature Astron.* 3.1 (2019), pp. 35–40. DOI: [10.1038/s41550-018-0658-y](https://doi.org/10.1038/s41550-018-0658-y). arXiv: [1811.08079](https://arxiv.org/abs/1811.08079) [gr-qc].
- [83] Pau Amaro-Seoane et al. “Laser Interferometer Space Antenna”. In: (Feb. 2017). arXiv: [1702.00786](https://arxiv.org/abs/1702.00786) [astro-ph.IM].
- [84] Jean-Baptiste Bayle et al. “Overview and progress on the Laser Interferometer Space Antenna mission”. In: *Nature Astron.* 6.12 (2022), pp. 1334–1338. DOI: [10.1038/s41550-022-01847-0](https://doi.org/10.1038/s41550-022-01847-0).
- [85] Pierre Auclair et al. “Cosmology with the Laser Interferometer Space Antenna”. In: *Living Rev. Rel.* 26.1 (2023), p. 5. DOI: [10.1007/s41114-023-00045-2](https://doi.org/10.1007/s41114-023-00045-2). arXiv: [2204.05434](https://arxiv.org/abs/2204.05434) [astro-ph.CO].

- [86] David Reitze et al. “Cosmic Explorer: The U.S. Contribution to Gravitational-Wave Astronomy beyond LIGO”. In: *Bull. Am. Astron. Soc.* 51.7 (2019), p. 035. arXiv: [1907.04833 \[astro-ph.IM\]](#).
- [87] Eugenio Coccia. “The Einstein Telescope”. In: *PoS ICRC2023* (2024), p. 1591. DOI: [10.22323/1.444.1591](#).
- [88] G. M. Harry et al. “Laser interferometry for the big bang observer”. In: *Class. Quant. Grav.* 23 (2006). [Erratum: *Class.Quant.Grav.* 23, 7361 (2006)], pp. 4887–4894. DOI: [10.1088/0264-9381/23/15/008](#).
- [89] Shuichi Sato et al. “DECIGO: The Japanese space gravitational wave antenna”. In: *J. Phys. Conf. Ser.* 154 (2009). Ed. by Alberto Lobo and Carlos F. Sopuerta, p. 012040. DOI: [10.1088/1742-6596/154/1/012040](#).
- [90] Seiji Kawamura. “Primordial gravitational wave and DECIGO”. In: *PoS KMI2019* (2019), p. 019. DOI: [10.22323/1.356.0019](#).
- [91] Michael S. Turner. “Coherent Scalar Field Oscillations in an Expanding Universe”. In: *Phys. Rev. D* 28 (1983), p. 1243. DOI: [10.1103/PhysRevD.28.1243](#).
- [92] Lev Kofman, Andrei Linde, and Alexei A. Starobinsky. “Reheating after Inflation”. In: *Physical Review Letters* 73.24 (Dec. 1994), pp. 3195–3198. ISSN: 0031-9007. DOI: [10.1103/physrevlett.73.3195](#). URL: <http://dx.doi.org/10.1103/PhysRevLett.73.3195>.
- [93] Y. Shtanov, Jennie H. Traschen, and Robert H. Brandenberger. “Universe reheating after inflation”. In: *Phys. Rev. D* 51 (1995), pp. 5438–5455. DOI: [10.1103/PhysRevD.51.5438](#). arXiv: [hep-ph/9407247](#).
- [94] Lev Kofman, Andrei D. Linde, and Alexei A. Starobinsky. “Towards the theory of reheating after inflation”. In: *Phys. Rev. D* 56 (1997), pp. 3258–3295. DOI: [10.1103/PhysRevD.56.3258](#). arXiv: [hep-ph/9704452](#).
- [95] Lev A. Kofman. “The Origin of matter in the universe: Reheating after inflation”. In: May 1996. arXiv: [astro-ph/9605155](#).
- [96] Kaloian D. Lozanov. “Lectures on Reheating after Inflation”. In: (July 2019). arXiv: [1907.04402 \[astro-ph.CO\]](#).
- [97] Mustafa A. Amin et al. “Oscillons After Inflation”. In: *Phys. Rev. Lett.* 108 (2012), p. 241302. DOI: [10.1103/PhysRevLett.108.241302](#). arXiv: [1106.3335 \[astro-ph.CO\]](#).
- [98] Kaloian D. Lozanov and Mustafa A. Amin. “Self-resonance after inflation: oscillons, transients and radiation domination”. In: *Phys. Rev. D* 97.2 (2018), p. 023533. DOI: [10.1103/PhysRevD.97.023533](#). arXiv: [1710.06851 \[astro-ph.CO\]](#).
- [99] Rafid Mahbub and Swagat S. Mishra. “Oscillon formation from preheating in asymmetric inflationary potentials”. In: *Phys. Rev. D* 108.6 (2023), p. 063524. DOI: [10.1103/PhysRevD.108.063524](#). arXiv: [2303.07503 \[astro-ph.CO\]](#).
- [100] Mohammed Shafi et al. “Formation and decay of oscillons after inflation in the presence of an external coupling, Part-I: Lattice simulations”. In: (May 2024). arXiv: [2406.00108 \[hep-ph\]](#).
- [101] Leonard Parker. “Quantized fields and particle creation in expanding universes. 1.” In: *Phys. Rev.* 183 (1969), pp. 1057–1068. DOI: [10.1103/PhysRev.183.1057](#).
- [102] Gary N. Felder, Lev Kofman, and Andrei D. Linde. “Instant preheating”. In: *Phys. Rev. D* 59 (1999), p. 123523. DOI: [10.1103/PhysRevD.59.123523](#). arXiv: [hep-ph/9812289](#).
- [103] Stefan Antusch et al. “Energy distribution and equation of state of the early Universe: matching the end of inflation and the onset of radiation domination”. In: *Phys. Lett. B* 811 (2020), p. 135888. DOI: [10.1016/j.physletb.2020.135888](#). arXiv: [2005.07563 \[astro-ph.CO\]](#).

- [104] Stefan Antusch et al. “Characterizing the postinflationary reheating history: Single daughter field with quadratic-quadratic interaction”. In: *Phys. Rev. D* 105.4 (2022), p. 043532. DOI: [10.1103/PhysRevD.105.043532](https://doi.org/10.1103/PhysRevD.105.043532). arXiv: [2112.11280](https://arxiv.org/abs/2112.11280) [[astro-ph.CO](#)].
- [105] Stefan Antusch, Kenneth Marschall, and Francisco Torrenti. “Characterizing the post-inflationary reheating history. Part II. Multiple interacting daughter fields”. In: *JCAP* 02 (2023), p. 019. DOI: [10.1088/1475-7516/2023/02/019](https://doi.org/10.1088/1475-7516/2023/02/019). arXiv: [2206.06319](https://arxiv.org/abs/2206.06319) [[astro-ph.CO](#)].
- [106] Daniel G. Figueroa et al. “Spectroscopy of particle couplings with gravitational waves”. In: *Phys. Rev. D* 106.6 (2022), p. 063522. DOI: [10.1103/PhysRevD.106.063522](https://doi.org/10.1103/PhysRevD.106.063522). arXiv: [2202.05805](https://arxiv.org/abs/2202.05805) [[astro-ph.CO](#)].
- [107] Rouzbeh Allahverdi et al. “The First Three Seconds: a Review of Possible Expansion Histories of the Early Universe”. In: (June 2020). DOI: [10.21105/astro.2006.16182](https://doi.org/10.21105/astro.2006.16182). arXiv: [2006.16182](https://arxiv.org/abs/2006.16182) [[astro-ph.CO](#)].
- [108] Kaloian D. Lozanov and Mustafa A. Amin. “Equation of State and Duration to Radiation Domination after Inflation”. In: *Phys. Rev. Lett.* 119.6 (2017), p. 061301. DOI: [10.1103/PhysRevLett.119.061301](https://doi.org/10.1103/PhysRevLett.119.061301). arXiv: [1608.01213](https://arxiv.org/abs/1608.01213) [[astro-ph.CO](#)].
- [109] Mustafa A. Amin et al. “Nonperturbative Dynamics Of Reheating After Inflation: A Review”. In: *Int. J. Mod. Phys. D* 24 (2014), p. 1530003. DOI: [10.1142/S0218271815300037](https://doi.org/10.1142/S0218271815300037). arXiv: [1410.3808](https://arxiv.org/abs/1410.3808) [[hep-ph](#)].
- [110] Kaloian D. Lozanov. *Lectures on Reheating after Inflation*. 2019. arXiv: [1907.04402](https://arxiv.org/abs/1907.04402) [[astro-ph.CO](#)].
- [111] Kaloian D. Lozanov and Mustafa A. Amin. “Self-resonance after inflation: Oscillons, transients, and radiation domination”. In: *Physical Review D* 97.2 (Jan. 2018). ISSN: 2470-0029. DOI: [10.1103/physrevd.97.023533](https://doi.org/10.1103/physrevd.97.023533). URL: <http://dx.doi.org/10.1103/PhysRevD.97.023533>.
- [112] Kaloian D. Lozanov and Mustafa A. Amin. “Gravitational perturbations from oscillons and transients after inflation”. In: *Phys. Rev. D* 99.12 (2019), p. 123504. DOI: [10.1103/PhysRevD.99.123504](https://doi.org/10.1103/PhysRevD.99.123504). arXiv: [1902.06736](https://arxiv.org/abs/1902.06736) [[astro-ph.CO](#)].
- [113] Kaloian D. Lozanov and Volodymyr Takhistov. “Enhanced Gravitational Waves from Inflaton Oscillons”. In: *Phys. Rev. Lett.* 130.18 (2023), p. 181002. DOI: [10.1103/PhysRevLett.130.181002](https://doi.org/10.1103/PhysRevLett.130.181002). arXiv: [2204.07152](https://arxiv.org/abs/2204.07152) [[astro-ph.CO](#)].
- [114] Steven Weinberg. “Damping of tensor modes in cosmology”. In: *Phys. Rev. D* 69 (2004), p. 023503. DOI: [10.1103/PhysRevD.69.023503](https://doi.org/10.1103/PhysRevD.69.023503). arXiv: [astro-ph/0306304](https://arxiv.org/abs/astro-ph/0306304).
- [115] Dominik J. Schwarz. “Evolution of gravitational waves through cosmological transitions”. In: *Mod. Phys. Lett. A* 13 (1998), pp. 2771–2778. DOI: [10.1142/S0217732398002941](https://doi.org/10.1142/S0217732398002941). arXiv: [gr-qc/9709027](https://arxiv.org/abs/gr-qc/9709027).
- [116] Yuki Watanabe and Eiichiro Komatsu. “Improved Calculation of the Primordial Gravitational Wave Spectrum in the Standard Model”. In: *Phys. Rev. D* 73 (2006), p. 123515. DOI: [10.1103/PhysRevD.73.123515](https://doi.org/10.1103/PhysRevD.73.123515). arXiv: [astro-ph/0604176](https://arxiv.org/abs/astro-ph/0604176).
- [117] Sachiko Kuroyanagi, Takeshi Chiba, and Naoshi Sugiyama. “Precision calculations of the gravitational wave background spectrum from inflation”. In: *Phys. Rev. D* 79 (2009), p. 103501. DOI: [10.1103/PhysRevD.79.103501](https://doi.org/10.1103/PhysRevD.79.103501). arXiv: [0804.3249](https://arxiv.org/abs/0804.3249) [[astro-ph](#)].
- [118] Jerome Martin, Christophe Ringeval, and Vincent Vennin. “Observing Inflationary Reheating”. In: *Phys. Rev. Lett.* 114.8 (2015), p. 081303. DOI: [10.1103/PhysRevLett.114.081303](https://doi.org/10.1103/PhysRevLett.114.081303). arXiv: [1410.7958](https://arxiv.org/abs/1410.7958) [[astro-ph.CO](#)].
- [119] Daniel G. Figueroa and Erwin H. Tanin. “Ability of LIGO and LISA to probe the equation of state of the early Universe”. In: *JCAP* 08 (2019), p. 011. DOI: [10.1088/1475-7516/2019/08/011](https://doi.org/10.1088/1475-7516/2019/08/011). arXiv: [1905.11960](https://arxiv.org/abs/1905.11960) [[astro-ph.CO](#)].



- [120] Massimo Giovannini. “Inflation, space-borne interferometers and the expansion history of the Universe”. In: *Eur. Phys. J. C* 82.9 (2022), p. 828. DOI: [10.1140/epjc/s10052-022-10800-4](https://doi.org/10.1140/epjc/s10052-022-10800-4). arXiv: [2206.08217](https://arxiv.org/abs/2206.08217) [gr-qc].
- [121] Massimo Giovannini. “Relic gravitons at intermediate frequencies and the expansion history of the Universe”. In: *Phys. Rev. D* 105.10 (2022), p. 103524. DOI: [10.1103/PhysRevD.105.103524](https://doi.org/10.1103/PhysRevD.105.103524). arXiv: [2203.13586](https://arxiv.org/abs/2203.13586) [gr-qc].
- [122] Sunny Vagnozzi. “Implications of the NANOGrav results for inflation”. In: *Mon. Not. Roy. Astron. Soc.* 502.1 (2021), pp. L11–L15. DOI: [10.1093/mnrasl/slaa203](https://doi.org/10.1093/mnrasl/slaa203). arXiv: [2009.13432](https://arxiv.org/abs/2009.13432) [astro-ph.CO].
- [123] Micol Benetti, Leila Lobato Graef, and Sunny Vagnozzi. “Primordial gravitational waves from NANOGrav: A broken power-law approach”. In: *Phys. Rev. D* 105.4 (2022), p. 043520. DOI: [10.1103/PhysRevD.105.043520](https://doi.org/10.1103/PhysRevD.105.043520). arXiv: [2111.04758](https://arxiv.org/abs/2111.04758) [astro-ph.CO].
- [124] Sunny Vagnozzi. “Inflationary interpretation of the stochastic gravitational wave background signal detected by pulsar timing array experiments”. In: *JHEAp* 39 (2023), pp. 81–98. DOI: [10.1016/j.jheap.2023.07.001](https://doi.org/10.1016/j.jheap.2023.07.001). arXiv: [2306.16912](https://arxiv.org/abs/2306.16912) [astro-ph.CO].
- [125] Basabendu Barman et al. “Gravity as a portal to reheating, leptogenesis and dark matter”. In: *JHEP* 12 (2022), p. 072. DOI: [10.1007/JHEP12\(2022\)072](https://doi.org/10.1007/JHEP12(2022)072). arXiv: [2210.05716](https://arxiv.org/abs/2210.05716) [hep-ph].
- [126] Basabendu Barman et al. “Gravitational wave from graviton Bremsstrahlung during reheating”. In: *JCAP* 05 (2023), p. 019. DOI: [10.1088/1475-7516/2023/05/019](https://doi.org/10.1088/1475-7516/2023/05/019). arXiv: [2301.11345](https://arxiv.org/abs/2301.11345) [hep-ph].
- [127] Basabendu Barman et al. “Measuring inflaton couplings via primordial gravitational waves”. In: *JHEP* 07 (2023), p. 231. DOI: [10.1007/JHEP07\(2023\)231](https://doi.org/10.1007/JHEP07(2023)231). arXiv: [2305.00027](https://arxiv.org/abs/2305.00027) [hep-ph].
- [128] Basabendu Barman et al. “Bremsstrahlung-induced gravitational waves in monomial potentials during reheating”. In: *Phys. Rev. D* 108.8 (2023), p. 083524. DOI: [10.1103/PhysRevD.108.083524](https://doi.org/10.1103/PhysRevD.108.083524). arXiv: [2305.16388](https://arxiv.org/abs/2305.16388) [hep-ph].
- [129] Basabendu Barman, Nicolás Bernal, and Yong Xu. “Resonant Reheating”. In: (Apr. 2024). arXiv: [2404.16090](https://arxiv.org/abs/2404.16090) [hep-ph].
- [130] Kin-Wang Ng. “Graviton mode function in inflationary cosmology”. In: *Int. J. Mod. Phys. A* 11 (1996), pp. 3175–3193. DOI: [10.1142/S0217751X96001528](https://doi.org/10.1142/S0217751X96001528). arXiv: [gr-qc/9311002](https://arxiv.org/abs/gr-qc/9311002).
- [131] Yann Gouttenoire, Geraldine Servant, and Peera Simakachorn. “Kination cosmology from scalar fields and gravitational-wave signatures”. In: (Nov. 2021). arXiv: [2111.01150](https://arxiv.org/abs/2111.01150) [hep-ph].
- [132] Yann Gouttenoire, Géraldine Servant, and Peera Simakachorn. “Revealing the Primordial Irreducible Inflationary Gravitational-Wave Background with a Spinning Peccei-Quinn Axion”. In: (Aug. 2021). arXiv: [2108.10328](https://arxiv.org/abs/2108.10328) [hep-ph].
- [133] Yann Gouttenoire, Géraldine Servant, and Peera Simakachorn. “Beyond the Standard Models with Cosmic Strings”. In: *JCAP* 07 (2020), p. 032. DOI: [10.1088/1475-7516/2020/07/032](https://doi.org/10.1088/1475-7516/2020/07/032). arXiv: [1912.02569](https://arxiv.org/abs/1912.02569) [hep-ph].
- [134] Yann Gouttenoire, Géraldine Servant, and Peera Simakachorn. “BSM with Cosmic Strings: Heavy, up to EeV mass, Unstable Particles”. In: *JCAP* 07 (2020), p. 016. DOI: [10.1088/1475-7516/2020/07/016](https://doi.org/10.1088/1475-7516/2020/07/016). arXiv: [1912.03245](https://arxiv.org/abs/1912.03245) [hep-ph].
- [135] Nathalie Deruelle and Viatcheslav F. Mukhanov. “On matching conditions for cosmological perturbations”. In: *Phys. Rev. D* 52 (1995), pp. 5549–5555. DOI: [10.1103/PhysRevD.52.5549](https://doi.org/10.1103/PhysRevD.52.5549). arXiv: [gr-qc/9503050](https://arxiv.org/abs/gr-qc/9503050).
- [136] Swagat S. Mishra, Edmund J. Copeland, and Anne M. Green. “Primordial black holes and stochastic inflation beyond slow roll. Part I. Noise matrix elements”. In: *JCAP* 09 (2023), p. 005. DOI: [10.1088/1475-7516/2023/09/005](https://doi.org/10.1088/1475-7516/2023/09/005). arXiv: [2303.17375](https://arxiv.org/abs/2303.17375) [astro-ph.CO].

- [137] Fien Apers et al. “String Theory and the First Half of the Universe”. In: (Jan. 2024). arXiv: [2401.04064](https://arxiv.org/abs/2401.04064) [[hep-th](#)].
- [138] Juan Martin Maldacena. “Non-Gaussian features of primordial fluctuations in single field inflationary models”. In: *JHEP* 05 (2003), p. 013. DOI: [10.1088/1126-6708/2003/05/013](https://doi.org/10.1088/1126-6708/2003/05/013). arXiv: [astro-ph/0210603](https://arxiv.org/abs/astro-ph/0210603).
- [139] Daniel Baumann. *TASI Lectures on Inflation*. 2012. arXiv: [0907.5424](https://arxiv.org/abs/0907.5424) [[hep-th](#)].
- [140] Sandipan Kundu. “Inflation with general initial conditions for scalar perturbations”. In: *Journal of Cosmology and Astroparticle Physics* 2012.02 (Feb. 2012), pp. 005–005. ISSN: 1475-7516. DOI: [10.1088/1475-7516/2012/02/005](https://doi.org/10.1088/1475-7516/2012/02/005). URL: <http://dx.doi.org/10.1088/1475-7516/2012/02/005>.
- [141] *NIST Digital Library of Mathematical Functions*. <https://dlmf.nist.gov/>, Release 1.1.12 of 2023-12-15. F. W. J. Olver, A. B. Olde Daalhuis, D. W. Lozier, B. I. Schneider, R. F. Boisvert, C. W. Clark, B. R. Miller, B. V. Saunders, H. S. Cohl, and M. A. McClain, eds. URL: <https://dlmf.nist.gov/>.
- [142] Y. Akrami et al. “Planck 2018 results. IX. Constraints on primordial non-Gaussianity”. In: *Astron. Astrophys.* 641 (2020), A9. DOI: [10.1051/0004-6361/201935891](https://doi.org/10.1051/0004-6361/201935891). arXiv: [1905.05697](https://arxiv.org/abs/1905.05697) [[astro-ph.CO](#)].
- [143] Anna Negro and Subodh P. Patil. “An Étude on the Regularization and Renormalization of Divergences in Primordial Observables”. In: (Feb. 2024). DOI: [10.1007/s40766-024-00053-0](https://doi.org/10.1007/s40766-024-00053-0). arXiv: [2402.10008](https://arxiv.org/abs/2402.10008) [[hep-th](#)].
- [144] Anna Negro and Subodh P. Patil. “Hadamard Regularization of the Graviton Stress Tensor”. In: (Mar. 2024). arXiv: [2403.16806](https://arxiv.org/abs/2403.16806) [[hep-th](#)].
- [145] Kazunori Kohri and Takahiro Terada. “Semianalytic calculation of gravitational wave spectrum nonlinearly induced from primordial curvature perturbations”. In: *Phys. Rev. D* 97.12 (2018), p. 123532. DOI: [10.1103/PhysRevD.97.123532](https://doi.org/10.1103/PhysRevD.97.123532). arXiv: [1804.08577](https://arxiv.org/abs/1804.08577) [[gr-qc](#)].
- [146] Massimo Giovannini. “Effective energy density of relic gravitons”. In: *Phys. Rev. D* 100.8 (2019), p. 083531. DOI: [10.1103/PhysRevD.100.083531](https://doi.org/10.1103/PhysRevD.100.083531). arXiv: [1908.09679](https://arxiv.org/abs/1908.09679) [[hep-th](#)].
- [147] Latham A. Boyle and Paul J. Steinhardt. “Probing the early universe with inflationary gravitational waves”. In: *Phys. Rev. D* 77 (2008), p. 063504. DOI: [10.1103/PhysRevD.77.063504](https://doi.org/10.1103/PhysRevD.77.063504). arXiv: [astro-ph/0512014](https://arxiv.org/abs/astro-ph/0512014).
- [148] Massimo Giovannini. “Relic gravitons and high-frequency detectors”. In: *JCAP* 05 (2023), p. 056. DOI: [10.1088/1475-7516/2023/05/056](https://doi.org/10.1088/1475-7516/2023/05/056). arXiv: [2303.11928](https://arxiv.org/abs/2303.11928) [[gr-qc](#)].
- [149] Dieter R. Brill and James B. Hartle. “Method of the Self-Consistent Field in General Relativity and its Application to the Gravitational Geon”. In: *Phys. Rev.* 135 (1964), B271–B278. DOI: [10.1103/PhysRev.135.B271](https://doi.org/10.1103/PhysRev.135.B271).
- [150] Richard A. Isaacson. “Gravitational Radiation in the Limit of High Frequency. II. Nonlinear Terms and the Effective Stress Tensor”. In: *Phys. Rev.* 166 (1968), pp. 1272–1279. DOI: [10.1103/PhysRev.166.1272](https://doi.org/10.1103/PhysRev.166.1272).
- [151] Kai Schmitz. *New Sensitivity Curves for Gravitational-Wave Experiments*. Version v1. Zenodo, Feb. 2020. DOI: [10.5281/zenodo.3689582](https://doi.org/10.5281/zenodo.3689582). URL: <https://doi.org/10.5281/zenodo.3689582>.
- [152] Varun Sahni, M. Sami, and Tarun Souradeep. “Relic gravity waves from brane world inflation”. In: *Phys. Rev. D* 65 (2002), p. 023518. DOI: [10.1103/PhysRevD.65.023518](https://doi.org/10.1103/PhysRevD.65.023518). arXiv: [gr-qc/0105121](https://arxiv.org/abs/gr-qc/0105121).
- [153] Chao Chen et al. “Enhanced primordial gravitational waves from a stiff post-inflationary era due to an oscillating inflaton”. In: (May 2024). arXiv: [2405.01679](https://arxiv.org/abs/2405.01679) [[hep-ph](#)].

- [154] Richard H. Cyburt et al. “Big bang nucleosynthesis: Present status”. In: *Rev. Mod. Phys.* 88 (1 Feb. 2016), p. 015004. DOI: [10.1103/RevModPhys.88.015004](https://doi.org/10.1103/RevModPhys.88.015004). URL: <https://link.aps.org/doi/10.1103/RevModPhys.88.015004>.
- [155] Thomas Kite et al. “Bridging the gap: spectral distortions meet gravitational waves”. In: *Mon. Not. Roy. Astron. Soc.* 505.3 (2021), pp. 4396–4405. DOI: [10.1093/mnras/stab1558](https://doi.org/10.1093/mnras/stab1558). arXiv: [2010.00040](https://arxiv.org/abs/2010.00040) [astro-ph.CO].
- [156] Bryce Cyr et al. “Disentangling the primordial nature of stochastic gravitational wave backgrounds with CMB spectral distortions”. In: *Mon. Not. Roy. Astron. Soc.* 528.1 (2024), pp. 883–897. DOI: [10.1093/mnras/stad3861](https://doi.org/10.1093/mnras/stad3861). arXiv: [2309.02366](https://arxiv.org/abs/2309.02366) [astro-ph.CO].
- [157] Karsten Danzmann and LISA Team. “LISA - An ESA Cornerstone Mission for the Detection and Observation of Gravitational Waves”. In: *Advances in Space Research, v.32, 1233-1242 (2003)* 32 (Oct. 2003). DOI: [10.1016/S0273-1177\(03\)90323-1](https://doi.org/10.1016/S0273-1177(03)90323-1).
- [158] Seiji Kawamura et al. “The Japanese space gravitational wave antenna—DECIGO”. In: *Classical and Quantum Gravity* 23.8 (Apr. 2006), S125–S131. DOI: [10.1088/0264-9381/23/8/S17](https://doi.org/10.1088/0264-9381/23/8/S17).
- [159] Matthew Evans et al. “A Horizon Study for Cosmic Explorer: Science, Observatories, and Community”. In: (Sept. 2021). arXiv: [2109.09882](https://arxiv.org/abs/2109.09882) [astro-ph.IM].
- [160] Aniello Grado. “Einstein Telescope, the future generation of ground based gravitational wave detectors”. In: *Journal of Physics: Conference Series* 2429.1 (Feb. 2023), p. 012041. DOI: [10.1088/1742-6596/2429/1/012041](https://doi.org/10.1088/1742-6596/2429/1/012041). URL: <https://dx.doi.org/10.1088/1742-6596/2429/1/012041>.
- [161] D. V. Martynov et al. “Sensitivity of the Advanced LIGO detectors at the beginning of gravitational wave astronomy”. In: *Phys. Rev. D* 93 (11 June 2016), p. 112004. DOI: [10.1103/PhysRevD.93.112004](https://doi.org/10.1103/PhysRevD.93.112004). URL: <https://link.aps.org/doi/10.1103/PhysRevD.93.112004>.
- [162] B. Zwiebach. *A first course in string theory*. Cambridge University Press, July 2006. ISBN: 978-0-521-83143-7.
- [163] J. Polchinski. *String theory. Vol. 1: An introduction to the bosonic string*. Cambridge Monographs on Mathematical Physics. Cambridge University Press, Dec. 2007. ISBN: 978-0-511-25227-3. DOI: [10.1017/CB09780511816079](https://doi.org/10.1017/CB09780511816079).
- [164] David Tong. “String Theory”. In: (Jan. 2009). arXiv: [0908.0333](https://arxiv.org/abs/0908.0333) [hep-th].
- [165] Michele Cicoli et al. “String cosmology: From the early universe to today”. In: *Phys. Rept.* 1059 (2024), pp. 1–155. DOI: [10.1016/j.physrep.2024.01.002](https://doi.org/10.1016/j.physrep.2024.01.002). arXiv: [2303.04819](https://arxiv.org/abs/2303.04819) [hep-th].
- [166] Joseph P. Conlon. “String Theory and the Early Universe: Constraints and Opportunities”. In: *58th Rencontres de Moriond on Cosmology*. May 2024. arXiv: [2405.19118](https://arxiv.org/abs/2405.19118) [astro-ph.CO].
- [167] Edmund J. Copeland, Andrew R. Liddle, and David Wands. “Exponential potentials and cosmological scaling solutions”. In: *Phys. Rev. D* 57 (1998), pp. 4686–4690. DOI: [10.1103/PhysRevD.57.4686](https://doi.org/10.1103/PhysRevD.57.4686). arXiv: [gr-qc/9711068](https://arxiv.org/abs/gr-qc/9711068).
- [168] Ivaylo Zlatev, Li-Min Wang, and Paul J. Steinhardt. “Quintessence, cosmic coincidence, and the cosmological constant”. In: *Phys. Rev. Lett.* 82 (1999), pp. 896–899. DOI: [10.1103/PhysRevLett.82.896](https://doi.org/10.1103/PhysRevLett.82.896). arXiv: [astro-ph/9807002](https://arxiv.org/abs/astro-ph/9807002).
- [169] Varun Sahni and Li-Min Wang. “A New cosmological model of quintessence and dark matter”. In: *Phys. Rev. D* 62 (2000), p. 103517. DOI: [10.1103/PhysRevD.62.103517](https://doi.org/10.1103/PhysRevD.62.103517). arXiv: [astro-ph/9910097](https://arxiv.org/abs/astro-ph/9910097).
- [170] Swagat S. Mishra, Varun Sahni, and Yuri Shtanov. “Sourcing Dark Matter and Dark Energy from  $\alpha$ -attractors”. In: *JCAP* 06 (2017), p. 045. DOI: [10.1088/1475-7516/2017/06/045](https://doi.org/10.1088/1475-7516/2017/06/045). arXiv: [1703.03295](https://arxiv.org/abs/1703.03295) [gr-qc].

- [171] Satadru Bag, Swagat S. Mishra, and Varun Sahni. “New tracker models of dark energy”. In: *JCAP* 08 (2018), p. 009. DOI: [10.1088/1475-7516/2018/08/009](https://doi.org/10.1088/1475-7516/2018/08/009). arXiv: [1709.09193](https://arxiv.org/abs/1709.09193) [gr-qc].
- [172] Xiao-Jin Liu et al. “Detecting Relic Gravitational Waves by Pulsar Timing Arrays: Effects of Cosmic Phase Transitions and Relativistic Free-Streaming Gases”. In: *Phys. Rev. D* 93.2 (2016), p. 024031. DOI: [10.1103/PhysRevD.93.024031](https://doi.org/10.1103/PhysRevD.93.024031). arXiv: [1509.03524](https://arxiv.org/abs/1509.03524) [astro-ph.CO].
- [173] Nicolás Bernal and Fazlollah Hajkarim. “Primordial Gravitational Waves in Nonstandard Cosmologies”. In: *Phys. Rev. D* 100.6 (2019), p. 063502. DOI: [10.1103/PhysRevD.100.063502](https://doi.org/10.1103/PhysRevD.100.063502). arXiv: [1905.10410](https://arxiv.org/abs/1905.10410) [astro-ph.CO].
- [174] Nicolás Bernal et al. “Primordial Gravitational Wave Signals in Modified Cosmologies”. In: *JCAP* 11 (2020), p. 051. DOI: [10.1088/1475-7516/2020/11/051](https://doi.org/10.1088/1475-7516/2020/11/051). arXiv: [2008.04959](https://arxiv.org/abs/2008.04959) [gr-qc].
- [175] Chiara Caprini et al. “Primordial gravitational wave backgrounds from phase transitions with next generation ground based detectors”. In: (June 2024). arXiv: [2406.02359](https://arxiv.org/abs/2406.02359) [astro-ph.CO].
- [176] Matteo Braglia et al. “Gravitational waves from inflation in LISA: reconstruction pipeline and physics interpretation”. In: (July 2024). arXiv: [2407.04356](https://arxiv.org/abs/2407.04356) [astro-ph.CO].
- [177] Lev Kofman, Andrei D. Linde, and Alexei A. Starobinsky. “Reheating after inflation”. In: *Phys. Rev. Lett.* 73 (1994), pp. 3195–3198. DOI: [10.1103/PhysRevLett.73.3195](https://doi.org/10.1103/PhysRevLett.73.3195). arXiv: [hep-th/9405187](https://arxiv.org/abs/hep-th/9405187).
- [178] Kevork Abazajian et al. “CMB-S4: Forecasting Constraints on Primordial Gravitational Waves”. In: *Astrophys. J.* 926.1 (2022), p. 54. DOI: [10.3847/1538-4357/ac1596](https://doi.org/10.3847/1538-4357/ac1596). arXiv: [2008.12619](https://arxiv.org/abs/2008.12619) [astro-ph.CO].
- [179] D. Paoletti et al. “LiteBIRD Science Goals and Forecasts: Primordial Magnetic Fields”. In: (Mar. 2024). arXiv: [2403.16763](https://arxiv.org/abs/2403.16763) [astro-ph.CO].
- [180] Claudio Gatti, Luca Visinelli, and Michael Zantedeschi. “Cavity Detection of Gravitational Waves: Where Do We Stand?” In: (Mar. 2024). arXiv: [2403.18610](https://arxiv.org/abs/2403.18610) [gr-qc].
- [181] Sugumi Kanno, Jiro Soda, and Akira Taniguchi. “Search for high-frequency gravitational waves with Rydberg atoms”. In: (Nov. 2023). arXiv: [2311.03890](https://arxiv.org/abs/2311.03890) [gr-qc].
- [182] Asuka Ito and Jiro Soda. “Exploring high-frequency gravitational waves with magnons”. In: *Eur. Phys. J. C* 83.8 (2023), p. 766. DOI: [10.1140/epjc/s10052-023-11876-2](https://doi.org/10.1140/epjc/s10052-023-11876-2). arXiv: [2212.04094](https://arxiv.org/abs/2212.04094) [gr-qc].
- [183] Nancy Aggarwal et al. “Challenges and opportunities of gravitational-wave searches at MHz to GHz frequencies”. In: *Living Rev. Rel.* 24.1 (2021), p. 4. DOI: [10.1007/s41114-021-00032-5](https://doi.org/10.1007/s41114-021-00032-5). arXiv: [2011.12414](https://arxiv.org/abs/2011.12414) [gr-qc].
- [184] Shi Pi et al. “Revisiting the Ultraviolet Tail of the Primordial Gravitational Wave”. In: (July 2024). arXiv: [2407.06066](https://arxiv.org/abs/2407.06066) [astro-ph.CO].
- [185] Kishore N. Ananda, Chris Clarkson, and David Wands. “The Cosmological gravitational wave background from primordial density perturbations”. In: *Phys. Rev. D* 75 (2007), p. 123518. DOI: [10.1103/PhysRevD.75.123518](https://doi.org/10.1103/PhysRevD.75.123518). arXiv: [gr-qc/0612013](https://arxiv.org/abs/gr-qc/0612013).
- [186] Guillem Domènech. “Scalar Induced Gravitational Waves Review”. In: *Universe* 7.11 (2021), p. 398. DOI: [10.3390/universe7110398](https://doi.org/10.3390/universe7110398). arXiv: [2109.01398](https://arxiv.org/abs/2109.01398) [gr-qc].
- [187] Hooshyar Assadollahi and David Wands. “Gravitational waves from an early matter era”. In: *Phys. Rev. D* 79 (2009), p. 083511. DOI: [10.1103/PhysRevD.79.083511](https://doi.org/10.1103/PhysRevD.79.083511). arXiv: [0901.0989](https://arxiv.org/abs/0901.0989) [astro-ph.CO].

- [188] Hooshyar Assadollahi and David Wands. “Constraints on primordial density perturbations from induced gravitational waves”. In: *Phys. Rev. D* 81 (2010), p. 023527. DOI: [10.1103/PhysRevD.81.023527](https://doi.org/10.1103/PhysRevD.81.023527). arXiv: [0907.4073](https://arxiv.org/abs/0907.4073) [[astro-ph.CO](#)].
- [189] Ryo Saito and Jun’ichi Yokoyama. “Gravitational wave background as a probe of the primordial black hole abundance”. In: *Phys. Rev. Lett.* 102 (2009). [Erratum: *Phys.Rev.Lett.* 107, 069901 (2011)], p. 161101. DOI: [10.1103/PhysRevLett.102.161101](https://doi.org/10.1103/PhysRevLett.102.161101). arXiv: [0812.4339](https://arxiv.org/abs/0812.4339) [[astro-ph](#)].
- [190] R. Saito and J. Yokoyama. “Gravitational-Wave Constraints on the Abundance of Primordial Black Holes”. In: *Progress of Theoretical Physics* 123.5 (May 2010), pp. 867–886. ISSN: 1347-4081. DOI: [10.1143/ptp.123.867](https://doi.org/10.1143/ptp.123.867). URL: <http://dx.doi.org/10.1143/PTP.123.867>.
- [191] N. Bartolo et al. “Testing primordial black holes as dark matter with LISA”. In: *Phys. Rev. D* 99.10 (2019), p. 103521. DOI: [10.1103/PhysRevD.99.103521](https://doi.org/10.1103/PhysRevD.99.103521). arXiv: [1810.12224](https://arxiv.org/abs/1810.12224) [[astro-ph.CO](#)].
- [192] Matteo Piani and Javier Rubio. “Preheating in Einstein-Cartan Higgs Inflation: oscillon formation”. In: *JCAP* 12 (2023), p. 002. DOI: [10.1088/1475-7516/2023/12/002](https://doi.org/10.1088/1475-7516/2023/12/002). arXiv: [2304.13056](https://arxiv.org/abs/2304.13056) [[hep-ph](#)].
- [193] Takashi Hiramatsu, Evangelos I. Sfakianakis, and Masahide Yamaguchi. “Gravitational wave spectra from oscillon formation after inflation”. In: *JHEP* 03 (2021), p. 021. DOI: [10.1007/JHEP03\(2021\)021](https://doi.org/10.1007/JHEP03(2021)021). arXiv: [2011.12201](https://arxiv.org/abs/2011.12201) [[hep-ph](#)].
- [194] Nicolas Herman, Léonard Lehoucq, and André Fúzfa. “Electromagnetic antennas for the resonant detection of the stochastic gravitational wave background”. In: *Phys. Rev. D* 108.12 (2023), p. 124009. DOI: [10.1103/PhysRevD.108.124009](https://doi.org/10.1103/PhysRevD.108.124009). arXiv: [2203.15668](https://arxiv.org/abs/2203.15668) [[gr-qc](#)].
- [195] Jose J. Blanco-Pillado et al. “Gravitational waves from cosmic strings in LISA: reconstruction pipeline and physics interpretation”. In: (May 2024). arXiv: [2405.03740](https://arxiv.org/abs/2405.03740) [[astro-ph.CO](#)].
- [196] Kai Schmitz and Tobias Schröder. “Gravitational waves from low-scale cosmic strings”. In: (May 2024). arXiv: [2405.10937](https://arxiv.org/abs/2405.10937) [[astro-ph.CO](#)].
- [197] D. J. Fixsen. “The Temperature of the Cosmic Microwave Background”. In: *Astrophys. J.* 707 (2009), pp. 916–920. DOI: [10.1088/0004-637X/707/2/916](https://doi.org/10.1088/0004-637X/707/2/916). arXiv: [0911.1955](https://arxiv.org/abs/0911.1955) [[astro-ph.CO](#)].
- [198] Gianpiero Mangano et al. “Relic neutrino decoupling including flavor oscillations”. In: *Nucl. Phys. B* 729 (2005), pp. 221–234. DOI: [10.1016/j.nuclphysb.2005.09.041](https://doi.org/10.1016/j.nuclphysb.2005.09.041). arXiv: [hep-ph/0506164](https://arxiv.org/abs/hep-ph/0506164).